Aus dem
Institut für Immunologie
Institut der Universität München
Direktor: Prof. Dr. Thomas Brocker

MFG-E8 - an antigen carrier to follicular dendritic cells

Dissertation
zum Erwerb des Doktorgrades der Medizin
an der Medizinischen Fakultät
der Ludwig-Maximilians-Universität zu München

vorgelegt von

Henning Thomas Hilgendorff

aus

Bremen

Jahr

2023

Aus dem
Institut für Immunologie
Institut der Universität München
Direktor: Prof. Dr. Thomas Brocker

MFG-E8 - an antigen carrier to follicular dendritic cells

Dissertation
zum Erwerb des Doktorgrades der Medizin
an der Medizinischen Fakultät
der Ludwig-Maximilians-Universität zu München

vorgelegt von

Henning Thomas Hilgendorff

aus

Bremen

Jahr

2023

Mit Genehmigung der Medizinischen Fakultät
der Universität München

Berichterstatter: Prof. Dr. Thomas Brocker

Mitberichterstatter: PD Dr. Christof Geldmacher

Prof. Dr. Barbara Schraml-Schotta

Mitbetreuung durch den
promovierten Mitarbeiter: Dr. Jan Kranich

Dekan: Prof. Dr. med. Thomas Gudermann

Tag der mündlichen Prüfung: 23.11.2023

TABLE OF CONTENTS

ABSTRACT

Previous studies establish that extracellular vesicles (EV) pulsed with antigen induce a specific humoral immune response, resulting in protective immunity. Our laboratory has created a fusion protein composed of MFG-E8 and the green fluorescent marker eGFP (MFG-E8-eGFP). It attaches to the membrane of extracellular vesicles based on MFG-E8´s property binding to phosphatidylserine (PS). Injecting the fusion protein induces quicker immune responses to eGFP than eGFP alone. This finding is comparable to studies, where EVs pulsed with antigen generate a specific humoral response in vivo. Injected MFG-E8-eGFP quickly accumulate in and around the germinal centres (GCs), while eGFP injected alone does not. Based on these results, we propose MFG-E8 as a carrier of antigen to follicular dendritic cells. We research whether this principle may apply to viral antigens, which hardly produce neutralising antibodies (nAbs) during infection. The lymphocytic choroid meningitis virus (LCMV) is widely used for immunosuppression and T-cell exhaustion research. Its GP1 is the primary protein for viral binding to the host cell and viral neutralisation. We fused the GP1 of the chronic LCMV variant Clone 13 to MFG-E8 (MFG-E8-260L-GP1). Second, we cloned the GP1 of the Armstrong LMCV (176N) similarly (MFG-E8-176N-GP1), an acute strain causing readily cleared infections within days. Third, we fused MFG-E8 to the nucleoprotein (NP) of LCMV (MFG-E8-NP). The NP produces a more rapid humoral response than GP1. We purified the fusion protein MFG-E8-176N-GP1 from stably transfected HEK cells via high-affinity FLAG chromatography. Then we injected it into mice naïve to LCMV to evaluate the production of anti-GP1 nAbs. In a neutralisation assay, we demonstrated that the serum from MFG-E8-176N-GP1 injected mice induced lower plaque-forming units than the control MFG-E8-eGFP. Moreover, MFG-E8-176N-GP1 caused lower PFU than the well-established GP1 nAb, KL-25. As a result, we concluded the presence of GP1 nAbs in the serum of MFG-E8-176N-GP1 injected mice. Consequently, it would be interesting to see if this principle applies to the other two fusion proteins, predominantly to MFG-E8-260L-GP1. It could give hints towards a new vaccine approach for immunosuppressive viruses.

ZUSAMMENFASSUNG (deutsch)

Frühere Studien zeigen, dass mit Antigen gepulste extrazelluläre Vesikel (EV) eine spezifische humorale Immunantworten auslösen und somit zu einer schützenden Immunität führen. Unser Labor hat ein Fusionsprotein kreiert, das aus MFG-E8 und dem grün fluoreszierenden Marker eGFP (MFG-E8-eGFP) besteht. Es heftet sich an die Membran von EVs aufgrund der Eigenschaft von MFG-E8 an Phosphatidylserin (PS) zu binden. Die Injektion des Fusionsproteins löst eine schnellere Immunreaktion gegen eGFP aus als eGFP allein. Dieses Ergebnis ist vergleichbar mit Studien, in denen mit Antigen gepulste EVs in vitro eine spezifische humorale Reaktion in vivo auslösen. Injiziertes MFG-E8-eGFP reichert sich schnell in und um die Keimzentren an, während allein injiziertes eGFP dies nicht tut. Auf der Grundlage dieser Ergebnisse haben wir MFG-E8 als Antigenträger zu follikuläre dendritische Zellen vorgeschlagen. Wir wollten untersuchen, ob dieses Prinzip auch für virale Antigene gilt, die bei einer Infektion kaum neutralisierende Antikörper (nAk) bilden. Das lymphozytären Choriomeningitis Virus (LCMV) wird häufig zur Erforschung von Immunsuppression und T-Zell Erschöpfung eingesetzt. Sein GP1 ist das wichtigste Protein für die Bindung des Virus an die Wirtszelle und die Neutralisierung des Virus. Wir fusionierten das GP1 der chronischen LCMV-Variante Klon 13 mit MFG-E8 (MFG-E8-260L-GP1). In ähnlicher Weise klonierten wir das GP1 des Armstrong LMCV (MFG-E8-176N-GP1), eines akuten Stammes, dessen Infektion innerhalb weniger Tage ausheilt. Als drittes protein fusionierten wir MFG-E8 mit dem Nukleoprotein (NP) von LCMV (MFG-E8-NP). Das NP erzeugt eine schnellere humorale Reaktion als GP1. Wir reinigten MFG-E8-176N-GP1 aus stabil transfizierten HEK-Zellen mittels hochaffiner FLAG-Chromatographie auf. Wir injizierten es in Mäusen, um die Produktion von GP1 nAk zu untersuchen. In einem Neutralisationstest konnten wir nachweisen, dass das Serum von Mäusen, denen MFG-E8-176N-GP1 injiziert worden war, weniger Plaque-bildende Einheiten (PFU) bildete als das Kontrollserum von MFG-E8-eGFP injizierten Mäusen. Es zeigte zudem weniger PFU als der bekannte GP1-nAk, KL-25. Daraus schlossen wir auf das Vorhandensein von anti-GP1 nAk im Serum von MFG-E8-176N-GP1 injizierten Mäusen. Folgend wäre es interessant zu sehen, ob dieses Prinzip auch für die beiden anderen Fusionsproteine gilt, vor allem für MFG-E8-260L-GP1. Dieses könnte Hinweise auf einen neuen Impfstoffansatz für immunsuppressive Viren liefern.

LIST OF FIGURES

LIST OF TABLES

ABBREVIATIONS

Ab	Antibody
Ag	Antigen
Arm	Armstrong
α-DG	Alpha-Dystroglycan
AID	Activation-induced cytidine deaminase
APE 1	Apurinic/apyrimidinic Endonuclease 1
ATF6	Activating transcription factor 6
BCR	B-cell receptor
Bcl6	B-cell lymphoma 6 protein
Blimp-1	B lymphocyte-induced maturation protein-1
Cat	Catalogue
Cl	Clone
Conjung.	Conjugate
CTL	Cytotoxic lymphocyte
CR	Complement receptor
CXCR	CXC-Motiv-Chemokinreceptor
d	Day
DC	Dendritic cell
ddH20	double distilled water
EBI2	Epstein-Barr virus-induced G-protein coupled receptor 2
ELISA	Enzyme-linked ImmunoSorbent Assay
EV	Extracellular vesicles
FACS	Fluorescence-activated cell sorting
FDC	Follicular dendritic cell
FLT3-L	Fms-related Tyrosine Kinase 3 Ligand
GPC	Glycoprotein precursor
GP	Glycoprotein
GC	Glomerular centre
GLT	Germline transcript
h	Hour
HEK	Embryogenic kidney cells

HRP	Horseradish peroxidase
IC	Immune complex
L	Large
LAMP-1	Lysosomal-associated membrane protein 1
LCMV	Lymphocytic choroid meningitis virus
LAG	Lymphocyte-activation gene
MFG-E8	Milk fat globule-epidermal growth factor 8
Min	Minute
MHC	Major histocompatibility complex
MZ	Marginal zone
mRNA	messenger ribonucleic acid
miRNA	Micro Ribonucleic acid
MP	Macrophage
NP	Nucleoprotein
nAb	Neutralizing antibody
d.p.i.	Days post-infection
d.p. im	Days post-immunization
PD	Programmed cell death protein
PS	Phosphatidylserine
RNA	Ribonucleic acid
SCS	Subcapsular sinus
S	Small
SN	Supernatant
UNG	Uracil-DNA glycosylase
S1Pr2	Sphingosine-1-phosphate receptor 2
SHM	Somatic hypermutation
Tfh-cell	T-follicular helper cell
TIM	T-cell immunoglobulin and mucin-domain containing
TCR	T-cell receptor
WB	Western Blot
WT	Wild type
Z	Zink finger

1 INTRODUCTION

1.1 Lymphocytic choriomeningitis virus

1.1.1 LCMV belonging to the family of the Arenaviridae

Arenaviridae are named after their sandy (Latin, arenosus) appearance under the electron microscope (1–3). Their grouping is mainly based on unity in their common Large and Small RNA (3,4). The family of the Arenaviridae is divided into three genera depending on the viral host: Mammarenavirus, Reptarenavirus, and Hartmanivirus (3,5). The genus of the Reptarenavirus and Hartmanvirus infect reptile hosts. Mammarenaviruses infect mammalian hosts (3,5). Mammarenaviridae are subdivided into new and old-world viruses based on their genetic, geographic, and epidemiological relationship (4,5). New world viruses located in South and North America are sectioned into A, B, C, and D. Clade B viruses, which include Junin, Machupo, Guanarito, and Sabia virus cause hemorrhagic fever (5,6) using transferrin-1 receptor as their mode of propagation (7).

Familiar representatives of the old-world viruses are the Lassa fever virus (LFV) present in West Africa and the Lymphocytic choroid meningitis virus (LCMV) located in America and Europe (CDC, 2013). Together with clade C, new world viruses use α-dystroglycan (DG) as a receptor of viral propagation (8–10). LFV´s host is the multimammate rat causing haemorrhagic fever (CDC, 2019) (11). The displayed symptoms are indistinguishable from other haemorrhagic fevers starting with febrile illness leading to mucosal bleeding, convulsions and death (12–14). In recovery, 29 % of seropositive patients with neurological sequelae display deafness (12,15,16). The natural host of LCMV is the mouse, in which the non-cytopathic virus can persist. The virus is transmitted to humans via direct contact with animal excrement, via aerosol or vertical from human to human. In immunocompetent humans, LCMV causes an undifferentiated febrile illness or meningitis. In immunosuppressed transplant patients, who receive organs from LCMV-infected donors, the virus leads to severe manifestations of aseptic meningitis and haemorrhagic symptoms with high fatality rates (17,18). The congenital infection leads to severe neurological malformations with cognitive impairment in newborns (19,20).

1.1.2 Discovery of LCMV

Lymphocytic choroid meningitis virus has been discovered in 1933 by Armstrong and Lillie in a patient with a general poor health condition. The patient has presented with acute meningeal symptoms during the St. Louis encephalitis epidemic. The virus transferred into monkeys and mice shows prominent lymphocytic infiltrations around choroid plexi, different from the virus causing the St. Louis epidemic (21). LCMV has been born.

Intracerebral injections of passaged LCMV into immunocompetent adult mice cause fatal meningitis (21,22). Intravenous, subcutaneous, and intraperitoneal injections cause a readily cleared infection in up to 10 days (23–25). An MHC-restricted CTL response and not Abs mediate the viral clearance (10,22,26–28). In utero or newborn mice infected with acute LCMV generate a persistent infection resulting from T-cell exhaustion. Mice that recover from a chronic illness by adoptively transferred LCMV-specific T-cells display a competent immune response against acute LCMV re-challenge (29–31). This contradicts the theory of deletion of LCMV-specific CD8 T-cells during neonatal LCMV infection in the thymus, called negative selection (23). In this theory, it has been thought that the omission of LCMV-specific T-cells induces viral persistence due to the viral antigen being recognised as "self-antigen".

Mice infected in immunosuppressed states ($CD8^{-/-}$, $CD4^{-/-}$, $perforin^{-/-}$, $TNF\text{-}alpha^{-/-}$) suffer from the persistent disease despite the LCMV strain. This changes the virus´ phenotype months after inoculation from acute to chronic (23,24,28). Two years after Armstrong´s findings, Traub et al. discovered that the first LCMV strain establishing a chronic infection without preceding immunosuppression (25). Intracerebral injection of LCMV in adult mice induces a persistent benign disease with enlarged spleens and signs of congestive hepatopathy instead of lethal meningitis (25).

Four decades after Traub´s and Armstrong's discovery, the strains Armstrong 53b and Clone13 LCMV were cloned and sequenced (32,33). Clone 13 LCMV ($LCMV_{Cl13}$) is derived from a mouse´s spleen infected neonatally with Armstrong 53b virus leading to chronic infection. $LCMV_{Cl13}$ has a Lysine at amino acid 260 (260L) comparable to WE and Traub virus, while Armstrong LCMV ($LCMV_{Arm}$) has a Phenylalanine at this position, determining their viral phenotypes. At amino acid (aa) 176 of the GP1, the Armstrong virus contains an asparagine (176N), while $LCMV_{Cl13}$ includes an aspartic acid (D). This aa change does not affect viral tropism or persistence (34,35). However,

it plays a role in our terminology of the LCMV_{Arm} GP1. LCMV-WE shares 94 % of amino acids with LCMV_{Arm} and LCMV_{Cl13} variants, implicating their close descendant and volatile evolution of the LCMV (24).

1.1.3 Organization of LCMV genome

Similar to other Arenaviridae, the genome of LCMV has two single-stranded RNA segments, the Large (L) and Small (S) RNA. Both RNA strands code in an anti-sense fashion for different proteins in 3´-5´ and 5´-3´ directions. The L RNA codes for the Zink finger protein in sense direction and in anti-sense order for L protein, which contains the viral RNA polymerase for replication (3,32). The S RNA codes for the Glycoprotein precursor (GPC) in anti-sense and sense direction for the NP (3,6). A non-coding intergenic region separates each RNA strand. The site-1 protease (S1P) cleaves the GPC post-translationally to its surface proteins GP1 and GP2 (3,36,37). Cryo-electron microscopy reveals that LCM virions are spherical vesicles composed of lipid bilayer decorated by GP1/GP2 spikes (2). Each spike composes 3 GP1/GP2 complexes. The Zink finger (Z) protein locates below the lipid bilayer acting as matrix protein for the GP1/GP2 heterodimers. It anchors the viral spikes on the virion surface (2,36). The NP encapsulates the viral RNA inside the virion, forming ribonucleoproteins (RNP). The RNP complexes connect to the L protein containing the viral polymerase to initiate viral replication (3).

1.1.4 Invading host cells

GP1 and GP2 attach non-covalently to each other forming trimers on the surface of the virion (2,37,38). GP2 is a distinct stalk anchoring on the virion surface, while the GP1 forms a spherical head for attachment to the host cell (2,37,38). GP1 utilises the α-DG receptor for attachment to the viral host cell. Its ability is due to its high-affinity binding to α-DG, competitively replacing extracellular matrix protein laminin (8,34,39,40). α-DG is an extracellular receptor binding to laminin, agrin, perlecan, and neurexin, all ECM proteins in different tissues (41–43). It is non-covalently attached to β-DG, located in the cell membrane. β-DG anchors the actin-based cytoskeleton to

the ECM via the adaptor proteins dystrophin and utrophin (42,44,45). α-DG´s wide expression in human and rodent tissue explains the broad host range of the LCMV (46).

The α-DG, GP1/GP2 virion complex is endocytosed into vesicles and transported within the endosomal compartment to the late endosomes (47,48). In the pre-fusion state, the crystal structure of GP2 consists of a signal peptide and fusion peptide at the C-terminus, which is connected to a heptad repeat (HR) 1 pattern. HR1 has 3 alpha-helical subunits fused via a T-loop to HR2 at the GP2´s N-terminus. The T-loop connects GP2 with GP1 via 2 anti-parallel β-strands forming a β-sheet (37).

The acidic milieu within the endosomal compartment induces the pH-dependent dissociation of GP1 and GP2 (47,49,50), followed by a conformational refolding of GP2. The result is the formation of a GP2 homotrimer separated from GP1, called a fusion state. HR1 and HR2 form a single α-helix, similar to the T loop. Three copies of each HR build a stable trimeric α-helical bundle, a hairpin structure. The C and N terminus connect to a hydrophobic fusion peptide and loop. Both anchor the GP2 in the endosomal vesicle´s host membrane, leading to membrane fusion and pore formation (37,38,51,52).

Viral RNA locates in the cell cytoplasm through the fusion pore, where its replication starts.

1.1.5 Replication of the virus

The Ribonucleoprotein mediates transcription and translation through its NP and L protein, which carries the RNA-dependent RNA polymerase (53). Function analysis and mutagenic experiments demonstrate that the L protein contains an endonuclease similar to the Influenza PA subunit (54). It facilitates cap snatching, using host RNA as primers to kick off viral transcriptions of the NP and L protein, the early gene transcripts during the LCMV life cycle (53,55). The process of cap snatching from host RNA is well established for the influenza virus (56,57).

After sufficient transcription and translation of NP, RNA depended RNA polymerases read through the intergenic regions to produce whole-stranded anti-genomic RNA necessary for replication and transcription of the late gen products, the GPC and Z protein (53,55). The late gen transcripts move to the rough endoplasmic reticulum,

where translation and glycosylation of the GPC take place (3,5,53). The Side-1 protease cleaves the GPC to its GP1/GP2 heterodimeric surface molecules in the late Golgi. Whereas the same protease processes the close related Lassa virus in the cis Golgi compartment using a different coded Site-1 protease binding site (58–60)

1.1.6 Importance of the Site-1 Protease

Site-1 protease (S1P), also called Membrane-bound transcription factor peptidase, resides in the cis, medial, and late Golgi apparatus of eukaryotic cells (58,59). The protease is responsible for the cleavage of host and viral proteins inducing cascades of downstream activation (61,62).

In vitro, S1P-deficient cell lines fail to propagate LCMV from cell to cell (58,63).

The breeding of $S1p^{-/-}$ mice is impossible because of embryogenic lethality during d 4 of embryogenesis (61).

$LCMV_{Cl13}$ infected mice with hypomorphic expression of S1P have decreased viral titres and no viral persistence compared to controls.

Infecting hypomorphic S1P mice with a recombinant (rec) $LCMV_{Cl13}$ variant containing a furin binding site instead of an S1P binding site prompts viral rescue due to enzymatic availability (64).

Commonly in LCMV, the binding site for the S1P is coded as $RRLA_{265}$ (58,59), with a consensus motif of R-(R/K/H)-L-(A/L/S/T/F)$_{265}$. Mutations beyond this consensus motive lead to complete or partial inhibition of GPC cleavage depending on the location of the modification. Accordingly, the following LCMV GPC mutants are not cleaved by S1P: R262A, R263A, and L264A (59).

While the in vitro surface expression of the GPC is not altered by the absence of cleavage, the infectivity is. This concludes that S1P is unnecessary for transporting the protein to the surface. However, for the cell-to-cell propagation of the virus, the cleavage of the GPC is vital (37,59,64).

Interestingly, Burri et al. suggest that the binding site's motive might hint at the location of endosomal processing. The Lassa virus´ GPC contains the S1P binding site RRLA but is processed in the cis-Golgi apparatus instead of the late Golgi (58–60). Cloning the Lassa virus´ S1P binding site into LCMV and replacing RRLL with RRLA leads to the processing of the GPC in the cis-Golgi apparatus instead of the late Golgi (58).

Finally, after endoproteolytic processing, GP1/GP2 heterodimers decorate the surface of the virion. These two GPs have specific sites for Ab-mediated binding.

1.1.7 Epitope mapping for antibody binding in LCMV

Competitive antibody-binding assays exhibit that different LCMV strains have common epitopes for antibody-mediated binding and neutralisation. Traub, Cl13 and LCMV-WE are all chronic strains, and Armstrong the prototype for acute strains (65). The discovered antibody (Ab)-binding topography is described as follows (26,65):

A major common conformational epitope GP-1A overlaps with epitope B; second, a minor linear GP-1C epitope is detected among chronic and acute strains. GP1-A locates on top of the GP1 near the S1P binding area on the rounded head of the viral spike (26,37). LCMV$_{Arm}$ has another GP1-D epitope. It resides nearby, is highly mutagenic and can induce viral neutralisation overlapping with specific GP1-A Abs (65,66). The GP1-A and -D epitopes locate near the α-DG binding site. They are the major neutralising sites for Abs by blocking attachment of GP1 to the α-DG receptor on the host cell (34,67). The GP1 main body has 6 N-linked glycosylation sides on its upper β-sheet (37,68). 1 glycan at aa 124 (37,68) shields the neutralising GP1-A epitope since recLCMV$_{Cl13}$ lacking this glycan exhibits enhanced sensitivity to KL-25 (68). KL-25 is a commonly used Ab for LCMV neutralisation experiments and known to bind specifically to the GP1-A epitope (26).

The GP2 has 3 epitopes, A, B and C, without neutralising abilities. They locate in aa 370-378 on the stem of the viral spike (38,69), residing on the T-loop connecting GP1 and GP2 in a prefusion state (37). 3 N-linked glycosylation sites are situated on the GP2´s T-loop shielding the mentioned Ab binding sites (37,38).

The GP2 binding Abs primarily have a non-neutralizing activity. Nevertheless, in the presence of excess complement factors, they induce virion lysis (69,70). GP1 binding Abs and neutralizing Abs of low affinity also cause complement-mediated virion lysis. Both decrease the spread of infection early after viral inoculation in the absence of high-affinity neutralizing Abs (nAbs) (71). Multiple studies conclude that the GP1 is the central region responsible for Ab-dependent virion lysis and viral propagation (26,28,65,72).

1.1.8 Pathogenesis of LCMV

GP1 has the characteristic of binding to α-DG in high or low affinity, which determines the tropism of the virus as it affects the chronicity of the disease. Chronic LCMV strains including Cl13, Traub, or WE, share a high affinity to α-DG. The association to this extracellular matrix receptor codes in the following 3 aa (24,34,37) located on the lower helix loop face of the GP1 (37): 260L, 153S and 155Y. These mutations induce a chronic infection independently of the LCMV backbone (34,37).

Acute strains missing these mutations have a 2-3 log lower affinity to α-DG and a different viral tropism. Thus, these strains infect different cell types (37,73,74). LCMV$_{Arm}$ use another unknown receptor for viral propagation (34,37,73,75). It could benefit from an apoptotic mimicry, an alternative propagation mechanism to α-DG mediated cell entry (74,76). The parental Armstrong virus differs further from his "Clone" 13 in having lysine in positions 1079 instead of glutamine coding for its viral polymerase in the L protein of the viral RNP (34,75,77). This aa change leads to increased viremia during the early stage of infection, contributing to increased T-cell exhaustion due to augmented antigen loads (35). Paradoxically, Sullivan et al. note that only 16% of observed LCMV persistent phenotypes acquire the K1079Q mutation (34). The pathogenesis during the first days post-infection is similar in acute and chronic LCMV. Each virus infects the marginal zone (MZ) cells in the splenic white pulp (24,75). Three days post-infection (d.p.i.), acute strains start to infect the splenic red pulp´s MPs (24,75). A cytotoxic lymphocyte response at 7 d.p.i. follows the infection. Chronic LCMV strains continue to infect the splenic white pulp´s CD11c+, DEC-205+ dendritic cells in an α-DG depended manner leading to an aborted cytotoxic lymphocyte (CTL) response (24,34,75,78). Infected dendritic cells (DC) downregulate MHC-I, MHC-II, and costimulatory molecules for T-cell activation but recover these with viral clearance (79). The ability of LCMV to infect bone marrow-derived DCs and their hematopoietic precursors leads to failure of maturation, proliferation and migration of mature CD11c+ DCs to the spleen (79).

During LCMV$_{Arm}$ infection, the stimulation of DCs with FLT3 ligand leads to a 20-fold increment of CD11c+ DCs in the spleen. In LCMV$_{Cl13}$ infected mice, DC mobilisation with FLT3 ligand fails (79,80). In persistently infected mice, DCs upregulate the negative immune regulators programmed cell death (PD)-ligand 1 and IL10 to prevent immunopathology (81–83).

The upregulation of negative immunomodulators, including Lymphocyte-activation gene 3 (LAG3), TIM3 (see abbreviations) and PD1, contributes to T-cell exhaustion, caused by persisting viremia and chronic T-cell stimulation (84,85). This overexpression leads to decreased CD4 and CD8 T-cell functions, described as a stepwise reduction of IL2, TNFα and IFNγ production (84–86). The Unresponsiveness of CD4 and CD8 T-cells can be reversed by IL10-receptor and PD1 Abs (83,87–89), which respond best in dual therapy. The LAG3 negative immunomodulator on T-cells shows promising results in different studies reversing T-cell exhaustion (84,90). Its inhibition, especially in dual treatment with anti-PD-L1 Abs, induces temporary viral remission and restores CD8 T-cell function (90). The clonal deletion corresponds primarily to CD8 T-cells. CD4 T-cells do not mainly undergo clonal deletion. They adjust their phenotype from IL2- to IL21-producing T-cells similar to a Tfh-phenotype (91). Tfh-cells are essential for a sufficient Ab response. This context is in line with the crucial task of nAbs for viral remission during the protracting phase of chronic viral infection (92).

1.1.9 Neutralizing antibodies in LCMV infections

Immunocompetent mice can clear $LCMV_{Cl13}$-infections within 2-3 months (90).
Mice infected with chronic LCMV in which the CTL response is abolished, the emergence of nAbs is detected at around 30 d.p.i. with start of virus clearance from the blood (26,28,93). But due to the emergence of viral mutants at around 70 d.p.i. clearance is quickly reversed, and the virus persists (28,93). While in high-dose infected WT mice, low-affinity GP1 nAbs reveal late at 80 d.p.i. with high titres of GP2 and NP Abs (26). In WT mice infected with a low dose of virus, no GP1 nAbs are found, but GP2 and NP Abs are readily detectable (26). A low number of emerging GP1 nAbs suggests that a small B-cell repertoire recognises the viral protein. Therefore, it needs a large amount of antigen (ag) to activate B-cells (26). In CTL-deficient and high-dose infected WT mice, high viremia translates into activation of B-cells and the emergence of Abs due to higher availability of ag and perseverance of follicular architecture (26,28). Interestingly WT mice show an early emergence of specific GP1 Abs with no or little neutralising capacity but very late emergence of nAbs

at 80 d.p.i. CTL-deficient mice develop nAbs at 30 d.p.i. (26). The late emergence of nAbs in persistently infected immunocompetent mice could have several reasons: First, high-dose infection with chronic LCMV strains induces profound CTL-mediated destruction of follicular architecture. Losing immune structures inhibits the cellular and humoral response from 7 d.p.i. due to the loss of the ag-presenting machinery and T-cell support (24,34,79). Immunosuppression and persistent infection follows (24,28,34,94). Second, the virus produces mutations in its variable regions of the receptor loops surrounding the virus´s binding site. They contribute to the evasion of ag from nAbs (26,95).

The WE-LCMV mutants present at around 70 d.p.i. have mutations at the following variable regions of the virus, at aa 119–133, 175–185, and 211–214 (28). These aa reside on loops 1, 2 and 3, respectively, of the GP1´s lower helix (37). Interestingly, aa 119 is the only position where mutations result in the evasion from nAbs in transgenic mice expressing the heavy and light chain of the KL-25 Ab (72). It is a well-established nAb specific for the GP1-A epitope (26,28,65). The isolated alteration suggests that either aa 119 binds directly in or induces a conformational change of the receptor region (28,72).

WT mice infected with recLCMV$_{Cl13}$ deficient in glycan at aa 119 prompt the production of nAbs from 4 d.p.i. From 12 d.p.i. The LCMV$_{Cl13}$ mutants cause lower viral titres due to effective viral clearance by nAbs. Complete viral clearance from blood is achieved at 19 d.p.i. WT LCMV$_{Cl13}$ infected mice achieve viral clearance at around 60 d.p.i. (68). We can summarise that LCMV has various strategies to evade the immune response (26): First, destroying the follicular architecture by an initial elicited CTL response, resulting in inhibition of the GC reaction and production of Abs. The destruction of the splenic white pulp containing CD11c+ DCs leads to poor CTL response and impaired humoral response. The host´s inability to clear the virus via CTL or nAbs leads to high viremia resulting in T-cell exhaustion and virus persistence. Second, changing the viral genetic makeup in its variable or receptor regions due to humoral mediated pressure by newly emerging nAbs. Third, successfully hiding nAbs binding regions by glycan shields (68). Similar strategies are used successfully by viruses like HIV or Hepatitis B and C invading immune cells and disrupting proper immune response.

1.2 Germinal centre response

1.2.1 Production of high-affinity antibodies

To initiate a germinal centre response, an ag needs to be presented by a follicular dendritic cell, macrophage or DC to a specific B-cell in the follicle.

Early as 1 d.p.im. T-cell start to upregulate B-cell lymphoma-6 (Bcl6) after interaction with ag-presenting DCs (96,97). In turn, T-cells start to express a Tfh-phenotype with C-X-C chemokine receptor (CXCR) 5, PD1 and the activation marker GL7 (98). Bcl6 upregulation is essential for the differentiation of Tfh-cells. B-lymphocyte-induced maturation protein 1 (Blimp1) antagonises Bcl6 and the Tfh-phenotype (99,100). Ag-specific Tfh-cells migrate into the interfollicular channels, where they undergo interaction with cognate B-cells (98). At 3 d.p. im. Tfh-cells migrate into the follicle 1 d. earlier than GC B-cells.

At d. 4 of the germinal centre (GC) response, pre-GC B-cells with higher affinity to presented ag outcompete lower affinity pre-GC B-cells and migrate into the follicle (101,102). The pre-selection process of high-affinity clones is due to the limiting factor of ag-specific Tfh-cell support (102,103). B-cells with the highest affinity to ag have a higher density of surface peptide MHC and receive more Tfh support prompting more cell proliferation. Thus, high-affinity pre-GC B-cells become GC seeding B-cells (102). High-affinity clones enter the follicle by upregulating Bcl6 and CXCR5 to migrate along the C-C motif chemokine (CCL) 13 gradient into the GC (98,104). GC seeding cells become B-cell blasts. When they increase in numbers, they displace IgM+ IgD+ follicular B-cells to the mantle zone forming an early GC. At d 7, several rounds of cell division have taken place, segregating the follicle into a dark area and light zone, respectively, in a CXCR5 and CXCR4 pole (98,103–105). Centroblast in the dark zone express CD86 low, CD83 low and CXCR4 high (103,106). They respond to CCL12 expressing reticular cells (106). Centrocytes in the light zone react to CCL13 produced by FDCs via overexpression of CXCR5 (CXCR4 low), CD83 high, and CD86 high (103,104,106,107).

Mice deficient in CXCR4 exhibit loss of dark and light zone segregation. Loss of CXCR5 prompts a disorganised follicle architecture, but dark and light zone differentiation persist (104).

The maintenance of follicle polarity in CXCR5 deficient mice is possibly due to the presence of Sphingosine-1-phosphate receptor 2 (S1Pr2) in the follicle centre

supporting its compartmentalisation (108). CXCR4 and CXCR5 deficient mice can still induce affinity maturation, questioning their importance for the differentiation of the GC response (106,109,110). Mice deficient in Bcl6 are not able to generate GC organisation. Thus, it is thought to be the master regulator of the GC reaction (111,112).

The dark zone comprises rapidly dividing blasts undergoing activation-induced deaminase (AID)-driven somatic hypermutation (SHM) in its variable regions CDR1, CDR2 and CDR3, increasing affinity to the presented ag (113,114).

Still, whether AID-driven class switching occurs before SHM or after it, the question must be asked. Liu et al. suggest the onset of class switch recombination (CSR) after the start of SHM due to the detection of germline transcripts in CD77+ B-cells, which have been thought to be centrocytes. But it is shown that CD77 is a universal marker for activated B-cells, centrocytes and centroblasts (115).

Most recent research indicates that CSR occurs before GC formation and the extrafollicular primary immune responses at the T-B border. Thus, higher Apurinic/apyrimidinic Endonuclease 1 (APE1) expression exists outside the follicle than inside the follicle in GC B-cells (116). APE1 is responsible together with AID and Uracil-DNA glycosylase (UNG) for class switch recombination (CSR). At the same time, APE2 and AID are necessary SHM (117,118). APE2 is higher expressed in the follicle (116). At d 3 and d 6, single-cell qPCRs for germline transcripts (GLT) are analysed. At d 6, pre-GC B-cells have 53% γ1-GLTs, contrary to GC B-cells, which have 3% γ1-GLTs. Similar percentages are seen in γ2-GLTs. These findings indicate that CSR is not a characteristic of mature GC B-cells but pre-GC B-cells (116).

After GC B-cells have undergone SHM in der dark zone to increase their affinity to ag, B-cells migrate into the light zone to become centrocytes. The light zone also comprises Tfh-cells, Follicular dendritic cells (FDC) and tingible body macrophages (103).

Centrocytes compared to centroblasts, are morphological alike in 2-photon microscopy experiments but not rapidly dividing. Instead, they upregulate genes for apoptosis, CD40 and B-cell receptor signalling (103).

Centrocytes recognise ag presented by FDCs via their B-cell receptor (BCR). The higher the affinity of the BCR to ag, the more ag centrocytes can internalise and present to Tfh-cells as peptide MHC II complexes. The more ag B-cells present via peptide-MHCII complexes, the more survival signalling the centrocytes receive from

Tfh-cells via Inducible T-cell Co-Stimulator (ICOS), CD40L and IL-21 and IL-4 (102,103). This process is called affinity maturation and leads to the selection of B-cells expressing high-affinity B-cell receptors. 70% of centrocytes entering the light zone undergo apoptosis and are removed by tingible macrophages (MP) with the help of MFG-E8 produced by FDCs (103,119). 30 % of B-cells receive enough survival signals (103). These centrocytes upregulate CXCR4 and migrate back into the dark zone along a CXCL12 chemokine gradient to undergo another round of affinity maturation. With upregulation of CXCR5, B-cells migrate back into the light zone for selection. Or the B-cell leaves the GC after positive selection to become a memory or plasma B-cell to produce high-affinity Abs (120,121).

1.2.2 Complement-mediated antigen delivery to FDCs

FDCs localise in the light zone of the GC. They are essential for presenting ag during affinity-based B-cell selection (122–124). To act as the ag library in the GC, ag has to be delivered to the FDCs. Immune complexes carry ag into the centre of the follicle. Immune complexes are formed by ag, IgM or IgG and a C3 or C4 degradation product (122). They are carried via afferent lymph vessels to the lymph node and blood into the spleen. Due to their large size, immune complexes (IC) cannot enter directly into the lymph conduit. Different subsets of MPs capture ICs working as flypaper and doorkeeper for ag (125,126).

In the lymph node, subcapsular sinus MPs catch ICs in a complement receptor 1 and complement receptor (CR) 2-dependent manner (122,127,128). CR1 captures C3b, C3b, C4b and iC4b bound ICs. CR2 catches C3d and iC3b mediated ICs (126,129). Subcapsular sinus (SCS) MPs do not phagocytose the ICs due to their low lysosomal and endocytic activity (128). The ICs move along their dendrites on the floor of the SCS to be carried on by follicular B-cells on their trailing ends, also called Uropod, as seen in multiple two-photon microscopy experiments (126,127,130). The formation of Uropods result from B-cell activation during Immunoglobulin capping (131). Immunoglobulin, microvilli and vesicles redistribute to the B-cell´s trailing end displaying a dendrite-like structure (131). So eventually, during the Uropod formation, CRs are redistributed, and its formation shows the CR-mediated capturing of ICs. MZ B-cells shuttle them onto FDCs using CR1 and CR2 (127,128). The shuttling of ICs

and B-cell between SCS and FDC is likely chemokine-dependent but needs further research (128). Deleting CR2 and C3 leads to a blunted immune response by decreased capturing of ICs.

The IC-mediated ag delivery mechanism is researched by Ferguson et al. in the spleen. Injected IgM-ICs deposit in the MZ onto metalophilic MPs and are captured by MZ B-cells (123). Later, MZ B-cells and IgM-bound ICs reside in juxtaposition to FDCs. This movement pattern suggests a transfer of the IgM-IC complex via MZ B-cells and a connection between the B-cells and the FCDs.

However, in adoptive transfer experiments, follicular B-cells cannot replace the MZ B-cell task when either cell line is depleted. Knocking out all B-cells leads to the failure of IgM-IC transport to the FDCs and the trapping of IgM-IC on the MPs (123).

Interestingly, adoptively transferred MZ B-cells incubated with IC can migrate to FDCs in MP-deficient mice. The ability to transport IC to the FDCs without MPs suggests a humoral response is possible without capturing MP but depends on an opsonin.

Injecting IgM-IC into CR2 and C3-deficient mice shows negligible binding outside the metallophilic MPs and no binding inside the follicle (123). The absence of ICs indicates that an intact complement system is crucial for capturing ICs and the resulting adaptive immune response.

Injected HIV-like particles are captured by MPs similar to ICs. HIV-like particles are commonly named virus-like particles (VLP). They are vesicle-like structures composed of a lipid layer with integrated immunogens for eliciting a humoral immune response (132). Injected VLP transfer into a Milk Fat Globule-Epidermal Growth Factor 8 (MFG-E8) rich area onto FDCs independently from B-cells. The expansion and contraction of the FDC network interact directly with the SCS MP, eliciting the transfer of the VLPs. In transfer experiments with genetically modified B-cells cognate to the HIV envelope protein GP120, display prolonged contact duration with SCS MPs carrying VLPs compared to non-cognate B-cells (126,130). This concludes that IC transfer from MPs toward FDCs might still be CR2 dependent, and the MFG-E8 rich area is a general gating area for ag delivery to FDCs (126).

We can assume different ag delivery mechanisms during a viral infection. During an early time point of the disease, the delivery mechanism might be due to a different opsonin than at a later point when IgM production increases and, in turn IC formation. Injected HIV-like particles do not infect cells (132). They could simulate an early time point during HIV infection, in which virus particles enter the human lymphoid system

(126). Consequently, MFG-E8 is an opsonin for ag delivery to FDCs, especially during the early time point of viral illness.

1.3 MFG-E8

1.3.1 The composition and function of MFG-E8

Milk fat globule-epidermal growth factor-factor 8 (MFG-E8), also called Lactadherin, is a glycoprotein containing 3 N-linked glycosylation. It is mainly produced by immature dendritic cells, MPs, retinal pigmental, mammary epithelial cells and FDCs (133–138). A long and alternative spliced short isoform of MFG-E8 is found in the mouse. The long-spliced version consists of one signal peptide on its N-terminus, which releases the protein into the extracellular space. Besides, it has two epidermal growth factor domains, a highly conserved arginine–glycine–aspartate (RGD) motive for $\alpha_V\beta_3$ and $\alpha_V\beta_5$ integrin-mediated binding. Further, it comprises a proline-/threonine-rich region between the C1 and epidermal growth factor domains. The PS binding region has a two-factor-VIII-homologous domain (C1C2) at its C-terminus (139,140). The proline-/threonine-rich area is responsible for the high-affinity binding of C2 to PS. The receptor acts as an "eat me signal" of apoptotic cells for MPs (138,141,142) or as apoptotic mimicry of enveloped viruses to invade host cells (76,143–145). The RGD domain of MFG-E8 binds to $\alpha_V\beta_3$ and $\alpha_V\beta_5$ integrins on MPs inducing phagocytosis of apoptotic cells. The short spliced version of MFG-E8 misses the proline-/threonine-rich regions, decreasing the affinity to PS and its ability to induce phagocytosis (135,138,146). Viable cells keep PS inside their phospholipidic cell membrane with help of a scramblase. In response to apoptotic stimuli, a flippase transfers PS outside the cell membrane (147,148). Deficiency of MFG-E8 leads to a lupus-like disease due to the development of auto-Ab against exposed DNA of unremoved apoptotic cells (142,149) (119). Thus, *Mfge8-/-* mice present with splenomegaly and enlarged follicles attributable to increased IgG production by plasma cells (119). In WT mice, CD68+ tingible body MPs remove sufficiently apoptotic B-cells from the GC with the help of MFG-E8. In *Mfge8-/-* mice, tingible MPs can recognise but not phagocytose apoptotic B-cells. Thus, these mice develop many anti-nuclear and anti-dsDNA Abs in serum inducing renal failure by glomerulonephritis (119,142). But in human systemic lupus

erythematosus (SLE) patients, high levels of MFG-E8 are present. This is caused by MFG-E8 antagonising integrin-mediated binding of MPs to apoptotic cells (142,149). Upregulation of cytokines in chronic inflammatory diseases like SLE increases levels of MFG-E8 in serum to remove apoptotic cells (142,149). Therefore, MFG-E8 is a regulator of the immune response downregulating autoimmunity by increasing phagocytosis. Another mechanism in SLE is to remove the apoptotic cell debris by the vicious cycle of auto-Ab production and the induction of ICs. Most recently and discussed below in more detail, $Mfge8^{-/-}$ mice display decreased ag loading of FDCs. Injection of recMFG-E8 improves ag delivery to FDCs. Thus MFG-E8 can be suggested as a delivery tool for ag onto FDCs promoting a humoral response (126).

1.3.2 MFG-E8, an antigen delivery tool to FDCs

MFG-E8 has 3 binding domains, 1 RGD domain connecting to $\alpha_V\beta_3$ and $\alpha_V\beta_5$. Second, it has a C1C2 domain binding to phosphatidylserine (PS).

HIV and other enveloped viruses use PS as a mode of viral propagation by binding to proteins, including MFG-E8 (144,145). Applying MFG-E8 with a blunted RGD cellular binding site inhibits viral propagation in vitro, implicating the importance of the RGD motive for cellular and viral interaction (144,145). Ag arriving from the afferent lymphatics are usually too big to enter the lymph conduits directly. Their size makes it essential for the ag to bind to an opsonin recognised by lining MPs (126). Many studies identify MFG-E8 as a mediator of phagocytosis through $\alpha_V\beta_3$ on MPs (150,151). The role of SCS MPs is contrary in the presence of MFG-E8.

Phan et al. reveal that SCS MPs CD169+ have lower endocytic and phagocytic activity due to lower expression of lysosomal-associated membrane protein 1 (LAMP-1) (128). SCS and MZ MPs process ag on their cellular surface instead of phagocytosing it. This characteristic promotes ag presentation to the underlying GC for further processing (127,128,130). HIV-like particles are captured by lining MPs similar to ICs. Their common name are virus-like particles (VLP). They are vesicle-like structures composed of a lipid layer with integrated immunogens (132).

Park et al. propose that MFG-E8 is an opsonin for the ag delivery to FDCs based on the VLP´s characteristic in binding via PS to MFG-E8 similar to a virion.

Flow cytometry demonstrates in vitro binding between MFG-E8, VLPs, and $\alpha_V\beta_3$. Injecting VLPs into mice induces an 85 % colocalization of $\alpha_V\beta_3$ with VLPs in an MFG-E8-rich compartment in the GC. This area locates below the SCS MPs and directly contacts the FDC network. In this zone, the high colocalization between $\alpha V\beta 3$, VLP and MFG-E8 implicates the linkage in vivo (126). Interestingly, injected fluorescent ICs overlap below the SCS in the MFG-E8-rich area with VLPs. However, no ties between IC and MFG-E8 in vitro are described (127,128).

Deleting the RGD binding domain of MFG-E8 in conjunction with the α_V part of $\alpha_V\beta_3$ in MPs abolishes ag delivery to FDCs. The result is the deposition of ICs on MPs surrounding the medullary sinuses, which phagocytose deposited IC and do not present them on the cell surface. The processing of the ag complexes to the GC is inhibited (128).

In contrast to the RGD-α_V mediated inhibition, FDC loading in $Mfge8^{-/-}$ mice is not wholly impaired. The capturing of ICs by MPs increases compared to WT mice, implicating multiple effective IC tethering mechanisms. However, the injection of recMFG-E8 into $Mfge8^{-/-}$ mice increases ag loading on FDCs (126). Enhanced IC delivery indicates that MFG-E8 is an opsonin similar to IgM. MFG-E8 directs ag to FDCs and elicits a humoral response (123,126).

Because VLPs highly mimic virions (132) and virions resemble exosomes in build (152), exosomes might similarly use MFG-E8 as a delivery mechanism.

MFG-E8 is a component of the membrane of extracellular vesicles secreted by immature DCs (153,154)

1.4 Extracellular vesicles

1.4.1 Characteristics of extracellular vesicle

Various cell types secrete extracellular vesicles, including DCs, T-cells, B-cells and MPs. Extracellular vesicles (EV) are highly immunologically active (155). Depending on their origin, they contain different immunologic markers and differ in their task and names (156,157). A clear differentiation based on immunologic surface markers is difficult due to overlapping (155,158). EVs are subdivided into exosomes, microvesicles and apoptotic bodies. Exosomes are roughly in size between 40-200 nm, microvesicles are up to 1 μm in length, and apoptotic bodies are 1-5 μm (157). Macrovesicles are created instead by low-speed centrifugation. Smaller EVs are produced by up to 100.000x g and segregated by sucrose gradient or immunologic markers (157,159).

In the cell, exosomes and multivesicular bodies are assembled as intraluminal vesicles from the lining membrane of the endosomal compartment. Intraluminal vesicles fuse with the lysosome undergoing degradation or leave the multivesicular bodies through exocytosis. Macrovesicles break off the cellular plasma membrane as blebs instead of being secreted. Markers of macrovesicles are associated with the corresponding plasma membrane (160).

EVs contain specific cytosolic proteins related to their production in the endosomal compartment (161). Further, they have miRNA and mRNA, which fuse with the host cell membrane and elicit viral-independent genetic transfer (162–164). The membrane of EVs consists of a bi-phospholipid layer. The lipid membrane contains several immunologic active transmembrane proteins depending on the secreted cell type. Immature DC-derived exosomes express MFG-E8 and PS (153,154). The bi-lipid layer of T-cells, B-cells, DCs and derived EVs have a separate array of active immunologic proteins from the tetraspanin family, including CD9, CD63, CD81 and CD82 (161,165). Peptide MHCII and MHCI complex presentation make EVs effective ag-presenting particles modulating the cellular and adaptive immune response (153,154,165,166).

1.4.2 Exosomes delivering antigen to FDCs

Peripherally injected exosomes rapidly migrate to secondary lymphoid organs. They transfer onto MZ-lining DCs and metalophilic MPs (167,168) (Kranich et al. unpublished results) and MZ B-cells 2-3 h after injection (169,170) (Kranich et al. unpublished results). The capturing mechanism of exosomes by ag-presenting cells is essential for an immune response induced by exosomes. Exosomes themselves hardly create T-cell activation in vivo. Without functional MHCI and MHCII, exosomes fail to generate solid CD4+ and CD8+ T-cell priming in vivo (167,171,172).

All splenic DC subtypes internalise exosomes and process them in the endosomal compartment. Immature to a lesser degree than mature DCs (167,168). The inhibition of endosomal processing in DCs leads to a failure of T-cell activation in vitro (168,171). Though in vitro experiments display successful T-cell activation without internalisation but by fixed externalisation of exosomes (167,173).

MZ B-cells show significant amounts of captured exosomes (1,3,4), which is more associated with binding than internalisation (167,169). So far, well-known is the complemented mediated delivery of ag via MZ B-cells to FDCs has been discussed before. $Cd19^{-/-}$ mice produce fewer MZ B-cells, leading to decreased transport of ICs to FDCs (123). OVA-pulsed exosomes injected into $Cd19^{-/-}$ mice exhibit reduced Ab production compared to WT mice (170). This could be due to a disturbed microenvironment in the MZ leading to decreased accumulation of DCs (174), translating into a reduced exosome transport. In confocal microscopes, peripherally injected DCs home to secondary lymphoid organs delivering exosomes to neighbouring DCs in the MZ (167).

Or second, it shows an essential transport mechanism of MZ B-cells for exosomes to FDCs. The finding of C3 on the membrane of exosomes produced by B-cells supports the notion of a complement-mediated delivery mechanism of exosomes to FDCs (175).

Immunoelectron microscopy detects exosomes carrying peptide MHCII complexes along the dendrites of FDCs (6). Due to the expression of tetraspanin proteins, peptide MHCI and MHCII complexes, these exosomes are of ag-presenting cell origin (166). Low phagocytic and endocytic capabilities of FDCs and the expression of CD55 and CD59 on antigen-presenting cell-derived exosomes inhibit phagocytosis. Thus, exosomes can stay on the surface over a more extended period, resistant to

complement-mediated opsonisation and lysis (176). This leads to the effective presentation of their peptide MHCII complexes to TCRs inducing T-cell activation (175,176).

Co-cultured biotinylated B-cell-derived exosomes with human tonsil tissue are more effective in binding to FDCs than any other cell type in the tonsil tissue (166). Because B-cells are the primary transporter of ag to FDC, it supports the idea of exosome transport in the GC similar to ICs. Finally, ELISA, WB and FACS experiments display that exosomes carry native ag anchored in or on their cell membrane for BCR activation to induce a GC reaction (170,177). It is evident in different studies that ag-pulsed exosomes produce a specific humoral immune response with protective immunity against invading pathogens (178,179). Similarly, apoptotic vesicles derived from tuberculosis-infected MPs induce protective immunity against tuberculosis. Statistical significant lower PFU is detected in the vesicle immunised mice compared to the controls (171).

1.4.3 Capturing mechanism of Exosomes

So far, the most accepted is the CR1/2 mediated capturing and transfer of ag-immune complexes on FDCs, which has been discussed before (122,127,128). The prior mentioned detection of C3 on the membrane of B-cell-derived exosomes influenced T-cell activation in vitro. Therefore, it supports the idea of a complement-mediated capture via CR1 and CR2 by B-cells. Different receptors might be used by other immune cells to capture exosomes. In the previous chapter, MFG-E8 is suggested as an opsonin for ag capture, increasing ag loading to FDCs (123,126). MFG-E8 could similarly enhance exosome capture and delivery to FDCs.

The opsonin is highly expressed by immature and less by mature DC-produced exosomes (153,154). Morelli et al. demonstrate in a competitive RGD binding domain essay decreased exosome endocytosis by DCs. Therefore, MFG-E8 is an opsonin for exosomes towards immature exosomes due to their higher endocytic capabilities than mature DCs (168).

Exosomes from mature DCs expressing little MFG-E8 are more T-cell stimulatory due to their overexpression of MHCII complexes and costimulatory molecules (154,180).

Moreover, *Mfge8^{-/-}* exosomes do not alter the activation of CD4+ T-cells compared to WT exosomes (153,154).

Especially the intercellular adhesion molecule 1 (ICAM-1) is highly expressed on exosomes from mature DCs, influencing T-cell activation positively (154,173). ICAM-1 plays a significant role in T-cell differentiation through its receptor lymphocyte-associated antigen-1 (LFA-1) (181). The ICAM-1/LFA-1 interaction drives T-cells into an inflammatory phenotype due to the induction of unresponsiveness to tissue growth factor-beta (181,182). Exosomes demonstrate a similar pattern. The activation of many costimulatory molecules, primarily ICAM-1, in mature DC-derived exosomes gives rise to a T-effector inflammatory phenotype (167,172). While immature DC-derived exosomes generate an immunosuppressive T-regulatory cell phenotype, enhancing allograft survival in vivo (180,183,184).

ICAM-1-expressing exosomes are captured via its natural ligand LFA-1 by T-cells in vitro (185) and DCs in vivo (173). LFA-1 Abs suppress in a dose-dependent manner capturing of DC-derived exosomes by T-cells (185). *Lfa^{-/-}* mice demonstrate lower T-cell activation mice due to diminished capture of exosomes. However, no complete inhibition of T-cell activation was observed (173). *Icam^{-/-}* exosomes injected into WT mice reduce but do not abolish T-cell activation (154).

These results indicate that the ICAM-1/LFA-1 relationship plays a significant role in binding exosomes by mature DCs and subsequent T-cell activation.

Moreover, exosomes from mature and immature DCs differ in function and, therefore, are captured by different receptor types.

The *Lfa^{-/-}* and *Icam^{-/-}* knockout experiments demonstrate that more than one receptor-ligand interaction is responsible for exosome capturing due to partial inhibition.

1.4.4 The function of Phosphatidylserine

Exosomes consist of a lipid bilayer containing PS (186,187). Usually, the enzyme flippase keeps PS in the cytosolic side of the cell and is exposed during apoptosis via the calcium-dependent scramblase (147,188,189). Exosomes originating from the endosomal pathway express PS outside their cell membrane independently of apoptosis (168,169,187,190). This natural ligand to MFG-E8 acts through its C1C2 domain as an "eat me signal" for apoptotic cells (138,141,142). Therefore, MFG-E8

can bind to exosomes expressing PS. In DCs, MFG-E8 increases endocytosis of exosomes in vitro (168) but does not influence T-cell activation in vivo (153,154). Through the C1C2 domain, the fusion protein MFG-E8-eGFP fluorescently labels PS+ exosomes attached to lymphocytes in vivo (169).

Kranich et al. detect that the fusion protein MFG-E8-eGFP, which lacks the RGD motif, bind with similar frequency to exosome-decorated lymphocytes like the full-length MFG-E8 in vivo (169). This finding indicates that MFG-E8 binds to exosomes, not via the RGD $\alpha_V\beta_3/\alpha_V\beta_5$ relationship, but binds to PS with its C1C2-binding domain. Also, MFG-E8 does not induce the association between immune cells and exosomes (169). The exposure of PS on living MZ B-cells seems to be apoptosis-independent. However, it is not shown if the exposure of PS is due to captured PS$^+$ exosomes or due to the cell-intrinsic display of PS (191). Therefore, it remains possible that the transfer of vesicles carrying ag during the GC reaction by MZ B-cells is responsible for this finding.

1.5 Aims

Previous work from the group suggested that chimeric fusion proteins with MFG-E8 induced much more potent and rapid immune responses than the proteins in question alone. Such results were obtained, for example, with GFP and with MFG-E8-eGFP.

In the present work, we aimed to investigate whether this principle also held for viral proteins, possibly leading to enhanced production of nAbs. To this end, we produced different MFG-E8 fusion proteins from viral components of LCMV.

2 MATERIAL AND METHODS

2.1 Methods

2.1.1 Agarose-Gel electrophoresis

We applied Agarose-Gel electrophoresis to establish the size of DNA fragments after cloning steps including Gibson Assembly, Ligation and restriction hydrolysis.

Depending on the length of the researched DNA fragment, a concentration of 0.5-4% agarose was used. 50 ml or 120 ml TAE was applied depending on the number of samples. 5 µl of 0.1% Ethidium bromide solution was added to make DNA bands visible under UV light. The gels were run for 45 min with a constant 120V.

To estimate the DNA´s length, a 100 bp and 1 kb DNA ladder was used depending on the predicted size of the tested DNA. Gel Doc XR+ with Image Lab 5.2.1 (BIO rad, Munich, Germany) visualised bands under ultraviolet light and photographed the gel.

2.1.2 Transformation of chemically competent E. coli.

After successful cloning, we transformed E. coli bacteria with the plasmid construct for more significant production of DNA via Miniprep.

For every transformation, 5 µl of ligation mix (see section 4.2.3 ligation mix) was added to 100 µl of chemically competent E. coli (SurePack Gold, Stragene).

Chemically competent E. coli were incubated with the ligation mix for 30 minutes on ice. They were heat-shocked for 30 seconds at 42°C. They were placed on ice for 1 min before adding 800 µl of lysogeny broth (LB) (Roth, Karlsruhe, Germany) medium without antibiotics.

The bacteria were placed into a shaker (Thermomixer compact, Eppendorf, Germany) at 37°C for 1 h, at 950 rounds per minute (RPM). 50 µl of the transformation mix was centrifuged at 5000 RPM. The pellet was resuspended in a 50 µl LB medium and plated onto plates containing the appropriate antibiotics (ampicillin or kanamycin) with a Pasteur pipette. The next day, colonies were picked and grown in a 5 ml LB medium with the appropriate antibiotics. Screening of the selected clones was done with colony PCR restriction digest analysis.

2.1.3 Bacterial culture

Positive colonies from the LB medium plate were used to inoculate the LB medium either with ampicillin or kanamycin, depending on the antibiotic resistance of the plasmid DNA.

The probes were taken with a Pasteur pipette and transferred into bacterial culture tubes containing 5 ml LB medium. For every positive bacteria colony, at least 3 cultures with a volume of 5 ml were prepared. The number of cultures depended on the amount of DNA required. They were placed into a bacteria shaker overnight.

2.1.4 Colony PCR

E. coli colonies from LB plates were taken and placed into a single PCR tube. Onto every sample, 15 µl of the master mix was added.

15 µl of the master mix were prepared like follows:

10.5 µl dH20

Three µl MyTaq ® Red DNA polymerase buffer (Bioline, London, United Kingdom)

0,6 µl (10 µM) Primer 1

0.6 µl (10 µM) Primer 2

0.3 µl of MyTaq® Red DNA polymerase (Bioline)

The PCR was running in a T3 thermocycler (Biometra, Göttingen, Germany) with the following program:

Step 1: 95°C 5 min.

Step 2: 95°C 15 sec.

Step 3: 54°C 15 sec.

Step 4: 72°C 10 sec.

Step 5: 4°C.

Steps 2-3 were repeated 27 times. The result was controlled on an agarose gel and stored at 4°C. Primer used for colonies PCR is listed in the appendix.

2.1.5 One-Step ISO Assembly of Overlapping dsDNA

After multiple cloning steps, we produced DNA templates containing *Mfge8 260L Gp1 r262a* and *Mfge8 176N Gp1 r262a (Fig.5)*.

We used the Gibson Assembly method to introduce cloned DNA fragments into plasmid Vectors. The instructions from Gibson et al.´s paper Enzymatic Assembly of Overlapping DNA Fragments, chapter five, were followed (192).

The Gibson assembly (GA) 5 Iso reaction buffer contained Phusion DNA Polymerase (Thermo-Fisher, USA), Taq ligase (Thermo-Fisher, USA), and T5 Exonuclease (Thermo-Fisher, USA) (193).

The exonuclease chews back overlapping ends of annealing DNA fragments to crease sticky ends. The polymerase filled the gaps created by the exonuclease, and the Taq ligase replaced the nicks (193).

The GA ligation mix contained 0.02 pmol of vector substrate and 0.2 pmol of DNA fragment. Both components were used in equimolar amounts.

5x GA reaction buffer was added in a ratio of 1:4. The GA ligation mix was incubated at 50°C for one hour. The reaction mix was analysed by agarose gel electrophoresis for the correct product size.

2.1.6 Isolation of DNA from agarose gel

After running an agarose gel in the electrophoresis device, the desired DNA fragments on the gel were visualised under UV light, Gel Doc XR+ (BIO rad laboratories, Munich) and cut out with a scalpel. DNA fragments were purified with GeneJet Gel Extraction Kit (Thermo-Fisher, USA) following the manufacturer's instructions. The DNA was eluted with an elution buffer (see section 2.2.3, chemicals and buffers). The DNA concentration was measured with a SimpliNano™ spectrophotometer (Biochrome Ltd., Cambridge, United Kingdom) and stored at -20 °C.

2.1.7 Protein harvesting from cell supernatant

Transfected human embryogenic kidney cells (HEK) (Sigmar-Aldrich) were cultured in a serum-free medium for protein production. The amount of serum used depended on

the desired protein production depending on the cell count and cell viability. The exact steps from HEK-cell culture to protein production were described in sections 2.1.21-2.1.23. Here we described a method to produce protein, less purified for testing reasons of correct protein expression before using complex purification steps described in section 2.1.23.

Serum-free supernatant from transfected HEK cells was centrifuged at 4100 rpm, at 4°C to remove cells and debris. The SN was taken and centrifuged at 30000 rpm, four °C for 90 minutes. For the concentration of the supernatant (SN), Vivaspin, 20 centrifugal concentrators (Sartorius, Göttingen, Germany) were used. The membranes of the spinning tubes were first washed with dH20 and then with serum-free medium. The SN was spun at 4100 rpm for 20 minutes to 1 ml. The concentrate was frozen in 100 µl aliquots in liquid nitrogen and stored at -80°C. We determined the protein concentration with the ELISA technique.

2.1.8 ELISA

A 96-well plate was coated with ab diluted in coating buffer (see section 2.2.3 chemicals and buffers) overnight at 4°C.

The plate was washed in ELISA washing buffer (see section 2.2.3, chemicals and buffers).

After 2 h of blocking with 0.1% tween 20 blocking buffer (see section 2.2.3), it was shaken off, and 100 µl of blocking buffer was placed in every well except in the first wells.

Each sample was applied in duplicates with 200 µl of sample in the first wells and diluted in serial dilution steps of 1:2 from row B till H obtaining 100 µl of equal sample size per well. Each ELISA plate contained the desired sample, a standard 50 ng/ml of purified MFG-E8-eGFP and a blank containing 1x PBS (see section 2.2.3). Serial dilution steps of the blank and standard from row B till H was performed in the same manner as the researched sample.

The plate was incubated for 2 h, at room temperature (RT). Afterwards, it was washed 6 times in ELISA washing buffer (see section 2.2.3 chemicals and buffers).

The primary Ab was added and incubated for 2 h at RT.

For an anti-MFG-E8 ELISA to determine protein concentration in HEK SN or purified protein of cloned constructs, we used antiMFG-E8 IgG unlabeled (Origene, Herford, Germany, BAF2805) in 1:1000 dilution as primary Ab.

The plate was washed 6 times and incubated with a secondary Ab HRP labelled IgG (Jackson Immuno Research, TA809279) in 1:10000 dilution for 1 h.

It was washed four times in ELISA washing buffer and 2 times in 1x PBS (see section 2.2.3, chemicals and buffers).

Stabilized chromogen (SeraCare, Massachusetts, USA) was applied with 100 µl per well and incubated. After good colouring of the standard 100 µl stop solution (see section 2.2.3, chemicals and buffers) was applied to each well.

The absorbance was read at A450 nm with Versa max absorption-ELISA-microplate-reader (Molecular Devices, LLC., San Jose, California, USA). The measured light absorbance represented the means of the protein values and was rendered by a standard curve produced by SoftMax Pro 7.0.3 (Molecular Devices, LLC.). 4-Parameter logics determined protein concentration in SN or purified protein of transfected HEK cells expressing cloned constructs.

2.1.9 SDS-page and Western Blot

The tested protein or SN was denatured in sodium dodecyl sulfate (SDS) at 95°C in the ThermoStat plus (Eppendorf, Germany) for 5 min. The samples were centrifuged at 13000 rpm for 1 min, with the centrifuge 5415 D (Eppendorf, Germany). The samples were frozen overnight at -20°C.

The next d the samples were thawed at RT and heated for 1 min at 95°C; then centrifuged, vortexed and centrifuged again.

The gel was placed into a Western blot (WB) cassette (Bio-Rad, Munich, Germany), containing running buffer (see section 2.2.3, chemicals and buffers). Equal amounts of samples were loaded into the pockets of the SDS gel. 10 µl of pre-stained protein ladder PageRuler™ (Thermo Fisher, USA) was applied as a control. The WB cassette was connected to the electrophoresis device (Bio-Rad, Germany) and run for approximately 1 h at 80V After the samples passed the stacking gel, the voltage was increased to 120V and run for another 3 h.

The gel was wrapped into the WB sandwich using one Amersham™ Protran™ 0.45 µm nitrocellulose blotting membrane (GE Healthcare, Chicago, Illinois, USA) above the SDS gel and two Whatman cellulose paper (Thermo-Fisher) from each side.

The WB sandwich was placed into a WB cassette containing transfer buffer (see section 2.3.3, chemicals and buffer) at 4°C and ran for 90 min at 90V. to transfer the separated proteins from the SDS gel onto the blotting membrane.

The success of the transfer was determined by the protein ladder being visible on the nitrocellulose membrane. The membrane was placed into a blocking buffer (see section 2.2.3) overnight at 4°C or for 2 h, at RT. The membrane was incubated at RT with the primary ab diluted in blocking buffer for 2 h and 1 h with the secondary Ab. After incubating with Ab, the membrane was washed 4 times in ELISA washing solution (see section 2.2.3) to remove excess Ab. The membrane was rinsed with PBS in the last washing step before applying enhanced chemiluminescence (ECL) WB substrate.

The membrane was placed into enhanced ECL WB substrate (PerkinElmer Inc., MA, USA) and developed onto Amersham Hyperfilm™ ECL (GE Healthcare).

2.1.10 Coomassie blue staining

A 12 % SDS gel was loaded with samples and pre-stained Protein Ladder PageRuler™ (Thermo-Fisher, USA). After running the SDS gel in a WB cassette (Bio-Rad, Munich, Germany), the SDS gel was shaken in 50 ml of fixation solution (see section 2.2.3, chemicals and buffers) for 1 h. The gel was washed in dH2O 4 times for 15 min. Afterwards, the gel was incubated in 50 ml 0.25% R-250 Coomassie® Brilliant Blue (AppliChem GmbH, Darmstadt, Germany) staining solution overnight. The subsequent background staining was removed with distilled H_2O till bands appeared clearly.

2.1.11 Polymerase chain reaction

Polymerase chain reaction (PCR) is a method to exponentially amplify DNA fragments with the help of primers, polymerase enzyme and nucleotides. Primers can induce single point mutations or add longer sequences including DNA fragments

coding for restriction enzyme binding sites. This property was useful for the cloning of complex plasmid DNA.

Heat-resistant polymerase used nucleotides as building bricks to amplify DNA fragments. Template DNA was needed as a base for the annealing of the primers and the action of the polymerase.

The PCR was done in a T3 thermocycler (Biometra, Göttingen, Germany).

The time of the PCR was determined by the time primers needed for annealing and elongation and by the number of base pairs (bp) contained in the desired PCR product. The DNA templates were diluted to a 2 ng/ml concentration with double distilled H_2O. Primers were diluted with double distilled (dd) H_2O to a concentration of 10 µM. The PCR mixes were pipetted as follows to a volume of 100 µl.

75.2 µl dH20

3 µl dNTPs

10 Pfx buffer (Thermo-Fisher, USA)

2 µl MgS04 (NEB, Ipswich, Massachusetts, USA)

3 µl primer 1

3 µl primer 2

3 µl template DNA (2 ng/ml)

0.8 µl Platinum Pfx polymerase (Thermo-Fisher, USA)

2.1.12   Restriction hydrolysis

Restriction hydrolysis (RH) was used to cleave double-stranded DNA with a particular endonuclease, which binds and cleaves specifically to one binding sequence.

Vector and insert DNA were cleaved by specific endonucleases to create complementary sticky ends for ligation.

There were either Age1 or Xba1 (New England Biolabs, Ipswich, MA, USA) restriction enzymes used. The instruction of the manufacturer was followed.

The RH mix contained Cut Smart buffer (New England Biolabs) and was prepared as follows:

Vector RH mix (1x):

15 µl DNA (1µg/µl)

7 µl buffer Cut Smart

1 µl restriction enzyme

47 µl ddH20

Insert RH mix (1x):

50 µl ddH2O

20 µl DNA (1 ug/ul)

8 µl buffer cut smart

2 µl restriction enzyme

The RH mix was placed into the T3 thermocycler (Biometra, Göttingen, Germany) with the following program: Age1 and Xba1 are activated by the same temperatures.

Thermocycler program:

1. Enzyme activation: 37°C for 10 h
2. Enzyme inactivation: 65°C for 65 min
3. Storage: 4°C

The digest was controlled by agarose gel electrophoresis and used for further dephosphorylation and ligation.

2.1.13   Dephosphorylation

After incubation of the restriction hydrolysis (RH) mix, the RH mix was dephosphorylated to prevent relegation of the plasmid
For dephosphorylation, Antarctic Phosphatase and Antarctic Phosphatase buffer (New England Biolabs, USA) were used. The information provided by the manufacturer was followed. The dephosphorylation mix was prepared as described below:

70 µl RH mix

8.2 µl Antarctic Phosphatase buffer

3 µl Antarctic Phosphatase

The dephosphorylation mix was placed into a T3 thermocycler (Biometra, Germany) with the following program:

1. Enzyme activation: 37°C for 3 h
2. Enzyme deactivation: 80 °C for 2 min
3. Storage: 4°C

2.1.14   Isolation of plasmid DNA from bacteria

DNA extracted from bacteria was either generated with Gen Jet Plasmid Miniprep Kit (Thermo-Fisher, Waltham, Massachusetts, USA) or via conventional miniprep. Using the Thermo-Fisher miniprep kit, the manufacturer's instructions were followed precisely. It was used for a small amount of DNA, up to 20 µg. The principle made use of the below in more detail described alkaline lysis to liberate DNA from transfected E. coli. The DNA was obtained via repetitive washing cycles via centrifugation through a silica membrane containing spin columns. The pellet was adsorbed in elution buffer (see section 2.2.3, chemicals and buffers), measured its DNA concentration, and adjusted as described below.

For large-scale production of DNA, Alkaline lysis followed by phenol: chloroform extraction was applied and prepared as follows: The d before the procedure, 6, 5 ml culture tubes LB medium containing were inoculated with transformed E. coli bacteria. The bacterial cultures were incubated shaking overnight at 37°C, 5 % CO_2.

The cultures were centrifuged for 10 min, at 4200 rpm. The SN was discarded, and the pellets were resuspended in 900 µl STE. 2-3 pellets were combined in 900 µl STE and placed in a 2 ml tube. The resuspended cells were centrifuged again as described before. All liquid was removed. 200 µl, Alkaline lysis solution 1 (see section 2.2.3, Chemicals and Buffers) was added to each pellet. The solution was resuspended and vortexed thoroughly.

Then 400 µl of Alkaline 2 solution (see section 2.2.3) was added to each tube and inverted carefully five times. 400 µl of Alkaline 3 solution (see section 2.2.3) was added and inverted five times. The mix was incubated for 3-5 min on ice. Afterwards, the mixture was centrifuged at 4200 rpm for 10 min. and the SN was transferred into a fresh tube. 3 ml RNase A (100 mg/ml) was added and incubated for 7 min at 57°C in a Thermo Stat plus (Eppendorf, Hamburg, Germany). 30 µl of Proteinase K (10 mg/ml) was added and vortexed.

In the next step, the Phenol: Chloroform extraction was performed. After incubation with Proteinase K, 900 µl Phenol: Chloroform: Isoamyl Alcohol 25:24:1, Saturated with 10 mM Tris, pH 8.0, 1 mM EDTA (Sigma-Aldrich, St. Louis, Missouri, USA) was added and mixed well.

The mixture was centrifuged for 10 min at 4200 rpm. Two phases appeared in the tube. The upper phase was transferred into a fresh tube. 450 µl Chloroform was added and mixed carefully. The mix was centrifuged as described before. The upper phase was pipetted into a new tube, and 900 µl ethanol absolute was added. It was incubated for 5 min at RT. The mixture was centrifuged for 15 min at 4200 rpm, the SN was removed carefully without losing the pellet. The pellet was washed with 200 µl of 70% ethanol. Excess fluid was removed, and the pellet dried at RT. After the pellet became see-through from white, it was resuspended in 150 µl of elution buffer. The elution buffer (see section 2.2.3, chemical and buffers) was taken from the Gen Jet Miniprep kit (Thermo-Fisher, USA).

The DNA concentration was determined by the SimpliNano™ spectrophotometer.
 (Biochrome Ltd., Cambridge, United Kingdom) and was adjusted to 1 µg/ml with elution buffer.

2.1.15   DNA Transfection for the establishment of transient cell lines

Before transfection, 2.4×10^6 HEK cells were seeded out in adherent 14 cm diameter dishes with 8 % FCS DMEM (Gibco). An eGFP expression plasmid was used to assess transfection efficacy.

1 h before transfection, the medium was refreshed. The working volume was 21 ml in the 14 cm diameter dishes.

The transfection mix was prepared (2.1x): 105 μl DNA (1 μg/ml) was added to 819 μl dH2O. 126 μl 2.5 M CaCl2 was added and vortexed. 1050 μl of 2x HBS, pH 7.05 was added dropwise while vortexing. We added 5.25 μl of 100mM Chloroquine to a final concentration of 100mM.

The DNA mix was added dropwise and uniformly to the cells. The dish was carefully shaken to mix the DNA with the cell medium. The cell dish was placed into the incubator at 37°C, 5% CO_2. After 16 h, the transfected cells were washed twice with PBS, and the medium was changed to serum-free Excell 293 medium.

The cells were incubated at 37 °C, 5 % CO_2 for 3 d. 1 d after transfection, efficacy was determined by evaluating the eGFP expression of transfected plasmid controls with fluorescent microscopy (Leica DM IRB, Leica Microsystems Wetzlar GmBH, Wetzlar, Germany). After the 3rd d, the protein was harvested from the cell SN and further analysed by WB and ELISA for correct protein size and concentration.

2.1.16   DNA Transfection for the establishment of stable cell lines

The day before transfection for the establishment of stable cell lines, HEK 293T 1.2×10^6 cells were seeded out in adherent 10 cm diameter dishes in 8 % FCS DMEM. The negative control contained no DNA in the transfection mix.

1 h before transfection, the medium was refreshed. The working volume was 10 ml.

The transfection mix was prepared as follows (1x): 50 μl of DNA (1μg/ml) was added to 390 μl of dH2O in a 15 ml falcon. Then 60 μl, 2.5 M, CaCl2 was added and vortexed. 500 μl of 2x HBS, pH 7.05, was added dropwise while vortexing. 2.5 μl of chloroquine (100 mM) was added to a final concentration of 25 mM.

The DNA mix was added dropwise and uniformly to the cells. The dish was carefully shaken to mix DNA and medium. The cell dish was placed into the incubator at 37°C, 5% CO_2.

16 h after transfection. cells were washed twice with PBS, and the DMEM medium changed.

The next d hygromycin (100 μg/ml) was added to the transfected HEK-cells to select stable expressers.

The selection process with antibiotics was continued over two weeks until the cells showed a regular growth pattern. The cells were evaluated for their viability and growth by light microscopy. Subsequently, the cells were adapted on a serum-free medium, which was necessary for the large-scale protein production in the cell fermenter

Gen	Primer	Annealing temperature
mMfge8_GS_fw	CTCTGGGGAGAGACCACACCCAAGCTGTCTAGAGAATTCTTTTCCCGCGTCCGC	77°C
GP1_176N_R262A_rv	CGTCATCGTCCTTGTAGTCGGAGCCACCGCCGCCTGCAAGTCTGGCAGTGAAGAATTTGG	79°C
GP1_260L_R262A_rv	CGTCATCGTCCTTGTAGTCGGAGCCACCGCCGCCTGCAAGTCTGGCAGTCAAGAATTTGG	79°C
GP1_rv2	AAGCTTCCCTATACATGGTGGCGGCTCTAGATTATTTGTCGTCATCGTCCTTGTAGTCGG	74°C

Tab. 1 Primer used for cloning and sequencing of MFG-E8-260L-GP1 R262A and -GP1-176N R262A

The table displayed the primer used for cloning of constructs MFG-E8-260L-GP1 R262A and MFG-E8 176 R262A and their respective annealing temperatures for the PCR. The primers were as well used for DNA sequencing for the construct DNA. The same MFG-E8 forward primer was used (mMfge8_GS_fw). The GP1 reverse primer was only used for sequencing purposes (GP1_rv2).

2.1.17 Organ harvesting and single-cell suspension

Mice were killed in a CO_2 chamber. Afterwards, the mice were pinned onto the dissecting board.

The mouse was opened up via the midline section to remove the spleen, lymph nodes and thymus.

The organs were placed into a tube containing FACS buffer on ice for preservation.

A single-cell suspension of the thymic cells was produced by grinding the thymus through a MACS ® SmartStrainer (100 µm) (Miltenyi Biotec, Bergisch Gladbach, Germany) and rinsing the cell strainer with FACS buffer (see section 2.2.3 chemicals and buffers).

The suspension was centrifuged at 1400 rpm for 5 min. Red blood cell lysis was performed when blood was visible in the sample.

For red blood cell lysis, the pellet was resuspended with 5 ml of ACK buffer (see section 2.2.3) for 5 min. Afterwards, 10 ml of FACS buffer was added to neutralise the suspension. The solution was centrifuged, and the SN was discarded. The pellet was resuspended in 3 ml FACS buffer. Cell count and viability were determined using a Casy® counter (Innovatis AG, CASY-Technology, Reutlingen, Germany).

Thymic cells were applied for induction of apoptosis with staurosporine and for measuring the binding ability of the MFG-E8 fusion proteins to apoptotic thymocytes: MFG-E8-260L-GP1, MFG-E8-176N-GP1 and MFG-E8 NP LCMV.

2.1.18 Induction of apoptosis

Thymic cells were produced by single-cell suspension and counted by a Casy® counter (Innovatis AG).

1 ml of the cell suspension was plated into a 12 cm dish with a 9 ml RPMI medium (see section 2.2.3 chemicals and buffers). 20 µl staurosporine (0.1 mg/ml) was added and mixed by careful movement of the dish. The mix was incubated for 2 h at 37 °C, with 5 % CO_2. 1 dish with thymocytes but without staurosporine was used as a control to assess apoptosis induction.

Afterwards, the cells were detached from the dish by pipetting and placed into a 15 ml falcon. The cells were centrifuged and washed three times in sterile 1x PBS and stored at 4°C.

Apoptotic thymocytes were used for the coating efficacy measurement of MFG-E8 and the cloned constructs containing MFG-E8.

2.1.19   Flow cytometry: Fluorescence-activated cell sorting

Flow cytometry is a method to measure and differentiate cell populations and their characteristics by using their light-scattering properties. These properties are either the size, granularity or fluorochrome coupled ab staining of a cell.

Fluorochrome coupled Ab were used to detect specific intra- or extracellular characteristics in a cell population.

Each cell has to bypass several lasers; then, the emitted light is passed through different bandpass filters and detected by other sensors. The signal produced is enhanced and analysed with the Software FlowJo (Becton, Dickinson & Company, USA). Flow cytometry was applied for measuring the coating efficacy of the MFG-E8-containing constructs to apoptotic thymocytes. The cells were either coated by cell SN of stably transfected HEK cells expressing MFG-E8 containing constructs or purified protein. Staining was performed by a biotinylated anti-MFG-E8 Ab and fluorochrome-coupled SA-APC (Caltag, UK). The FACS data was acquired by FACS Canto 2 (Becton, Dickinson & Company, Franklin Lakes, New Jersey, U.S.). Further data analysis was performed with Flow Jo software version 10.4 (Becton Dickinson).

2.1.20   Preparation of FACS staining

To prepare the FACS staining, all steps were performed on ice (4°C) and covered from light sources. The staining volume was 100 µl. Every centrifugation step was done for 5 min at 1500 rpm.

1×10^6 apoptotic thymocytes were pipetted into each desired well of 96 well tissue culture plates. It was centrifuged, and the SN was discarded.

The cells were coated with 100 µl protein SN or purified protein dilution and incubated for 25 min. We used 1:2 diluted HEK SN expressing MFG-E8 NP (0.32 µg/ml), SN of HEK expressing MFG-E8-260L-GP1 in 1:3 dilution and purified MFG-E8-176N-GP1 in 1:3 dilution. 100 ng of recMFG-E8 (100 µg/ml) was used to control coating efficacy. Unstained staurosporine-treated thymocytes were the negative control.

The plate was centrifuged, and the SN was discarded. The pellet was resuspended in 100 µl of 1:300 biotinylated monoclonal anti-MFG-E8 IgG (R&D Systems cat. # BAF2805) dilution and incubated for 25 min. 100 µl of FACS buffer was added, the plate was centrifuged, and the SN was discarded. The cells were centrifuged and resuspended in 200 µl of FACS buffer for another three times to remove the unbound Ab.

The pellet was resuspended in 100 µl of 1:700 fluorochrome coupled, Streptavidin-allophycocyanin (SA-APC) (Caltag, UK) dilution and incubated for 25 min. The washing procedure was repeated as described before.

In the last step, the pellet was resuspended in 200 µl of FACS buffer and pipetted through a polyamide mesh into a 5 ml FACS tube. 200 µl of FACS buffer was added additionally. The FACS tubes were stored on ice and covered from light exposure before acquiring the FACS data.

Controls were produced evenly using staurosporine untreated cells or apoptotic thymocyte staining without SA-APC or biotinylated anti-MFG-E8.

Third, we used MFGE8-eGFP (1:500) without additional antibodies to stain apoptotic thymocytes. Here the steps were followed as described above. Instead of incubating with ab, FACS buffer was used when prepared on the same plate.

2.1.21   Culture of HEK 293T cells

HEK 293 T cells were cultured in Greiner T75 or T175 flask, depending on if the expansion of cells was required.

The cells were grown to confluency in DMEM 8% FCS medium, containing 1 % Penicillin/ Streptomycin (PS) and split twice per week.

The vitality and cell count were observed using a Casy cell counter (Innovatis AG, Germany) and light microscopy.

2.1.22   Adaptation of HEK 293T cells

For the large-scale production of cloned construct protein, stable HEK cell lines expressing MFG-E8 fusion proteins had to be adapted from 8% FCS containing

DMEM medium (see section 2.2.3, chemicals and buffers) to serum-free Excell 293 medium (see section 2.2.3).

The cells were adapted in steps from 25%, 50%, and 75%, to 100% serum-free medium.

To increase the concentration of the serum-free medium, the cells needed to show a healthy morphology and growth pattern. A healthy growth pattern was determined as confluency within 5 d with a splitting ratio of at least 1:4. The cells were then placed into an FCS medium containing a higher percentage of serum-free medium. This procedure was done till 100% serum-free medium was reached. Morphology and growth pattern were estimated by light microscopy.

After the cells were adapted to a 100% serum-free medium, the cells had to be adapted to shaking cultures. Shaking cultures should adapt the cells to rotation motions in the cell fermenter.

Cells had to be seeded in a high ratio into a 250 ml corning Erlenmeyer flask containing 50 ml serum-free Excell 293 medium. The flasks were shaken at 80 rpm in the incubator Galaxy 170 S (New Brunswick, Eppendorf). The vitality and cell count were observed by using a Casy cell counter (Innovatis AG, Germany)

With achieving 80 % vitality count and surviving splitting ratio of 1:8, the cells were ready for large-scale production in the cell fermenter.

2.1.23   Protein purification

The constructs MFG-E8-176N-GP1, MFG-E8-260L-GP1 and MFG-E8 NP LCMV were transfected into HEK cells, selected to stable cell lines by their respective plasmid hygromycin antibiotic resistance and adapted to serum-free medium and shaking cultures. The procedure was recently published by Kranich et al. (169). The steps were similarly followed. The cells were grown in a Labfors Bioreactor (Infors, Switzerland) for 5 d in 3 liters of serum-free Excell 293 medium (Sigma). The cells were continuously monitored for vitality using a Casy cell counter (Innovatis AG, Germany) The SN was harvested and centrifuged (300g, 10 min) to remove cells and debris. 0,5% Triton was added to the SN to solubilise membrane vesicles. Incubation followed for 1 h on a magnetic stirrer.

The SN was then centrifuged once more for 1:30 h at 30.000 g to clear the protein of the left-over cell debris. The protein was filtered using first a 1.2 µm filter, followed by a 0.2 µm filtration on ice. Recombinant MFG-E8 proteins were captured by FLAG affinity chromatography using M2-FLAG agarose beads (Sigma-Aldrich, USA). FLAG-bound protein was eluted using 7,5 mg Flag peptide (Genscript, China) in 25 mM HEPES 2% Glycerol, 200 mM L-Arginine, 200 mM L-Glutamic acid and 150 mM NaCl, pH 7.4. The eluate was concentrated using a spin column (Sartorius, Göttingen, Germany) with the cut of the value of 30 kDa. Gel Filtration was applied to the eluate in an Äkta prime system with a Superdex 200 Increase 10/300 GL column (GE Healthcare, USA) at -6°C in the cold room. The protein concentration was determined using a Spectrophotometer (Biochrome, UK).

The final purified product MFG-E8-176N-GP1 was stored in 25 mM HEPES 2% Glycerol, 200 mM L-Arginine, 200 mM L-Glutamic acid and 150 mM NaCl at pH 7.4 snap-frozen in liquid nitrogen and held at 80°C.

2.1.24   Plaque assay

Before performing the neutralisation assay, a plaque assay had to be applied to determine plaque count and plaque-forming units per ml (PFU/ml) of the used virus batch.

We performed the virus batch production and virus titer determination in-house with the AG Baumjohann from the Institute for Immunology of the Ludwig-Maximilians-University, Munich.

To evaluate the best ab´s neutralising efficacy, we wanted to achieve a plaque count between 30 and 60 per well. For this reason, we prepared 1:10000 and 1:20000 LCMV$_{Arm}$ dilutions. For controls, we applied cells only to exclude viral contamination. Vero cells were trypsinised from T 75 cell culture flask and diluted in 5 % FCS DMEM to 8×10^5 cells per ml. 200 µl of the Vero cell dilution was pipetted in triplets onto the 24 well tissue culture plate. The Vero cells were overlaid with 200 µl of the virus dilutions or medium only for controls. Incubation was done for 3 h at 37 %, 5 % CO_2. A mix of 2x DMEM (Gibco), 2x Penicillin/Streptomycin, and 10 % FCS was prepared in a ratio of 1:1 with 2 % methylcellulose (Viscosity 400 cP) (Sigmar Aldrich, Cat.

#M0430). 400 µl of the mix were used to overlay each well carefully. The plate was incubated for 60-72 h, after which the staining was performed.

The SN was aspirated carefully without touching the cell layer. 400 µl of 4% paraformaldehyde (PFA) was pipetted dropwise against the side of the well to fixate the cells. It was incubated for exactly 30 min. 400 µl of 1:100 Triton-x (Sigmar-Aldrich, USA) solution was added to permeabilise the cell membranes. It was incubated for 20 min. The Triton solution was aspirated and washed with 400 ul PBS. 200 µl of 5 % FCS PBS was added and set for 30 min.

Afterwards, it was aspirated, and 200 µl of unlabelled anti-LCMV NP VL-4 Rat IgG2$_{a,}$ $_{k}$ (Bio Cell, Cat. #AB_10949017) 1:100 Ab dilution was added. It was incubated for 1 h at RT. It was washed twice with 400 µl PBS.

200 µl in 1:100 dilution of secondary Ab, polyclonal HRP labelled goat anti-rat IgG (Jackson Immuno Research, Cat. #112-035-003) was applied to each well. It was incubated for 1 h. The SN was aspirated and washed twice with 400 µl 1x PBS. O-Phenylenediamine (OPD) substrate solution was prepared by dissolving one tablet of OPD (Thermo-Fisher, USA) in 12.5 ml 0.1 M citric acid, 12.5 ml 0.2 M NA$_2$HPO$_4$, 25 ml dH$_2$O and 50 µl H$_2$O$_2$ (Sigmar-Aldrich, USA).

400 µl of the substrate was added to each well and incubated for 15 min until visible colouring of the plaques appeared. The number of plaques was counted, and the PFU/ml was calculated. After establishing the plaque assay, we set up the neutralisation assay using the GP1 nAb KL-25.

2.1.25   Neutralization assay using anti-GP1 LCMV antibody

To set up a neutralisation assay using the serum of immunised mice, we first needed a sophisticated control. Therefore, we used the KL-25 Ab, a well-known anti-GP1 LCMV nAb. It was received from the Pinschewer AG of the University of Basel. To test its efficacy for optimal titration, we incubated it with LCMV$_{Arm.}$

KL-25, anti-GP1 LCMV nAbs were incubated for 30 min on ice in dilutions of 1:100, 1:300 and 1:10000 with 1:10000 and 1:20000 LCMV$_{Arm}$ virus dilution. The virus was diluted in 5 % FCS DMEM (Gibco). 400 µl of the mix was used to overlay each well carefully. The plate was incubated for 60-72 h, after which the staining was performed as described in the plaque assay. The number of plaques was counted under light

microscopy, and the PFU/ml was calculated. We continued immunising C57BL/6 mice with MFG-E8 176N and MFG-E8-eGFP purified protein.

2.1.26   Mice used for experiments

C57BL/6 mice were obtained from Jackson Immuno Research (Cambridge, UK) and bred at the Core animal facility of the Biomedical Center Munich under SPF conditions.

2.1.27   Immunization of mice

Three C57BL/6 mice were injected intraperitoneally with 30 µl (50 µg) MFG-E8-eGFP mixed with 100 µl sterile alum and 70 µl arginine glutamine buffer. 4 C57BL/6 mice were injected intraperitoneally with 33.1 µl (50 µg) MFG-E8-176N-GP1 protein mixed with 100 µl sterile alum and 66.9 µl arginine glutamine buffer. The injections were repeated after two weeks. 7 d after the second injection, blood from the mice was taken by cutting into the tail vein. We proceeded with the production of serum.

2.1.28   Serum production

The blood received from the mouse tail vein was collected in BD Vacutainers (Beckton Dickinson, Franklin Lakes, New Jersey, USA). The guidelines of the manufacturer were followed. The blood was incubated in the tubes for 30 min at RT and centrifuged for 10 min at 2000 g. Aliquots of the serum were snap-frozen in liquid nitrogen and frozen at -80°C.

The serum was evaluated for the presence of nAbs against $LCMV_{Arm}$ by a neutralisation assay.

2.1.29   Neutralization assay using serum of immunised mice

Different amounts of serum from each injected mouse with MFG-E8-176N-GP1 protein were obtained. The serum was divided by two, and each sample was incubated as a doublet with 1:10000 LCMV$_{Arm}$ dilution. Different amounts of serum were incubated with the virus. The volume was equalised using a 5% FCS DMEM (Gibco) medium. It was overlaid on Vero cells and incubated for three days at 37°C. Staining was done for anti-NP of the LCMV$_{Arm}$ (see section 2.1.24, plaque assay). Plaques were counted, and the PFU/ml was calculated.

Serum from MFG-E8-eGFP immunised mice was used as negative controls due to no expectations of development nAbs against LCMV$_{Arm}$. The obtained Serum was again divided by 2, laid over Vero cells of the same plate and incubated for 3 d at 37 °C. Different amounts of serum were incubated. Staining was done, plaques counted and PFU/ml calculated. KL-25 GP1 LCMV$_{Arm}$ 1:100 diluted ab was used as the positive control (see section 2.1.25, Neutralization assay using anti-GP1 LCMV antibody). 400 µl of the antibody dilution was laid over Vero cells and incubated for 3 d at 37 °C. Staining was performed in the same manner. Plaques were counted and PFU/ml was calculated.

2.1.30   Statistics

The statistics were calculated using GraphPad Prism software version 8.3.0 for Windows (GraphPad Software, San Diego, California USA). P-values were analysed by applying the T-test and Welch test. Statistical significance was defined as P<0,05.

2.2 Materials

2.2.1 Consumable supplies

Consumables	Company
Disposable cell strainer (100 µm nylon)	Falcon a Corning Brand, One Riverfront Plaza, Corning, USA
Disposable glass Pasteur pipettes	VWR International bvba, Leuven, Belgium
Serological pipette, sterile (10 ml)	Greiner, Frickenhausen, Deutschland TipOne filter
TipOne filter tips (10 µl, 200 µl, 1000 µl)	STARLAB GmbH, Hamburg, Germany
Laboratory gloves Latex Gentle Skin Grip	
PCR strips tubes (0.2 mL)	VWR International, West, Belgium
Reaction container 1.5 ml, 2 ml	Eppendorf, Hamburg, Germany
Reaction container 5 ml (FACS)	BD, Franklin Lakes, NJ, USA
Petri dish	Greiner Bio-One GmbH, Germany
Tissue culture plates (96 wells-U and 24 well sterile)	VWR International bvba, Leuven, Belgium
Tissue culture flasks (T25, T75 and T175)	Nunc
Erlenmayer flasks (250 ml, 500 ml, 1000 ml)	
Disposable injection needle (26 G x ½"), (23 G X ½"), (21 G x ½")	Terumo Medical Corporation, Tokyo, Japan
Photographic film	Amersham Hyperfilm^{TM} ECL, GE Healthcare, Chicago, Illinois, USA
Disposable syringe (1+5+20 ml) Reaction	Braun, Melsungen, Germany
0.45 µm nitrocellulose blotting membrane	Amersham^{TM} Protran^{TM} GE healthcare, Chicago, Illinois, USA

Cell strainer	MACS ® Smart Strainer (100 µm) , Miltenyi Biotec, Bergisch Gladbach, Germany

2.2.2 Devices

Devices	Company
Spectrophotometer,	SimpliNano™, Biochrome Ltd., Cambridge, United Kingdom
PCR machine	T3 Thermocycler (Biometra, Goettingen, Germany)
Temperature adjuster	ThermoStat plus (Eppendorf, Hamburg, Germnay
Agarose gel reader	Gel Doc XR+ with the software Image Lab 5.2.1 (BIO rad laboratories, Munich, Germany)
ELISA Microplate reader	Versa max absorption-ELISA-microplate- reader (Molecular Devices, LLC., San Jose, California, USA)
Pipettes	Gilson, Middleton, WI, USA
Water bath	Grant Instruments Ltd., Barrington Cambridge, UK
Vortex-Genie2	Scientific Industries, Bohemia, NY, USA
Magnetic stirrer	Ika Labortechnik, Staufen, Germany
Bench centrifuge	Centrifuge 5415 D, Eppendorf, Germany
Centrifuge	Rotixa RP, Hettich, Tuttlingen, Germany
Incubator	
Laminar airflow cabinet	Heraeus, Hanau, Germany
Cell counter	CASY cell counter and analyser, OMNI life science, Bremen, Germany

Gel electrophoresis	BIO-RAD, Hercules, CA, USA
Flow cytometer	FACS Canto II, BD, Heidelberg, Germany

2.2.3 Chemicals and buffers

All chemicals were obtained from Merck (Darmstadt, Germany), Roth (Karlsruhe, Germany) or Thermo-Fisher unless stated differently. All buffers and solutions are prepared with double distilled water (ddH20).

Buffers and solution	Components
Alkaline lysis solution 1 (ALS1)	50 mM Glucose 25 nM Tris-Cl pH 8.0 10mM EDTA pH 8.0
Alkaline lysis solution 2 (ALS2):	0.2 N NaOH 1% SDS
Alkaline lysis solution 3 (ALS3):	60ml 5M Potassiumaccetate 11.5 ml glacial acetic acid 28.5 ml H20
ACK lysis buffer	8.29 g NH4Cl 1 g KHCO3 37.2 mg Na2EDTA H2O add 1 lt pH 7.2-7.4 adjusted with HCl sterilised by 0.2 µm filtration
STE	10mM Tris-Cl pH 8.0 0.1 M NaCl 1mM EDTA pH 8.0
Coomassie blue staining solution	0.25 % R-250 Coomassie® Brilliant Blue (AppliChem, Darmstadt, Germany) 20 % methanol 10 % acetic acid

	70% H$_2$O
Fixation solution for Coomassie blue staining	10% acetic acid 30 % methanol 60% H20
2x HBS	280 mM NaCl 50 mM HEPES 1,5 mM Na2HPO4-Dihydrate pH 7.05 adjustment with NaOH, sterile filtration with 0.2 µm filters. Storage at -20 °C (max. six months)
50x TAE Buffer	50x TAE Buffer 242 g Tris 57,1 ml 100% Acetic acid v/v) 100 ml 0,5 M EDTA (pH 8,0) H2O ad 1 l
PBS	150 mM NaCl 10 mM Na2HPO4 2 mM KH2PO4 pH 7,4, adjustment with 5 N NaOH
FACS buffer	1x PBS 2% FCS
PBS for cell culture	Dulbecco's PBS without Ca2+ /Mg2+ (PAA)
Elution buffer	10 mM Tris-HCl, pH 8.5
5x SDS sample buffer	50 % Glycerin 250 mM Tris, pH 6,8 adjusted with HCl 500 mM DTT 10 % SDS 0,5 % Bromophenol blue
SDS running buffer	192 mM Glycin 25 mM Tris 0.1 % SDS
Separating gel 12%	H2O (6.6 ml)

	30 % acrylamide mix (8 ml)
	1.5 M Tris/HCL, pH 8.8 (5 ml)
	10 % SDS (200 µl)
	10 % ammonia persulphate (200 µl)
	TEMED (20 µl)
Stacking Gel 5%	H2O (2.1 ml)
	30 % acrylamide mix (500 µl))
	1 M Tris/HCL, pH 6.8 (380 µl)
	10 % SDS (30 µl)
	10 % ammonia persulphate (30 µl)
	TEMED (3 µl)
RIPA Lysis buffer	1 M NaCl
	1% Nonident P-40
	0.5% Sodium deoxycholate
	0.1% SDS
	50 mM Tris, pH 7.4
Transfer buffer	192 mM Glycine
	25 mM Tris
	20 % Methanol
	0.002 % SDS
ELISA Washing buffer	1x PBS, 0.1% Tween-20
5x ISO reaction buffer	25 % PEG-8000
	500 mM Tris HCL pH 7.5
	50 nM $MgCl_2$
	50 mM DTT
	1 mM of each dNTPs
	5 mM NAD
CaCl2	2.5 M CaCl2
	Sterile filtration with 0.2 µm filters
	Storage at -20 °C
Coating buffer	0.1 M sodium carbonate buffer pH 9.6
	1.58 g Na2CO3
	2.94 g BaHCO3

	In 500 ml ddH20
Methylcellulose	10g (viscosity 400 cP, Sigmar-Aldrich Cat. #M0430) in 500 ml dH_2O
Arginine glutamine buffer	3.5 mM L-Leucine 18 mM L-Arginine 5.7 mM L-Glutamic acid 350 mM NaCl 0.5 % Triton X
Elution buffer	
Sample/ blocking buffer	1x Casein Blocking Buffer with 0.1% tween® 20
FCS containing cell culture medium for HEK 293T cells	Dulbecco's modified Eagle medium (DMEM) GlutaMAX™ (Gibco) 5-8% fetal calve serum (inactivated) 1% Penicillin Streptomycin (PS)
Serum-free medium for HEK 293T cells	Excell 293 20 nM HEPES 1% L-glutamic acid 1% PS.
Cell culture medium for thymocytes	RPMI medium 1640 (1x) + GlutaMAX™-I (Gibco) 1% PS
Cell culture medium for Vero cells	1. DMEM GlutaMAX™ (Gibco), 5 % FCS (inactivated), 2 % PS 2. 2x DMEM with L-Glutamine without Na Pyruvate and NaHCO, 9000 MG/L Glucose
Stabilized chromogen	KPL TMB Microwell Peroxidase Substrate System (Cat. # 5120-0053): 1. 100 mL KPL TMB Peroxidase Substrate

	2. 100 mL KPL Peroxidase Substrate Solution B
STOP solution for ELISA	0.5M H_2SO_4

2.2.4 Antibodies for WB

Epitope	Clones	Conjug.	Isotype	Dilution	Origin	Cat. number
Anti-MFG-E8	18A2–G10	Unlabeled	Hamster IgG	1:1000	Origene, Herford, Germany	TA809279
IgG (H + L)	Polyclonal	HRP	Rabbit Anti-Armenian hamster IgG	1:3000	Abcam, Cambridge, UK	ab5745
Anti-FLAG	Monoclonal, M2 clone	HRP	Mouse IgG_1	1:1000	Sigma-Aldrich, St. Louis, Missouri, US	A8592
Anti-FLAG	Monoclonal, M2 clone	unlabeled	Mouse IgG_1	1:4000	Sigma-Aldrich	F3165
IgG (H)	Polyclonal	HRP	Goat IgG	1:5000	Southern Biotech	1020-05
Anti-LCMV NP	VL-4	Unlabeled	Rat $IgG_{2a, \kappa}$	1:1000	Bio Cell	AB_10949017
IgG (H + L)	Polyclonal	HRP	Goat Anti-Rat, IgG	1:10000	Jackson Immuno Research	TA809279

2.2.5 Antibodies for ELISA

Epitope	Clones	Conjug.	Isotype	Dilution	Origin	Cat. number
Anti-MFG-E8	Polyclonal Goat IgG	Biotin	Goat IgG	1:300	R&D Systems	BAF2805
Streptavidin		A-APC		1:700	Caltag, Buckingham, UK	

2.2.6 Antibodies for FACS

Epitope	Clones	Conjug.	Isotype	Dilution	Origin	Cat. number
Anti-MFG-E8	18A2 - G10	unlabeled	Hamster IgG	Origene, Herford, Germany	1:1000	BAF2805
IgG (H + L)	Polyclonal	HRP	Goat Anti-Rat, IgG	Jackson Immuno Research	1:10000	TA809279

2.2.7 Antibodies for neutralisation assay

Epitope	Clones	Conjug.	Isotype	Dilution	Origin	Cat. number
Anti-LCMV NP	VL-4	Unlabeled	Rat $IgG_{2a, \kappa}$	1:100	Bio Cell	AB_10949017
IgG (H + L)	Polyclonal	HRP	Goat Anti-Rat, IgG	1:100	Jackson Immuno Research	112-035-003

3 RESULTS

3.1 Generation of recombinant MFG-E8 NP protein.

NP of the LCMV produces a more rapid humoral immune response than GP1 (26). Based on that principle, we generated MFG-E8-NP (Fig.1) as the control for our immunisation and neutralisation experiments. The fusion protein contains a FLAG-tag necessary for purification with FLAG high-affinity chromatography (194). We applied the long spliced version of MFG-E8, having the C1C2 domain and a proline-threonine-rich region (138,141,142).

We fused the NP to the C terminus of MFG-E8 via an oligo linker sequence. At its C terminus, the construct contained a FLAG-tag (Fig.2A). The cloned DNA was inserted into the commercial vector pcDNA3.1(+) (Thermo-Fisher, USA), which included a cytomegalovirus promoter for high protein expression in mammalian cells. The vector expresses 2 antibiotic resistances, one against ampicillin for selection of transformed E. coli and one against hygromycin for creating stably expressing mammalian cell lines.

Moreover, the vector includes multiple cloning sites in forward and reverse direction available for insertion of cloned DNA via RH and ligation. We utilised pcDNA3.1(+) MFG-E8-eGFP as the base for our final construct pcDNA3.1 MFG-E8-NP-FLAG. The base vector construct was digested by its respective enzymes producing pcDNA3.1 MFG-E8. Digested *Lcmv Np* was then ligated into the vector resulting in pcDNA3.1 MFG-E8-NP. Annealed FLAG-tag oligonucleotides were ligated into pcDNA3.1 MFG-E8-NP giving rise to the final vector construct pcDNA3.1 MFG-E8-NP-FLAG.

The newly created plasmid was successfully sequenced to confirm the *Np* and *Mfge8* (See tab. 2, primers used for sequencing of MFG-E8-NP). We continued to transform the construct DNA into competent E. coli. Positive clones were selected for large-scale DNA production and transfection into HEK cells.

For protein expression we applied HEK293T cells derived from human embryogenic kidney cells (HEK) (195). Transfection was performed utilizing the $CaP0_4$ method. Next, we tested cell SN of the transfected HEK cells for protein expression. To check the size of our recombinant protein, we applied WB staining using anti-FLAG Ab (194). We detected bands for MFG-E8-NP at the expected molecular weight at approximately 120 kDa (Fig. 2B), for MFG-E8-eGFP at about 80 kDa. Both bands were consistent

with the calculated protein sizes. Staining for recMFG-E8 was absent because it contained a HIS-tag and not a FLAG-tag.

We concluded that HEK cells transfected with pcDNA3.1 MFG-E8-NP-FLAG correctly expressed the protein. Stable cell lines expressing recombinant MFG-E8-NP were adapted to serum-free medium, larger volumes and shaking grounds to acclimate them to conditions in a cell fermenter for large scale protein production. After reaching good viability in shaking cultures, the cells were snap-frozen and stored in liquid nitrogen.

We measured the concentration of MFG-E8-NP in SN of stably expressing HEK cells with an anti-MFG-E8 ELISA. The estimated protein concentration of MFG-E8-NP in SN of stably transfected HEK cells was 0,32 µg/ml applying 4-Parameter logics. The result confirmed that the transfected HEK cells express MFG-E8-NP in small but sufficient amounts. To assess MFG-E8's functionality as part of the recombinant protein, we tested its coating efficacy to staurosporine treated thymocytes applying FACS staining. Apoptotic thymocytes were overlaid with SN of HEK cells expressing MFG-E8-NP. FACS staining was acquired for MFG-E8 using a biotinylated anti-MFG-E8 Ab (R&D Systems) followed by Streptavidin A-APC (Caltag, UK). MFG-E8-NP labelled 2,95% of the apoptotic thymocytes. The positive control recMFG-E8 detected 66.6 %, while the background of unstained cells was 0.56 % (Fig. 2C). We concluded that the PS binding domains C1C2 of recombinant MFG-E8-NP were functional. The low labelling frequency might be due to low amount of functional MFG-E8-NP in SN. In addition, NP folding could eventually interfere with PS-binding sites of the MFG-E8 fusion protein.
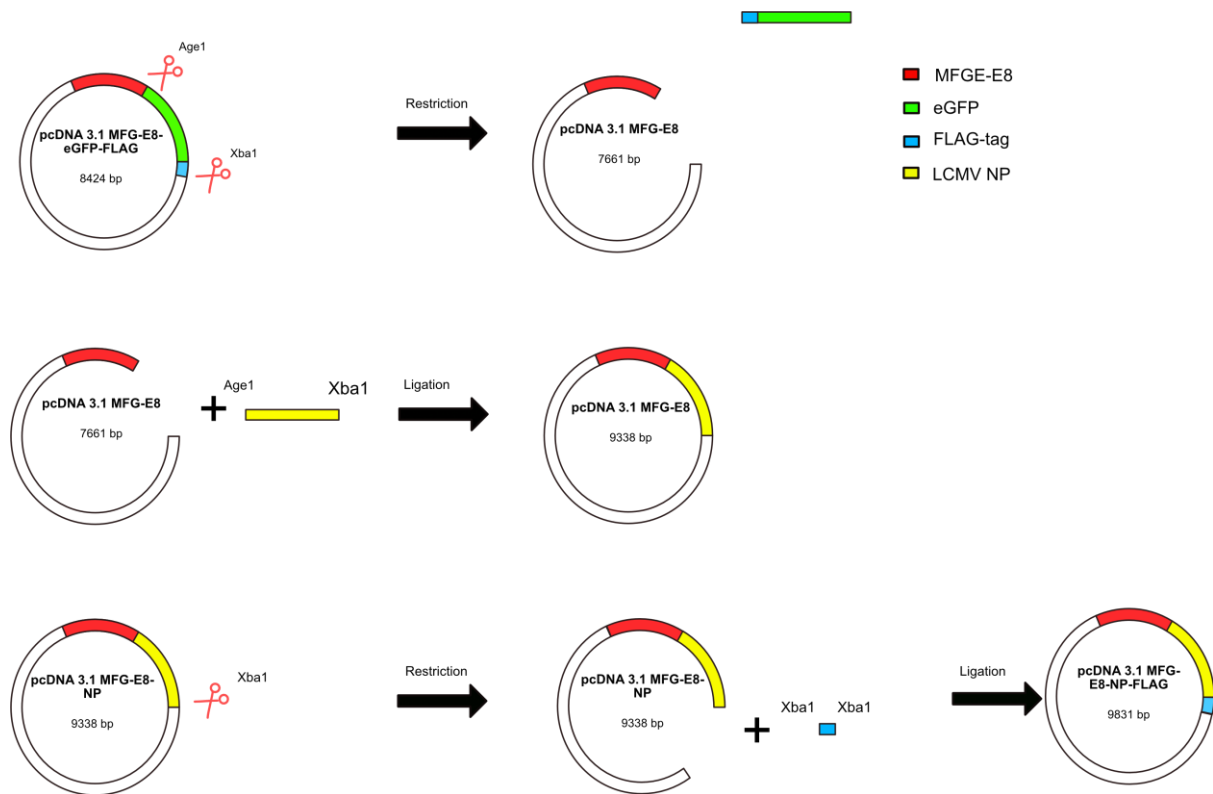
Fig. 1 Cloning of Mfge8-Np

We utilized the construct pcDNA3.1 MFG-E8-eGFP based on the commercial vector pcDNA3.1(+) from Invitrogen (Thermo-Fisher, USA) as cloning vector. The plasmid construct was evaluated by sequencing with the primer MFG-E8_3end_pcDNA3.1 to control if the vector contained the correct FLAG-tag sequence. We cleaved the construct pcDNA3.1 MFG-E8-eGFP-FLAG with the enzymes Age1 and Xba1 by restriction digestion. This cloning step removed *Egfp-Flag*. The result pcDNA3.1 MFG-E8, 7661bp, was first controlled with 0.5% agarose gel electrophoresis. Second, the vector DNA was dephosphorylated to maintain the cleavage. After dephosphorylation, the product was purified using a PCR purification kit (Thermo-Fisher). *Lcmv Np* containing *Age1* and *Xba1* cutting sites was cleaved by restriction enzyme digestion. The DNA template containing *Np* was then ligated into the plasmid yielding pcDNA3.1 MFG-E8-NP. Afterwards, the construct DNA was transformed into chemo competent E. coli. The transformed E. coli bacteria were controlled with colony PCR. DNA of the positive colony was sequenced twice in 3 steps: LCMV_NP_fw_pos622 LCMV_NP_fw_pos1372 for the correct position of the *Lcmv Np* sequence. MFG-E8_3end_pcDNA3.1. for the correct *Mfge8* sequence.

DNA was produced by conventional mini prep for the next ligation step. pcDNA3.1 MFG- E8-NP was cleaved by Xba1 and dephosphorylated. The product was extracted with a GenJet PCR purification kit (Thermo-Fisher Scientific, USA) and controlled by 0.5% agarose gel electrophoresis. FLAG-tag oligos were annealed and confirmed using 4% agarose gel electrophoresis. The annealed FLAG-tag oligos were cleaved by Xba1 and ligated into pcDNA3.1 MFG-E8-NP (9338 bp), obtaining the final construct pcDNA 3.1 MFG-E8-NP-FLAG (9831 bp). The final vector construct was transformed into competent E. coli bacteria and evaluated with colony PCR. From positive E. coli colonies, DNA was produced by miniprep and sequenced with LCMV_NP_fw_pos1372 for correct *Np* expression. One positive clone without mutation was obtained and used for DNA transfection into HEK293T cells.

Gen	Forward primer (5´-3´)	Reverse primer (5´- 3´)	Annealing Temperature
NP at aa622	CCTTGGCTTGCTTT ACACAGTC	AGTCTTTCAC ATCCCAAACTCTTACC	59°C
NP at aa1372	GGTTCTAAGCTGTC AAGGCTCC	AGTCTTTCAC ATCCCAAACTCTTACC	59°C
MFG-E8	GTGTCCTTCCAGT CCTGG	AGTCTTTCAC ATCCCAAACTCTTACC	59°C

Tab. 2 Primers used for Sequencing of Mfge8-Np
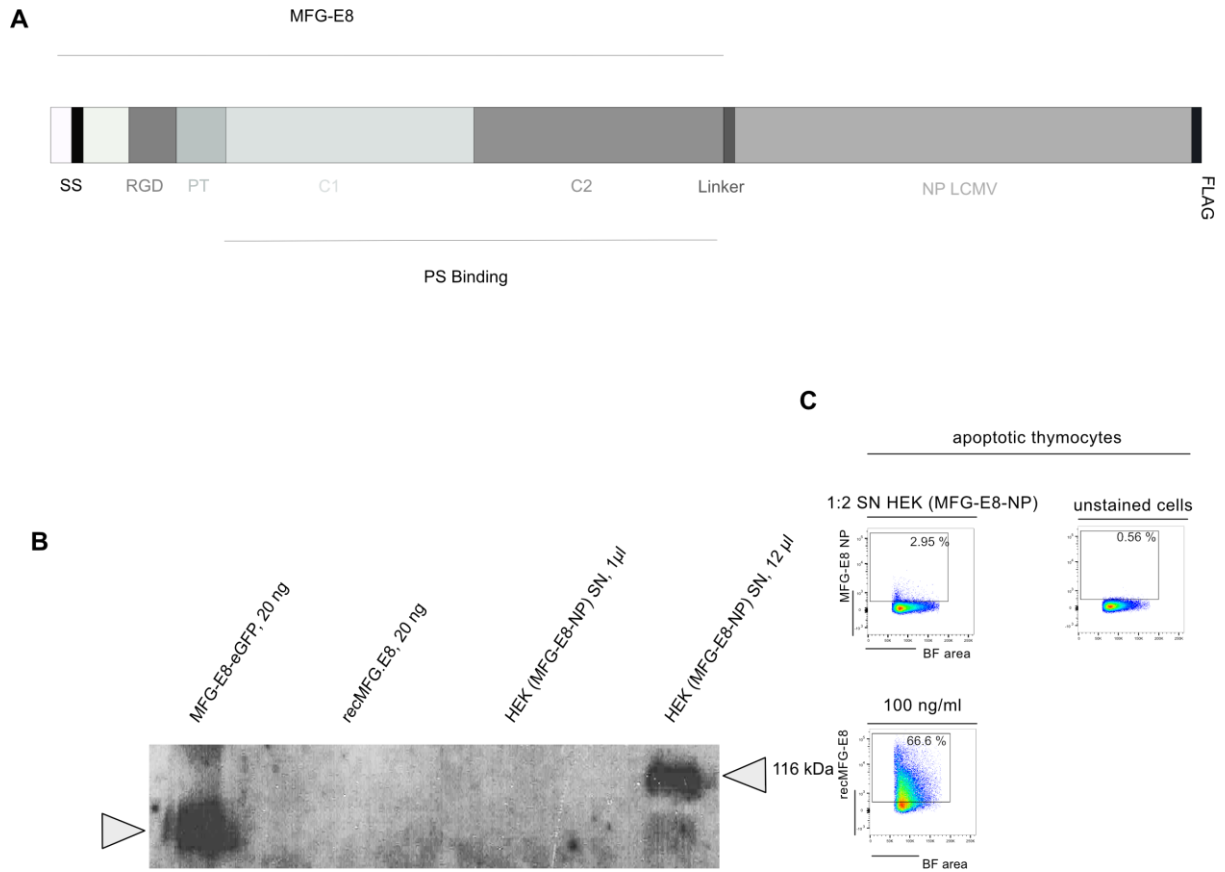This table contains the primers used to sequence pcDNA3.1 MFG-E8 NP-FLAG.

Fig. 2 Evaluation of MFG-E8-NP

(A) displays a schematic representation of the fusion protein MFG-E8-NP. It is composed of MFG-E8 with its PS-binding region C1C2, the RGD-domains connected to its C terminal with the Nucleoprotein (NP) and the FLAG-tag.

(B) Western Blot staining for anti-Flag: Different volumes, 12 µl and 1 µl, from SN of stably transfected HEK cells expressing MFG-E8-NP, purified MFG-E8-eGFP and recMFG-E8 were loaded onto an SDS gel, transferred onto a membrane and stained for anti-FLAG using unlabelled anti-FLAG mouse IgG1 M2 (Sigma-Aldrich, US, Cat. # F3165), followed by polyclonal HRP labelled rabbit anti-Armenian hamster IgG1 (1:3000, Abcam, Cambridge, UK, Cat. #ab5745). Bands were detected for MFG-E8-eGFP and MFG-E8-NP at expected sizes. No band was seen for recMFG-E8 and 1 µl of MFG-E8-NP. RecMFG-E8 contains a HIS-tag.

(C) shows the ability of MFG-E8-NP to coat staurosporine treated thymocytes. The data shown was from one experiment. Supernatant from HEK cells stably expressing MFG-E8-NP (1:2) stained 1×10^6 apoptotic thymocytes. The binding frequency (BF) was measured by flow cytometry. We stained for MFG-E8 using a biotinylated MFG-E8 Ab followed by streptavidin A-APC.

3.2 Generation of MFG-E8-R262A-GP1(260L/176N)

The GP1 of the LCMV is next to MFG-E8, one of the interests of this research. It is the viral protein responsible for attachment to host cells. Furthermore, it is the location for ab mediated binding and neutralization of the virus. In contrast to the NP, it induces hardly a humoral response, due to its vigorous strategies evading recognition by the host's adaptive immune response (1.1.9 Neutralizing antibodies in LCMV infections). We fused MFG-E8 to GP1 to enhance the humoral response against the GP1.

A FLAG-tag is crucial for large scale production via FLAG affinity chromatography. Therefore, it was necessary to evaluate the correct FLAG-tag expression by the cloned constructs. To this end, we evaluated MFG-E8-260L-GP1 and MFG-E8-176N-GP1 via WB staining for valid FLAG-tag expression but could not detect any signal. As a possible reason for the absence, we noticed the well-characterised S1P binding site within *Lcmv-Gp1*, located at aa 265. Such an S1P binding site would allow cleavage of the following FLAG-tag located at the C-terminal end of the GP1. In vivo, the S1P binding site is vital for viral endoproteolytic processing of the GPC to GP1 and GP2. GP1 is responsible for attachment to α-DG of host cells. Studies show that abolishing this binding site in genetically modified LCMV strains leads to inhibition of viral cell-to-cell propagation due to loss of GPC differentiation into GP1 (58,59). We expected that the S1P binding site was responsible for the absence of the FLAG-tag due to cleavage during endosomal processing in HEK cells. We inserted an R262A mutation into the 260L-GP1 and 176N-GP1 of their respective fusion proteins. This modification is shown in multiple studies to silence the S1P-activity (37,59). The DNA of MFG-E8-260L-GP1 and MFG-E8-176N-GP1 was enzymatically cleaved. The desired mutation was inserted together with their respective *Gp1* and the *Flag-tag* in various cloning steps (Fig. 3A, B). We confirmed the *r262a* mutation by sequencing in each construct (See tab. 1 Primer used for cloning and sequencing of MFG-E8-260L-GP1 R262A and -GP1-176N R262A). HEK cells stably expressing the constructs were developed. SN was assessed for protein expression via WB staining. We calculated molecular weights using the Ape plasmid editor (v. 3.0.0, April 9, 2021). The size 77 kDa was gauged for both fusion proteins, MFG-E8-260L-GP1-R262A and MFG-E8-176N-GP1-R262A. Staining for anti-MFG-E8 displayed large and blurry bands due to strong protein expression by the transfected HEK cells (data not shown). Staining the SN of HEK cells expressing MFG-E8-176N-GP1 and MFG-E8-260L-GP1 displayed bands

at approximately 130 kDa (Fig. 7B). We confirmed MFG-E8 expression in all constructs due to positive staining. Next, we continued staining for anti-FLAG. No bands were revealed applying unlabelled anti-FLAG mouse IgG1 M2 (Sigma-Aldrich) utilised to dye the FLAG-tag of MFG-E8-NP (Fig. 2B). We repeated the anti-FLAG staining with a monoclonal HRP labelled mouse IgG1 ab (Sigma-Aldrich). Bands ranged between 120 and 130 kDa for the fusion proteins containing the GP1-R262A, MFG-E8-260L-GP1 and MFG-E8-176N-GP1 (Fig. 4, 7C). All recombinant proteins expressed the FLAG-tag correctly, including those containing the R262A mutation. The bands of the GP1 containing proteins run at 130 kDa compared to MFG-E8-eGFP at 70-90 kDa. The larger size is due to heavy N-linked glycosylation of the GP1 during posttranslational processing in the Golgi apparatus (37). Even MFG-E8 is a GP containing 3 N-linked glycosylation contributing to slowing migration during the SDS page. The apparent glycosylation of the fusion proteins confirms that GP1 is similarly expressed to the original viral protein. A correctly presented GP1 is vital for the induction of nAbs to LCMV. Studies demonstrate that changing the N-linked glycan makeup of the GP1 alters its antigenic behaviour (68). Therefore, we did not remove the glycans from the GP1 by PNgase F. Due to possible immunological changes induced by the R262A modification, we preceded with MFG-E8-260L-GP1 and MFG-E8-176N-GP1 without the S1P mutation. The question of why a directly labelled ab was more sensitive in detecting the FLAG-tag stayed elusive.
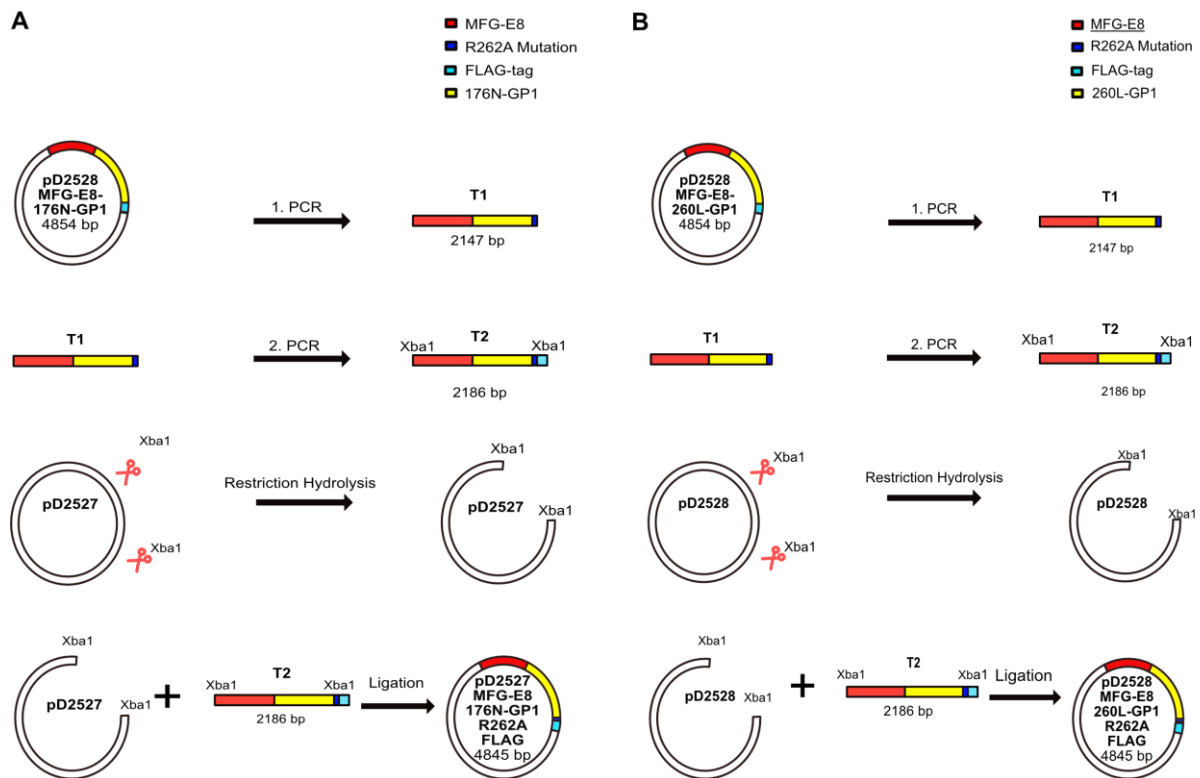
Fig. 3 Cloning of MFG-E8-260L-GP1-R262A and MFG-E8-176N-R262A

(A) displays the cloning of the MFG-E8-260L-GP1-R262A construct. It was based on the vector construct pD2528 (Newark, CA, USA) MFG-E8-260L-GP1. Two PCR steps were applied as follows: In the first step, we created a DNA template (T1) containing *Mfge8* and *Gp1* of the LCMV$_{Cl13}$ with a point mutation at the amino acid position 262 of the GP1 exchanging arginine for alanine (R262A). This mutation changes the S1P binding site from KFFTRR to KFFTAR and abolishes its activity. In the second PCR step, we added a FLAG-tag to the template (T2) *Mfge8-260l-Gp1-r262a*, yielding *Mfge8-260l-Gp1-r262a-Flag*. The product was restricted by its respective enzymes and ligated into the digested pD2528 vector with the "one-step ISO assembly of overlapping dsDNA method" presented by Gibson et al. (2,3). All cloning steps were controlled by DNA sequencing. The final vector constructs pD2528 MFG-E8-260L-GP1-R262A-FLAG was transfected into HEK cells using the CaPO4 method. We evaluated correct protein expression via Western Blotting and ELISA.

(B) visualizes the cloning strategy of MFG-E8-176N-GP1. The vector construct was cloned similarly. A template (T1) was produced by PCR containing *Mfge8* and *Gp1* from the LCMV$_{Arm}$. At amino acid residue 262 of the GP1, we introduced a point mutation, exchanging arginine for alanine (R262A). This mutation changes the S1P binding site from KFFTRR to KFFTAR. It was based on the vector construct PD 2528 (Newark, CA, USA) MFG-E8-176N-GP1. The template (T2) was digested by its respective enzymes and ligated with the "one-step ISO assembly of overlapping dsDNA method" presented by Gibson et al. (192,193) into the digested pD2527 vector. The construct DNA was transfected into HEK cells, stabilised, and purified by FLAG affinity chromatography and peptide elution.
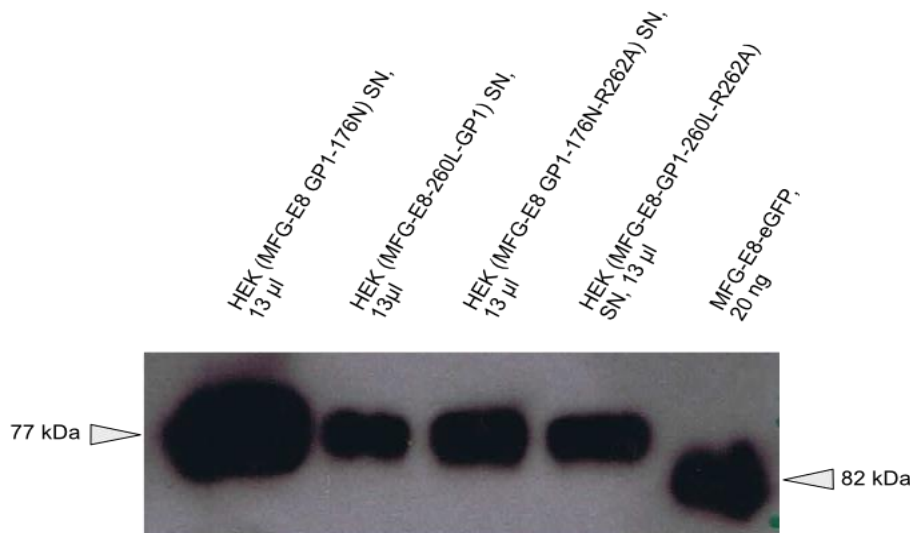
Fig. 4 Detection of FLAG-tag in all MFG-E8-GP1 fusion proteins
MFG-E8-176N-GP1-R262A, MFG-E8-260L-GP1-R262A, MFG-E8-176N-GP1, MFG-E8-GP1 and MFG-E8-eGFP
were loaded onto an SDS-gel, transferred onto a membrane and stained with a direct HRP labelled IgG$_1$ anti-FLAG
antibody (Sigma-Aldrich). Bands were detected in all constructs at expected sizes. The GP1 fusion proteins run
higher due to glycosylation of the GP1.

3.3 Purification of MFG-E8-176N-GP1

Following the cloning the experiments, we purified MFG-E8-176N-GP1 from SN of
stably transfected HEK. The purification step was necessary for the immunisation of
mice.

SN from stably transfected HEK cells expressing MFG-E8-176N-GP1 was utilised to
purify protein using FLAG affinity chromatography. To quantify the protein
concentration, we applied an anti-MFG-E8 ELISA. A 4-parametric analysis calculated
the final concentration of the protein. The result of the MFG-E8-176N-GP1 purification
process was 1.5 mg/ml (Fig. 5).

Following, we controlled the purified protein's correct size and potential contamination
with SDS page and Coomassie staining. The expected molecular weight was 77 kD.
However, due to heavy glycosylation of the GP1, the recombinant protein ran at 130
kDa (Fig. 6B)., as noticed in previous WB staining (Fig 4,7B, C). No other bands were
obtained, which indicated no contamination with other proteins. We concluded correct
protein expression by MFG-E8-176N-GP1 transfected HEK cells used for large scale
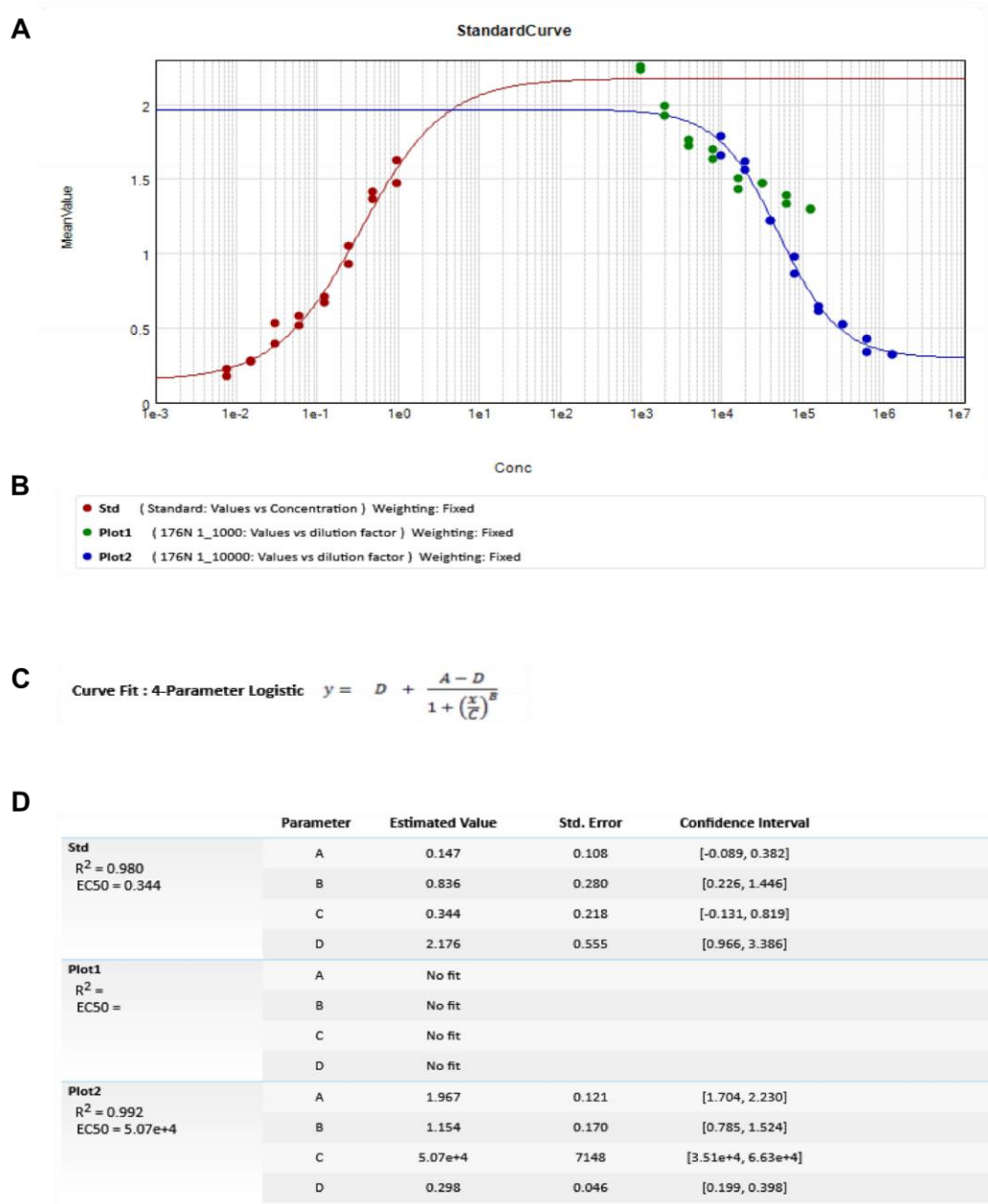protein production.

A

StandardCurve

B

- **Std** (Standard: Values vs Concentration) Weighting: Fixed
- **Plot1** (176N 1_1000: Values vs dilution factor) Weighting: Fixed
- **Plot2** (176N 1_10000: Values vs dilution factor) Weighting: Fixed

C

Curve Fit : 4-Parameter Logistic $\quad y = D + \dfrac{A-D}{1+\left(\frac{x}{C}\right)^B}$

D

	Parameter	Estimated Value	Std. Error	Confidence Interval
Std $R^2 = 0.980$ EC50 = 0.344	A	0.147	0.108	[-0.089, 0.382]
	B	0.836	0.280	[0.226, 1.446]
	C	0.344	0.218	[-0.131, 0.819]
	D	2.176	0.555	[0.966, 3.386]
Plot1 $R^2 =$ EC50 =	A	No fit		
	B	No fit		
	C	No fit		
	D	No fit		
Plot2 $R^2 = 0.992$ EC50 = 5.07e+4	A	1.967	0.121	[1.704, 2.230]
	B	1.154	0.170	[0.785, 1.524]
	C	5.07e+4	7148	[3.51e+4, 6.63e+4]
	D	0.298	0.046	[0.199, 0.398]

Fig. 5 Quantification ELISA of MFG-E8-176N-GP1

(A) presents the quantification of protein gained from transfected HEK cells. An ELISA plate was coated with an MFG-E8 18A2 antibody (Ab) and stored at 4 °C overnight. MFG-E8-176M-GP1 diluted in1:1000 and 1:10000 was pipetted into the first wells. Serial 1:2 dilution was performed. Biotinylated anti-MFG-E8 ab was used as the secondary ab. After applying stabilised chromogen (SeraCare, USA), the light absorbance was measured by Versa max microplate reader (Molecular Devices, USA), represented in a standard curve seen in figure A. The standard MFG-E8-eGFP is designated as the red-lined graph. The blue chart displays the 1:10000 dilution, the green one the 1:1000 dilution of MFG-E8-176N-GP1. The standard curve is based on the mean values of the protein concentration.

(B) legend to (A).

(C) for calculating the protein concentration, 4-Parameter logics were applied as shown.

(D) values of plot (A) were inserted into the formula (C) to calculate the protein concentration. The final concentration of the purified MFG-E8-176N-GP1 protein was 1.5 µg/ml. The graphs and tables were produced by SoftMax Pro 7.0.3 (Molecular Devices, USA).

3.4 The function of MFG-E8 GP1 (176N/260L) fusion proteins

We tested the function of the recombinant proteins by evaluating their binding efficacy to apoptotic thymocytes. Binding would show us if the C1C2 domain of the MFG-E8 containing fusion proteins were functional. We applied FACS staining for MFG-E8 using a biotinylated MFG-E8 Ab (R&D System) followed by Streptavidin A-APC (Caltag, UK) to measure the labelling efficacy. We acquired the following results using different dilutions of the protein. Coating with 600 ng/ml MFG-E8-176N-GP1 dilution had a binding frequency of 55.8 %, 300ng/ml 50.1 % and the 150 ng/ml dilution 40.3 %. 100 ng/ml recMFG-E8 had a comparably higher coating efficacy of 63.9 %. A binding frequency of 0.18 % was found in unstained thymocytes (Fig. 6C).

SN of MFG-E8-260L-GP1 stably expressing HEK cells was utilised to coat apoptotic thymocytes in a separate experiment. We prepared the FACS staining evenly. The binding frequency was counted 14.4 % (Fig. 7D).

We concluded that MFG-E8-176N-GP1 and MFG-E8-260L-GP1 bound to PS. Therefore, MFG-E8 as part of the fusion proteins was functional.

300 ng/ml of MFG-E8-176N-GP1 was the optimal coating dilutions to achieve similar coating efficacy to recMFG-E8. Higher protein concentrations induced more extensive background staining and did not represent valid results. Higher protein concentration required compared to recMFG-E8 might be due to GP1 interfering with MFG-E8´s C1C2 domain inhibiting binding to PS. We proceeded using the purified MFG-E8-176N-GP1 for an immunisation protocol to find out if GP1 linked to MFG-E8 induces nAbs against LCMV$_{Arm}$.
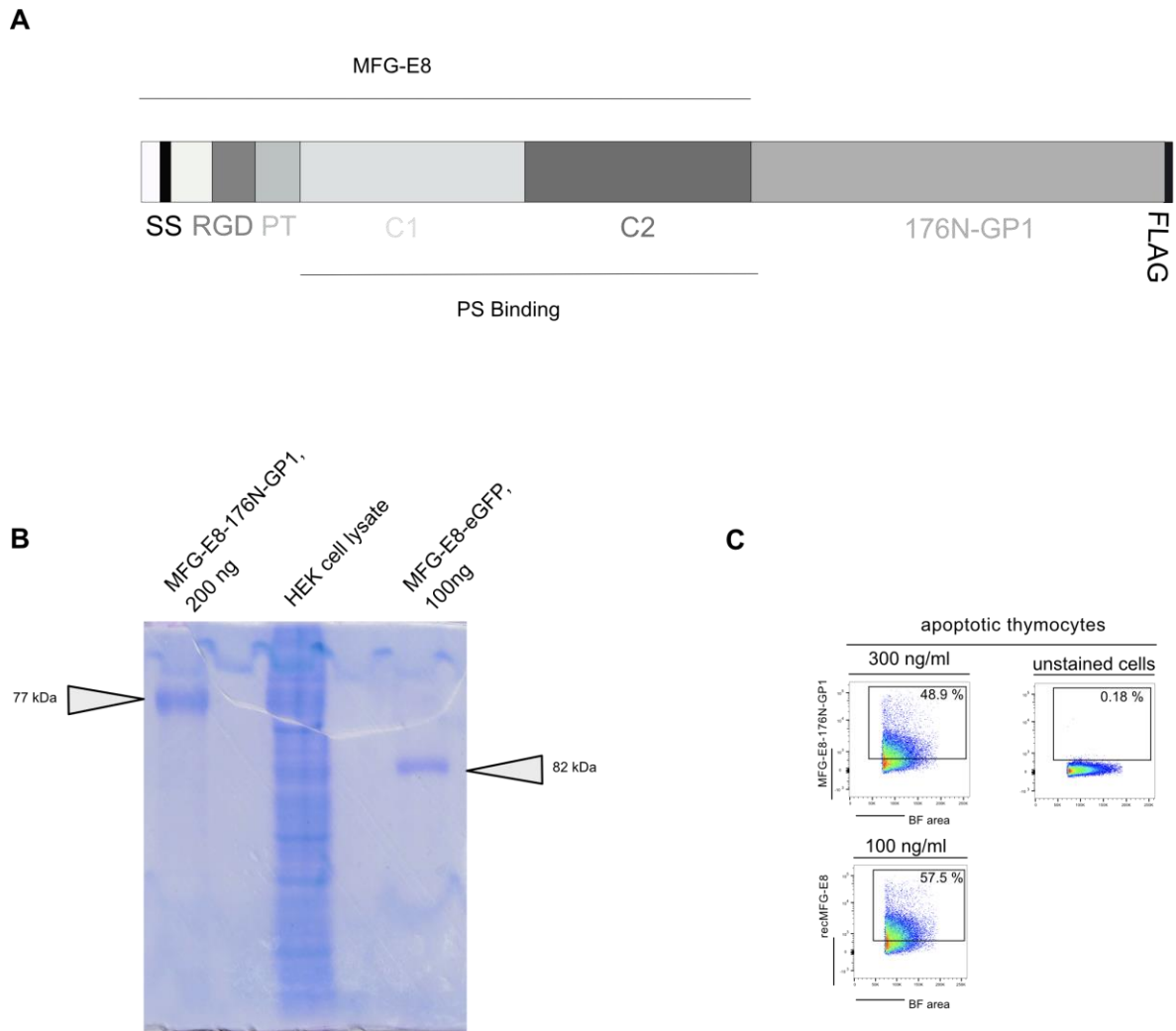
A

B

C

Fig. 6 Purified MFG-E8-176N-GP1

(A) presents the fusion protein MFG-E8-176N-GP1. MFG-E8 was fused to the N-Terminus of the $LCMV_{Arm.}$ GP1 and to the FLAG-tag.

(B) shows the Coomasie staining (Thermo-Fisher) of MFG-E8-176N-GP1 purified via FLAG chromatography. 200 ng of MFG-E8-176N-GP1 (77 kDa), 100 ng of MFG-E8-eGFP (82 kDa) as positive and HEK lysate as negative control were loaded onto an SDS gel. The gel was stained overnight in Coomassie staining solution. H_2O washed off the Coomassie. Bands were detected at the expected size. MFG-E8-176N-GP1 run higher than MFG-E8-eGPF due to the heavy glycosylation of GP1.

(C) displays the functionality of MFG-E8-176N-GP1 by measuring its binding efficacy to staurosporine treated thymocytes. $1x10^6$ apoptotic thymocytes were coated with purified MGF-E8-176N-GP1 (1.5 mg/ml). Fluorescent anti-MFG-E8 staining was performed with biotinylated anti-MFG-E8 IgG, 1:300 (R&D Systems, Cat. # BAF2805) and Streptavidin A-APC, 1:700 (Caltag, UK). The Coating efficacy was measured using 300 ng/ml of MFG-E8-176N-GP1 achieving 48,9 % coating efficacy. Unstained apoptotic thymocytes were the negative control. RecMFG-E8 was utilised as a positive control.
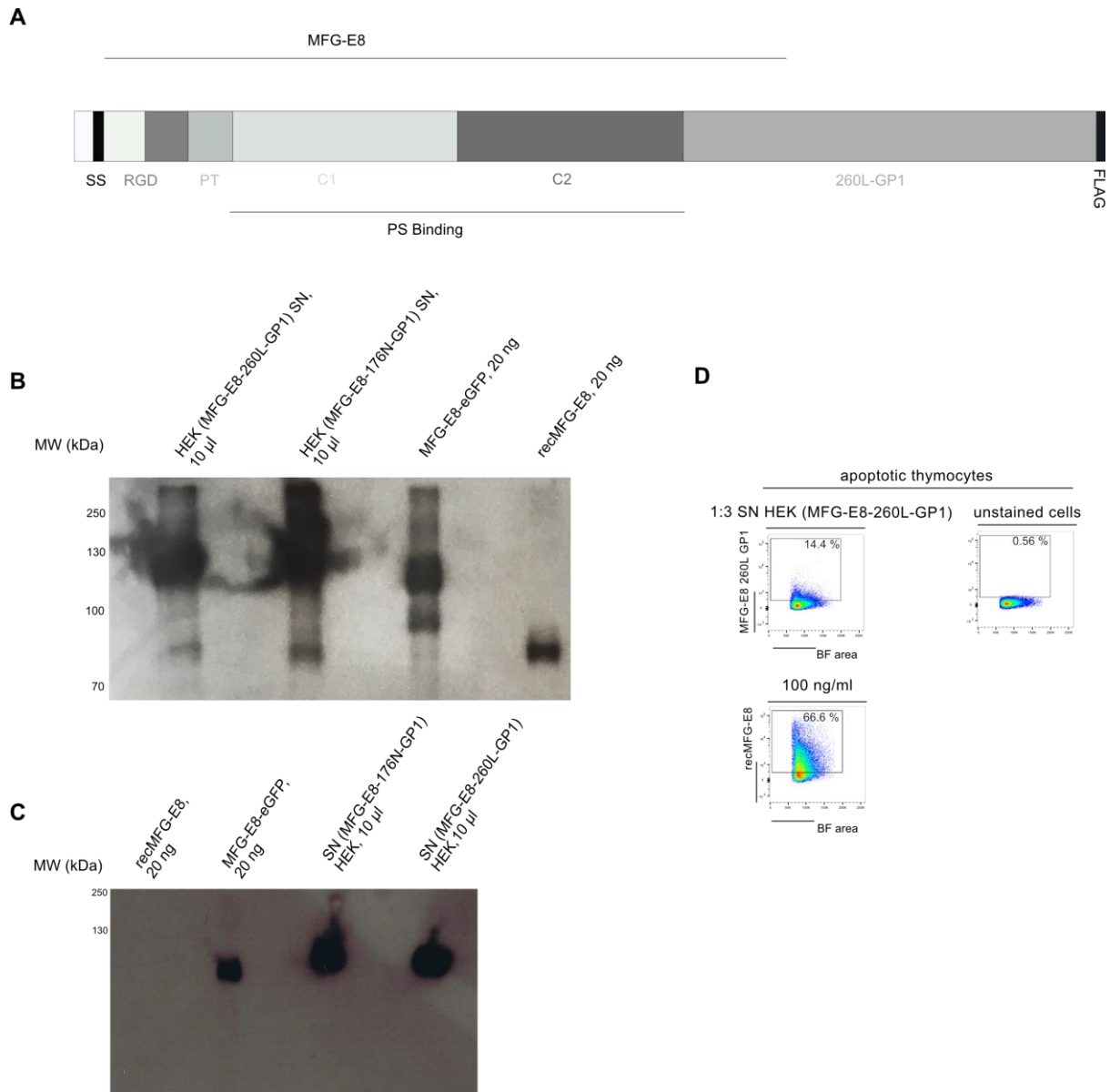
A

MFG-E8

SS | RGD | PT | C1 | C2 | 260L-GP1 | FLAG

PS Binding

B

HEK (MFG-E8-260L-GP1) SN, 10 µl
HEK (MFG-E8-176N-GP1) SN, 10 µl
MFG-E8-eGFP, 20 ng
recMFG-E8, 20 ng

MW (kDa)
250
130
100
70

C

recMFG-E8, 20 ng
MFG-E8-eGFP, 20 ng
SN (MFG-E8-176N-GP1) HEK, 10 µl
SN (MFG-E8-260L-GP1) HEK, 10 µl

MW (kDa)
250
130

D

apoptotic thymocytes

1:3 SN HEK (MFG-E8-260L-GP1)   unstained cells

MFG-E8 260L GP1   14.4 %   0.56 %

BF area

100 ng/ml

recMFG-E8   66.6 %

BF area

Fig. 7 Functionality of MFG-E8-260L-GP1

(A) presents the fusion protein MFG-E8 connected at its C Terminal to GP1 of the LCMV$_{Cl13}$ strain bound to a FLAG-tag.

(B) shows the Western Blot (WB) staining for MFG-E8 in the supernatant (SN) of MFG-E8-GP1(260L/176N). The SN of the stably transfected HEK cells expressing MFG-E8-176N-GP1 or MFG-8-260L-GP1 were loaded with recMFG-E8 and MFG-E8-eGFP protein onto an SDS gel transferred onto a nitrocellulose membrane. Blotting was done with an anti-MFG-E8 18A2-G10, and HRP labelled Armenian hamster IgG. Bands for MFG-E8-260L-GP1 (77 kDa), recMFG-E8 (60 kDa) and MFG-E8-eGFP (82 kDa) were detected at the expected size. Blurred staining was acquired for MFG-E8-176N-GP1.

(C) displays the WB staining for the FLAG-tag. Equal amounts from the SN of stably transfected HEK cell lines expressing MFG-E8-176N-GP1 and MFG-E8-260L-GP1 (77 kDa) were loaded onto an SDS gel. recMFG-E8 (60 kDa) and MFG-E8-eGFP were the control proteins (82 kDa). The gel was transferred onto a nitrocellulose membrane and stained for anti-FLAG. Bands were detected. The GP1 incorporating constructs run higher than MFG-E8-eGFP due to N-linked glycosylations.

(D) demonstrates the coating capability of MFG-E8-260L-GP1 to staurosporine treated thymocytes. SN from HEK cells stably expressing MFG-E8-260L-GP1 was utilised to coat 1x106 apoptotic thymocytes. Staining was accomplished with biotinylated anti-MFG-E8 IgG, 1:300 (R&D Systems, Cat. # BAF2805), followed by Streptavidin A-APC, 1:700 (Caltag, UK). The binding frequency (BF) was measured using flow cytometry.

3.5 Antibody detection in mice

MFG-E8-eGFP injected in mice induces an accelerated humoral immune response to eGFP shown by ELISA experiments (Kranich et al. unpublished results). Comparably, we evaluated the presence of nAbs to GP1 using an Ab mediated neutralisation assay. B6 mice naïve to LCMV were injected either with MFG-E8-176N-GP1 or with MFG-E8-eGFP protein at equimolar protein amounts. The injections were done twice in 2 weeks. 7 d after the second injection, serum of the mice was taken and assessed with a plaque-forming neutralisation assay for nAbs against LCMV$_{Arm}$.

The serum of MFG-E8-eGFP injected mice was designed as the negative control because there were no nAbs against LCVM$_{Arm}$ to be expected.

LCMV$_{Arm}$ incubated with the serum of MFG-E8-176N-GP1 injected, mice exhibited a lower PFU/ml mean than mice injected with MFG-E8-eGFP (Fig. 8A, B). The mean difference was 0.00333 PFU/ml. However, the PFU difference to the negative control was statistically insignificant (t-test, P=0.0670; Welch´s test, P=0.1128).

The PFU/ml mean of LCMV$_{Arm}$ incubated without serum or ab was higher than the virus incubated with the serum of MFG-E8-176N-GP1 injected mice (Fig. 8A).

The PFU/ml mean difference between these wells was 0.01083 PFU/ml concluding the result statistically significant (t-test, P<.0001; Welch´s test, P<.0001).

The PFU/ml mean of LCMV$_{Arm}$ only was higher than the one obtained upon incubation with the KL-25 ab. The mean difference was 0.00458 PFU/ml (Fig. 8A). The outcome was statistically significant (t-test, P= 0.058; Welch´s test P=0.0066).

The PFU/ml mean of KL-25 ab, the positive control, incubated with the virus was higher than with serum of MFG-E8-176N-GP1 injected mice (Fig. 8A). The mean difference was 0.0625 PFU/ml and statistically significant (t-test P=0.0002; Welch´s test P=0.0008).

The PFU/ml mean of virus only was higher than the virus incubated with the serum of MFG-E8-eGFP injected mice (Fig. 8A). The mean difference was 0.01083 PFU/ml, which was statistically significant (t-test, P=0.0024; Welch´s test P=0.0049).

Virus incubated with KL-25 ab revealed a higher PFU/ml than virus incubated with the serum of MFG-E8-eGFP injected mice (Fig. 8A). The PFU/ml difference was 0.002917 PFU/ml resulting in statistical insignificance (t-test, P=0.1741; Welch´s test, P=0.1798).

First, KL-25, a well-established GP1 nAb, was successful as a control for this experiment. KL-25 displayed statistically significant lower PFU/ml (Welch´s test P=0.0066) than virus only. Therefore, the KL-25 ab contained adequate neutralising capacity (Fig. 8A).

Both fusion proteins MFG-E8-176N-GP1 and MFG-E8-eGFP generated lower PFU/ml than virus only. This result could indicate that the sera of immunised mice contained proteases, complement factors and unspecific immunoglobulins which have affected viral lysis. Interestingly, both fusion proteins caused lower PFU/ml than KL-25, a specific anti-GP1 nAbs exemplified to induce viral lysis. Consequently, the amount of immunologically active substances in their sera was far greater than in the used KL-25 dilution. However, MFG-E8-eGFP's PFU/ml mean was more soaring than MFG-E8-176N-GP1 and statistically not significantly different from KL-25. Additionally, MFG-E8-176N-GP1 yielded lower PFU/ml (t-test, P=0.0670) close to significance than MFG-E8-eGFP (Fig. 8B). Accordingly, it was possible that result was due to the presence of nAbs against LCMV$_{Arm}$ in serum of MFG-E8-176N-GP1 immunised mice. The concern was that different amounts of serum from each mouse were incubated with the same LCMV concentration. Some of the mice yielded more serum than others. As a result, the comparison of the PFU/ml between the sera obtained from each mouse is inaccurate. The greater the amount of serum used for an assay, the more lysis-inhibitory factors might have been present. Equal parts of serum incubated with the same virus concentration would be validly comparable. However, a larger test group of mice or repetition of the experiment was not possible due to the limited amount of protein. Both could have drawn a clearer picture of whether nAbs were present in the sera of MFG-E8-176N-GP1 immunised mice.

A all conditions vs. virus only

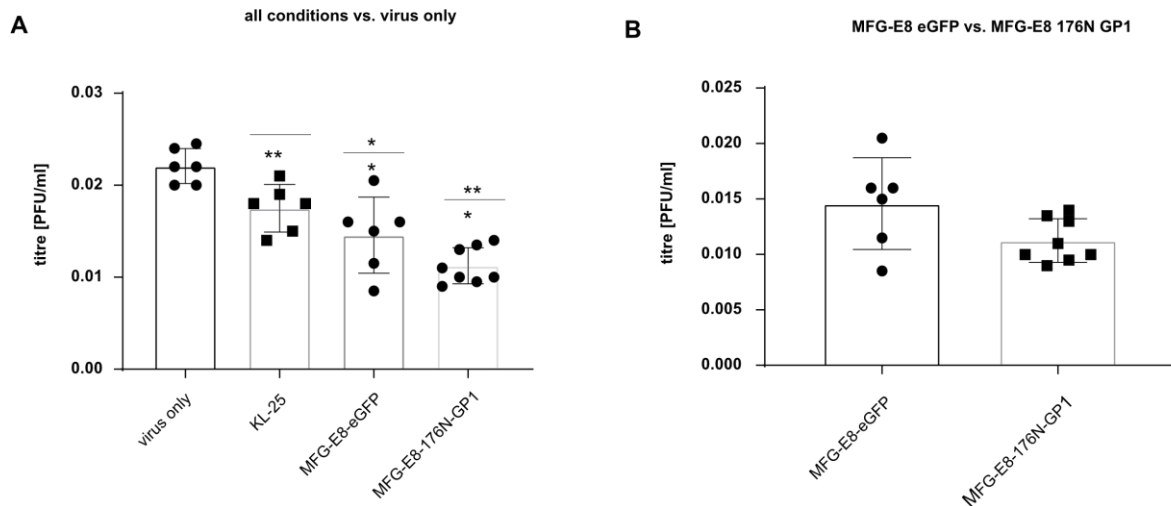**B** MFG-E8 eGFP vs. MFG-E8 176N GP1

Fig. 8 Comparison of infectious titres

Three C57BL/6 mice were injected intraperitoneally with MFG-E8-eGFP. 4 mice of the same breed were injected with MFG-E8-176N-GP1. The injections were repeated after 2 weeks. 7 d after the second injection, blood from the tail vein of the mice was taken, and serum was produced. The serum was divided by two, and each sample was incubated as doublets with the same 1:10000 $LCMV_{Arm}$. dilution. The serum amount per doublet (wells, n=6, n=8) was equal, the amounts between doublets differed. The volume was balanced using a 5% FCS DMEM (Gibco) medium. The mix was overlaid on Vero cells and incubated for 3 d at 37°C. Staining was completed for the nucleoprotein of the $LCMV_{Arm}$. Plaques were counted, and the PFU/ml was figured. Serum from MFG-E8-eGFP immunised mice were used as the negative control. KL-25, anti-GP1 antibody $LCMV_{Arm}$, was applied as a positive control in 1:100 dilution and incubated in triplets with the (n=6) same virus dilution. Plaques were counted and PFU/ml calculated. The histograms display the measured viral titres (PFU/ml) from $LCMV_{Arm}$. incubated with KL-25 antibody, serum from mice (n=3) injected with MFG-E8-eGFP, serum from mice (n=4) injected with purified MFG-E8-176N-GP1 and virus only. (A) shows infectious titres from all conditions to $LCMV_{Arm}$ only. (B) shows the comparison of infectious titers from the serum of MFG-E8-eGFP and MFG-E8-176N-GP1 injected mice incubated with $LCMV_{Arm}$. The data presented originated from one experiment. Each dot in the graph indicates one well. Statistical significance is denoted by asterisks (ns P > 0.5; *P ≤ 0.05; **P ≤ 0.01; ***P ≤ 0.001; T-test or Welch-test

4 DISCUSSION

4.1 Successful cloning of constructs

We verify the successful induction of the R262A mutation into the fusion proteins MFG-E8-260L-GP1 and MFG-E-176N-GP1, yielding MFG-E8-176N-GP1- R262A and MFG-E8-176N-GP1-R262A. Each fusion protein express GP1, MFG-E8 and a FLAG-tag shown by sequencing and WB. We conclude that the S1P is not vital for expressing our fusion proteins in HEK cells. Burri et al. demonstrated that the S1P binding site is essential for processing the viral GPC into GP1 and GP2. The induction of the R262A mutation in recLCMV lead to the failure of viral propagation (58,59). That S1P-deficient LCMV clones could not present GP1 contradicts in some way our findings. HEK cells correctly express our GP1-fusion protein despite abolishing the S1P binding site. Transport of native GPC in the absence of a functional S1P-binding site to the cell surface was examined (196). However, our GP1 did not need further cleavage from the viral precursor protein. We figur that the binding site is active in GPC composition, cleaving it into GP1 and GP2. The MFG-E8-GP1 fusion proteins differ from the original GPC in design. Consequently, they are independent of the S1P processing. Various studies showed that different proteases can achieve correct GP1 cleavage with their respective binding sites at the same aa position. Exchanging the S1P-binding site of recLCMV with a different coded S1P of the Lassa virus or a furin binding site of the HIV, resulted in correct LCMV-GP1 expression. However, cleavage occurred in a different part of the Golgi apparatus than in native LCMV-GP1 (58,64).

Despite assuming that our MFG-E8-GP1 fusion proteins are processed differently than the native LCMV-GP1, correct GP1 expression is feasible in other parts of the Golgi apparatus. Therefore, we believe that our GP1-MFG-E8 fusion proteins induce an accurate humoral response to GP1

4.2 Correct glycosylation of the GP1 in HEK cells

The GP1 of the LCMV was highly enriched in glycans, shielding the virus from lysis by nAbs (37,68). GPs run slower on the SDS pages and display larger sizes due to their large glycan expression (26). Similar, our MFG-E8-GP1 fusion proteins advance in WB slower than MFG-E8-eGFP. Thus, it hints at proper glycosylation of the GP1 in HEK cells. Therefore, we can consider that the GP1's antigenicity is preserved during cloning procedures. Eschli et al. used PNGase F digestion to deglycosylate their IgG-GP1 fusion protein to display its actual protein size. Thereby they proved that proper glycosylation in the transfected mammalian cells occurs (26). An aspect of future experiments can be to demonstrate the actual size of the MFG-E8-GP1 fusion proteins via PNGase F digestions. Further determining correct protein folding, Eschli et al. characterized their IgG-GP1 fusion protein by epitope mapping of known neutralising and binding Ab sites, respectively GP1-A, GP1-B and GP1-C (26,65). They applied an ELISA with specific Ab to each binding site, including our KL-25 ab, to map the GP1. Specific binding to each epitope was obtained, and correct protein folding of GP1 in a non-trimeric, native state was concluded. These discoveries support the notion that valid GP1 expression is possible in our MFG-E8-GP1 fusion proteins expressed by HEK cells. However, epitope mapping of GP1 fusion proteins would be an exciting aspect to further research correct protein folding of the GP1.

4.3 PS binding of constructs

Several studies demonstrated that apoptotic cells express PS as an "eat-me-signal" on their outer cell membrane to elicit MFG-E8 binding for removal by MPs (133,141). In this context, we demonstrate that the MFG-E8-GP1/NP fusion proteins bind to PS expressing thymocytes. The induction of PS by staurosporine underlines its characteristic as an inductor of apoptosis (171,196). These findings were in line with Kranich et al. recently published study where the fusion protein MFG-E8-eGFP bound to apoptotic thymocytes via its C1C2 domain. Kranich et al. created the fusion protein with similar cloning and expression techniques using FLAG affinity chromatography as a purification method (169).

4.4 Induction of neutralizing antibodies

Our LCMV neutralisation assay confirms that the KL-25 ab has sufficient neutralisation power to LCMV$_{Arm}$ (26). This finding aligns with Ab studies for similar LCMV neutralisation assays (26,71). Kranich et al. demonstrated that living lymphocytes capture MFG-E8-eGFP marked EVs due to their characteristic of expressing PS (169). Therefore, we present MFG-E8 as a new in vivo pulsing method for exosomes. Different studies showed that peripherally injected exosomes produced by ag-pulsed DCs provide protective immunity against invading pathogens (178,179). In immunohistochemical staining, MFG-E8-eGFP accumulated in and around the GC, while eGFP only did not. Kranich et al. revealed that MFG-E8-eGFP generates an accelerated B-cell activation compared to eGFP only injection with increased specific ab titres to eGFP (Kranich et al. unpublished results). Our finding that MFG-E8-176-GP1 induces lower PFU/ml than the negative control MFG-E8-eGFP exhibits a positive trend towards the production of nAbs. This result supports studies from Kranich et al., where MFG-E8 is established to be a carrier of ag to FDCs, accelerating the humoral immune response. Histochemical staining of the MFG-E8-176N-GP1 binding to GC was unfortunately not part of the present thesis-project. Staining spleen sections for anti-GP1 and anti-MFG-E8 are future challenges to further characterize the properties of this molecule.

Measuring GP1 ab titres by ELISA is another critical experiment to make a definitive statement about quantification and the presence of Abs. It is also necessary to further quantify the neutralising capacity of the emerged nAbs in the serum of our immunised mice. We demonstrate that MFG-E8-176N-GP1 induces lower PFU than KL-25. However, potentially many proteases and complement factors in the serum influences the results. Studies show that early binding Ab preceded the production of nAbs (26,71). Complement-mediated lysis inhibited viral spread

during an earlier time point of LCMV (71). Purifying the serum for GP1-specific ab from different timepoint post immunisation and comparing their neutralising efficacy could have solved that issue.

Eschli et al. differentiated between the emergence of nAbs and binding Ab elegantly by applying a competitive binding assay to GP1 (26). They used a competition assay to evaluate the binding efficacy of nAbs in the serum of mice by ELISA. Thereby they noticed the emergence of nAbs from 30 d.p.i. in CTL-deficient mice with less impaired

GCs compared to WT-mice where nAbs occurs at 80 d.p.i. (26). We detected neutralisation of LCMV at 21 d.p. im. by serum of MFG-E8-176N-GP1 injected mice. This time point is 9 d before the earliest detection of nAbs described in the literature. The result demonstrates the potential acceleration of the humoral response induced by MFG-E8, but it requires further studies. Additionally, infecting the immunized mice with LCMV could have tested clinically if they developed protective immunity against the viral disease.

We can summarise that we have promising results, making further experiments compelling.

The fusion protein MFG-E8-260L-GP1 was ready to be purified, but could not be analysed for the sake of time. It would be interesting to see if immunisation with this protein could exhibit similar results.

Immunisation experiments with these MFG-E8-coupled constructs could hint at vaccine approaches towards HIV or Lassa fever virus. Both are still enormous burdens to mankind. The fusion protein MFG-E8-NP was cloned, transfected, and ready to be purified. A strong non-neutralising Ab response against the NP would have been expected (26). Therefore, it would be potentially better comparable than using MFG-E8-eGFP as control.

5 SUMMARY AND OUTLOOK

In the present doctoral thesis, recombinant fusion proteins based on MFG-E8 were produced. The aim was on the one hand to test or optimize the production of such proteins and on the other hand to apply and functionally analyze these proteins. In the short time available, it was possible to answer both main questions. Future projects should now deal with the in vivo application and evaluation of the proteins, and hopefully show that the use of such modified viral proteins leads to an increased and improved production of virus nAbs. Based on the pandemic situation lately, it became apparent that new vaccination approaches are still needed. Vaccination with recombinant proteins, which mixed with adjuvants leads to protection from SARS-CoV-2 infections, was recently approved by the EMA for the EU. Novavax's protein vaccine is based on the receptor binding domain of the SARS-CoV-2 virus and leads to abs and protection against infection. If our approach was used here, this receptor binding domain coupled to MFG-E8 eventually would be able to induce stronger and faster ab responses. But such studies would have to be performed in the future.

REFERENCES

1. Rowe WP, Murphy FA, Bergold GH, Casals J, Hotchin J, Johnson KM, et al. Arenoviruses: Proposed Name for a Newly Defined Virus Group. J Virol [Internet]. 1970;5(5):651–2. Available from: https://jvi.asm.org/content/5/5/651

2. Neuman BW, Adair BD, Burns JW, Milligan RA, Buchmeier MJ, Yeager M. Complementarity in the Supramolecular Design of Arenaviruses and Retroviruses Revealed by Electron Cryomicroscopy and Image Analysis. J Virol [Internet]. 2005 Mar 15;79(6):3822–30. Available from: http://jvi.asm.org/cgi/doi/10.1128/JVI.79.6.3822-3830.2005

3. Radoshitzky SR, Buchmeier MJ, Charrel RN, Clegg JCS, Gonzalez J-PJ, Günther S, et al. ICTV Virus Taxonomy Profile: Arenaviridae. J Gen Virol [Internet]. 2019 Aug 1;100(8):1200–1. Available from: https://www.microbiologyresearch.org/content/journal/jgv/10.1099/jgv.0.001280

4. Charrel RN, de Lamballerie X, Emonet S. Phylogeny of the genus Arenavirus. Curr Opin Microbiol. 2008;11(4):362–8.

5. Hallam SJ, Koma T, Maruyama J, Paessler S. Review of mammarenavirus biology and replication. Front Microbiol. 2018;9(AUG):1–8.

6. GONZALEZ JPJ, BOWEN MD, NICHOL ST, RICO-HESSE R. Genetic Characterization and Phylogeny of Sabiá Virus, an Emergent Pathogen in Brazil. Virology [Internet]. 1996 Jul;221(2):318–24. Available from: https://linkinghub.elsevier.com/retrieve/pii/S0042682296903815

7. Radoshitzky SR, Abraham J, Spiropoulou CF, Kuhn JH, Nguyen D, Li W, et al. Transferrin receptor 1 is a cellular receptor for New World haemorrhagic fever arenaviruses. Nature. 2007;446(7131):92–6.

8. Cao W, Henry MD, Borrow P, Yamada H, Elder JH, Ravkov E V., et al. Identification of α-dystroglycan as a receptor for lymphocytic choriomeningitis virus and Lassa fever virus. Science (80-). 1998;282(5396):2079–81.

9. Burri DJ, Ramos da Palma J, Seidah NG, Zanotti G, Cendron L, Pasquato A, et al. Differential Recognition of Old World and New World Arenavirus Envelope

Glycoproteins by Subtilisin Kexin Isozyme 1 (SKI-1)/Site 1 Protease (S1P). J Virol. 2013;87(11):6406–14.

10. Oldstone MBA, Campbell KP. Decoding arenavirus pathogenesis: Essential roles for alpha-dystroglycan-virus interactions and the immune response. Virology [Internet]. 2011 Mar;411(2):170–9. Available from: http://dx.doi.org/10.1016/j.virol.2010.11.023

11. Lecompte E, Fichet-Calvet E, Daffis S, Koulemou K, Sylla O, Kourouma F, et al. Mastomys natalensi s and Lassa Fever, West Africa. Emerg Infect Dis [Internet]. 2006;12(12):1971–4. Available from: http://wwwnc.cdc.gov/eid/article/12/12/06-0812_article.htm

12. Richmond JK, Baglole DJ. Lassa fever: Epidemiology, clinical features, and social consequences. Br Med J. 2003;327(7426):1271–5.

13. Martínez MJ, Salim AM, Hurtado JC, Kilgore PE. Ebola Virus Infection: Overview and Update on Prevention and Treatment. Infect Dis Ther. 2015;4(4):365–90.

14. Zapata JC, Cox D, Salvato MS. The Role of Platelets in the Pathogenesis of Viral Hemorrhagic Fevers. Powers AM, editor. PLoS Negl Trop Dis [Internet]. 2014 Jun 12;8(6):e2858. Available from: https://dx.plos.org/10.1371/journal.pntd.0002858

15. Cummins D. Acute Sensorineural Deafness in Lassa Fever. JAMA J Am Med Assoc [Internet]. 1990 Oct 24;264(16):2093. Available from: http://jama.jamanetwork.com/article.aspx?doi=10.1001/jama.1990.03450160063030

16. Mateer EJ, Huang C, Shehu NY, Paessler S. Lassa fever–induced sensorineural hearing loss: A neglected public health and social burden. Rabaa MA, editor. PLoS Negl Trop Dis [Internet]. 2018 Feb 22;12(2):e0006187. Available from: https://dx.plos.org/10.1371/journal.pntd.0006187

17. States U, Macneil A, Ströher U, Farnon E, Campbell S, Cannon D, et al. Solid Organ Transplant – associated. 2012;18(8).

18. Fischer SA, Graham MB, Kuehnert MJ, Kotton CN, Srinivasan A, Marty FM, et al. Transmission of lymphocytic choriomeningitis virus by organ transplantation.

N Engl J Med. 2006;354(21):2235–49.

19. Barton LL, Mets MB, Beauchamp CL. Lymphocytic choriomeningitis virus: Emerging fetal teratogen. Am J Obstet Gynecol [Internet]. 2002 Dec;187(6):1715–6. Available from: https://linkinghub.elsevier.com/retrieve/pii/S0002937802004970

20. Bonthius DJ. Lymphocytic Choriomeningitis Virus: A Prenatal and Postnatal Threat. Adv Pediatr [Internet]. 2009;56(1):75–86. Available from: http://dx.doi.org/10.1016/j.yapd.2009.08.007

21. Amstrong C, Lillie RD. Experimental Lymphocytic Choriomeningitis of Monkeys and Mice Produced by a Virus Encountered in Studies of the 1933 St . Louis Encephalitis Epidemic Authors (s): Charles Armstrong and R . D . Lillie Published by : Association of Schools of Public Healt. Public Health Rep. 1934;49(35):1019–27.

22. Baenziger J, Hengartner H, Zinkernagel RM, Cole GA. Induction or prevention of immunopathological disease by cloned cytotoxic T cell lines specific for lymphocytic choriomeningitis virus. Eur J Immunol [Internet]. 1986 Apr;16(4):387–93. Available from: http://www.ncbi.nlm.nih.gov/pubmed/3084281

23. Oldstone MBA. Biology and pathogenesis of lymphocytic choriomeningitis virus infection. Curr Top Microbiol Immunol. 2002;263:83–117.

24. Sevilla N, Kunz S, Holz A, Lewicki H, Homann D, Yamada H, et al. Immunosuppression and resultant viral persistence by specific viral targeting of dendritic cells. J Exp Med. 2000;192(9):1249–60.

25. Traub E. Special Articles. Lancet. 1952;260(6738):772–4.

26. Eschli B, Zellweger RM, Wepf A, Lang KS, Quirin K, Weber J, et al. Early Antibodies Specific for the Neutralizing Epitope on the Receptor Binding Subunit of the Lymphocytic Choriomeningitis Virus Glycoprotein Fail To Neutralize the Virus. J Virol. 2007;81(21):11650–7.

27. Traub E. Immunization of guinea pigs with a modified strain of lymphocytic choriomeningitis virus. J Exp Med [Internet]. 1937;66(3):317–24. Available from:

https://www.ncbi.nlm.nih.gov/pmc/articles/PMC2133621/

28. Ciurea A, Klenerman P, Hunziker L, Horvath E, Senn BM, Ochsenbein AF, et al. Viral persistence in vivo through selection of neutralizing antibody-escape variants. Proc Natl Acad Sci U S A. 2000;97(6):2749–54.

29. Traub E. EPIDEMIOLOGY OF LYMPHOCYTIC CHORIOMENINGITIS IN A MOUSE STOCK OBSERVED FOR FOUR YEARS. J Exp Med [Internet]. 1939 Jun 1;69(6):801–17. Available from: https://www.ncbi.nlm.nih.gov/pmc/articles/PMC2133762/

30. Jamieson BD, Somasundaram T, Ahmed R. Abrogation of tolerance to a chronic viral infection. J Immunol [Internet]. 1991 Nov 15;147(10):3521–9. Available from: https://www.jimmunol.org/content/147/10/3521

31. Jamieson BD, Ahmed R. T-cell tolerance: exposure to virus in utero does not cause a permanent deletion of specific T cells. Proc Natl Acad Sci [Internet]. 1988 Apr 1;85(7):2265–8. Available from: http://www.pnas.org/cgi/doi/10.1073/pnas.85.7.2265

32. Salvato M, Shimomaye E, Oldstone MBA. The primary structure of the lymphocytic choriomeningitis virus L gene encodes a putative RNA polymerase. Virology. 1989;169(2):377–84.

33. Salvato M, Shimomaye E, Southern P, Oldstone MBA. Virus-lymphocyte interactions IV. Molecular characterization of LCMV Armstrong (CTL+) small genomic segment and that of its variant, clone 13 (CTL-). Virology. 1988;164(2):517–22.

34. Sullivan BM, Emonet SF, Welch MJ, Lee AM, Campbell KP, De La Torre JC, et al. Point mutation in the glycoprotein of lymphocytic choriomeningitis virus is necessary for receptor binding, dendritic cell infection, and long-term persistence. Proc Natl Acad Sci U S A. 2011;108(7):2969–74.

35. Bergthaler A, Flatz L, Hegazy AN, Johnson S, Horvath E, Lohning M, et al. Viral replicative capacity is the primary determinant of lymphocytic choriomeningitis virus persistence and immunosuppression. Proc Natl Acad Sci [Internet]. 2010 Dec 14;107(50):21641–6. Available from:

http://www.pnas.org/cgi/doi/10.1073/pnas.1011998107

36. Capul AA, Perez M, Burke E, Kunz S, Buchmeier MJ, de la Torre JC. Arenavirus Z-Glycoprotein Association Requires Z Myristoylation but Not Functional RING or Late Domains. J Virol [Internet]. 2007 Sep;81(17):9451–60. Available from: https://journals.asm.org/doi/10.1128/JVI.00499-07

37. Hastie KM, Igonet S, Sullivan BM, Legrand P, Zandonatti MA, Robinson JE, et al. Crystal structure of the prefusion surface glycoprotein of the prototypic arenavirus LCMV. Nat Struct Mol Biol. 2016;23(6):513–21.

38. Eschli B, Quirin K, Wepf A, Weber J, Zinkernagel R, Hengartner H. Identification of an N-Terminal Trimeric Coiled-Coil Core within Arenavirus Glycoprotein 2 Permits Assignment to Class I Viral Fusion Proteins. J Virol [Internet]. 2006 Jun 15;80(12):5897–907. Available from: http://jvi.asm.org/cgi/doi/10.1128/JVI.00008-06

39. Kunz S, Rojek JM, Kanagawa M, Spiropoulou CF, Barresi R, Campbell KP, et al. Posttranslational Modification of -Dystroglycan, the Cellular Receptor for Arenaviruses, by the Glycosyltransferase LARGE Is Critical for Virus Binding. J Virol [Internet]. 2005 Nov 15;79(22):14282–96. Available from: http://jvi.asm.org/cgi/doi/10.1128/JVI.79.22.14282-14296.2005

40. Imperiali M, Thoma C, Pavoni E, Brancaccio A, Callewaert N, Oxenius A. O Mannosylation of -Dystroglycan Is Essential for Lymphocytic Choriomeningitis Virus Receptor Function. J Virol [Internet]. 2005 Nov 15;79(22):14297–308. Available from: http://jvi.asm.org/cgi/doi/10.1128/JVI.79.22.14297-14308.2005

41. Reissner C, Stahn J, Breuer D, Klose M, Pohlentz G, Mormann M, et al. Dystroglycan Binding to α-Neurexin Competes with Neurexophilin-1 and Neuroligin in the Brain. J Biol Chem [Internet]. 2014 Oct;289(40):27585–603. Available from: https://linkinghub.elsevier.com/retrieve/pii/S0021925820483978

42. Ervasti JM, Campbell KP. A role for the dystrophin-glycoprotein complex as a transmembrane linker between laminin and actin. J Cell Biol. 1993;122(4):809–23.

43. Kunz S. Receptor binding and cell entry of Old World arenaviruses reveal novel

aspects of virus – host interaction. Virology [Internet]. 2009;387(2):245–9. Available from: http://dx.doi.org/10.1016/j.virol.2009.02.042

44. Ervasti JM, Campbell KP. Membrane organization of the dystrophin-glycoprotein complex. Cell [Internet]. 1991 Sep;66(6):1121–31. Available from: https://linkinghub.elsevier.com/retrieve/pii/009286749190035W

45. Johnson EK, Li B, Yoon JH, Flanigan KM, Martin PT, Ervasti J, et al. Identification of New Dystroglycan Complexes in Skeletal Muscle. Gaetano C, editor. PLoS One [Internet]. 2013 Aug 8;8(8):e73224. Available from: https://dx.plos.org/10.1371/journal.pone.0073224

46. Blasdell KR, Becker SD, Hurst J, Begon M, Bennett M. Host Range and Genetic Diversity of Arenaviruses in Rodents, United Kingdom. Emerg Infect Dis [Internet]. 2008 Sep;14(9):1455–8. Available from: http://wwwnc.cdc.gov/eid/article/14/9/08-0209_article.htm

47. Borrow P, Oldstone MBA. Mechanism of Lymphocytic Choriomeningitis Virus Entry into Cells. Virology [Internet]. 1994 Jan;198(1):1–9. Available from: https://linkinghub.elsevier.com/retrieve/pii/S0042682284710014

48. Quirin K, Eschli B, Scheu I, Poort L, Kartenbeck J, Helenius A. Lymphocytic choriomeningitis virus uses a novel endocytic pathway for infectious entry via late endosomes. Virology [Internet]. 2008 Aug;378(1):21–33. Available from: https://linkinghub.elsevier.com/retrieve/pii/S0042682208002948

49. Di Simone C, Zandonatti MA, Buchmeier MJ. Acidic pH Triggers LCMV Membrane Fusion Activity and Conformational Change in the Glycoprotein Spike. Virology [Internet]. 1994 Feb;198(2):455–65. Available from: https://linkinghub.elsevier.com/retrieve/pii/S0042682284710579

50. Di Simone C, Buchmeier MJ. Kinetics and pH Dependence of Acid-Induced Structural Changes in the Lymphocytic Choriomeningitis Virus Glycoprotein Complex. Virology [Internet]. 1995 May;209(1):3–9. Available from: https://linkinghub.elsevier.com/retrieve/pii/S0042682285712251

51. Parsy M-L, Harlos K, Huiskonen JT, Bowden TA. Crystal Structure of Venezuelan Hemorrhagic Fever Virus Fusion Glycoprotein Reveals a Class 1

Postfusion Architecture with Extensive Glycosylation. J Virol [Internet]. 2013 Dec 1;87(23):13070–5. Available from: http://jvi.asm.org/lookup/doi/10.1128/JVI.02298-13

52. Igonet S, Vaney M-C, Vonrhein C, Bricogne G, Stura EA, Hengartner H, et al. X-ray structure of the arenavirus glycoprotein GP2 in its postfusion hairpin conformation. Proc Natl Acad Sci [Internet]. 2011 Dec 13;108(50):19967–72. Available from: http://www.pnas.org/cgi/doi/10.1073/pnas.1108910108

53. Meyer BJ, de la Torre JC, Southern PJ. Arenaviruses: genomic RNAs, transcription, and replication. Curr Top Microbiol Immunol [Internet]. 2002;262:139–57. Available from: http://www.ncbi.nlm.nih.gov/pubmed/11987804

54. Morin B, Coutard B, Lelke M, Ferron F, Kerber R, Jamal S, et al. The N-terminal domain of the arenavirus L protein is an RNA endonuclease essential in mRNA transcription. PLoS Pathog. 2010;6(9).

55. Meyer BJ, Southern PJ. Concurrent sequence analysis of 5' and 3' RNA termini by intramolecular circularization reveals 5' nontemplated bases and 3' terminal heterogeneity for lymphocytic choriomeningitis virus mRNAs. J Virol [Internet]. 1993 May;67(5):2621–7. Available from: https://jvi.asm.org/content/67/5/2621.long

56. Pflug A, Guilligay D, Reich S, Cusack S. Structure of influenza A polymerase bound to the viral RNA promoter. Nature [Internet]. 2014;516(7531):355–60. Available from: http://dx.doi.org/10.1038/nature14008

57. Sikora D, Rocheleau L, Brown EG, Pelchat M. Influenza A virus cap-snatches host RNAs based on their abundance early after infection. Virology [Internet]. 2017;509(April):167–77. Available from: http://dx.doi.org/10.1016/j.virol.2017.06.020

58. Burri DJ, Pasqual G, Rochat C, Seidah NG, Pasquato A, Kunz S. Molecular Characterization of the Processing of Arenavirus Envelope Glycoprotein Precursors by Subtilisin Kexin Isozyme-1/Site-1 Protease. J Virol. 2012;86(9):4935–46.

59. Beyer WR, Po D, Garten W, Laer D Von, Lenz O. Endoproteolytic Processing of the Lymphocytic Choriomeningitis Virus Glycoprotein by the Subtilase SKI-1 / S1P. 2003;77(5):2866–72.

60. Wright K. Post-translational processing of the glycoproteins of lymphocytic choriomeningitis virus. Virology [Internet]. 1990 Jul;177(1):175–83. Available from: https://linkinghub.elsevier.com/retrieve/pii/0042682290904713

61. Yang J, Goldstein JL, Hammer RE, Moon YA, Brown MS, Horton JD. Decreased lipid synthesis in livers of mice with disrupted Site-1 protease gene. Proc Natl Acad Sci U S A. 2001;98(24):13607–12.

62. Chen X, Shen J, Prywes R. The luminal domain of ATF6 senses endoplasmic reticulum (ER) stress and causes translocation of ATF6 from the er to the Golgi. J Biol Chem. 2002;277(15):13045–52.

63. Rojek JM, Pasqual G, Sanchez AB, Nguyen N-T, de la Torre J-C, Kunz S. Targeting the Proteolytic Processing of the Viral Glycoprotein Precursor Is a Promising Novel Antiviral Strategy against Arenaviruses. J Virol. 2010;84(1):573–84.

64. Popkin DL, Teijaro JR, Sullivan BM, Urata S, Rutschmann S. Hypomorphic mutation in the site-1 protease Mbtps1 endows resistance to persistent viral infection in a cell specific manner. 2012;9(3):212–22.

65. Parekh BS, Clinic S, Jolla L. Proteins of Lymphocytic Choriomeningitis Virus : Antigenic Topography of the Viral Glycoproteins. 1996;178(1986):168–78.

66. Wright KE, Salvato MS, Buchmeier MJ. Neutralizing epitopes of lymphocytic choriomeningitis virus are conformational and require both glycosylation and disulfide bonds for expression. Virology. 1989;171(2):417–26.

67. Borrow P. Characterization of Lymphocytic Choriomeningitis Virus-Binding Protein (s): a Candidate Cellular Receptor for the Virus. 1992;66(12):7270–81.

68. Sommerstein R, Flatz L, Remy MM, Malinge P, Igonet S, Rigo D, et al. Arenavirus Glycan Shield Promotes Neutralizing Antibody Evasion and Protracted Infection. 2015;1–25.

69. Weber EL, Buchmeier MJ. Fine Mapping of a Peptide Sequence Containing an

Antigenic Site Conserved among Arenaviruses. 1988;38:30–8.

70. Buchmeier MJ, Lewicki HA, Tomori O, Oldstone MBA. Monoclonal antibodies to lymphocytic choriomeningitis and pichinde viruses: Generation, characterization, and cross-reactivity with other arenaviruses. Virology. 1981;113(1):73–85.

71. Hangartner L, Zellweger RM, Giobbi M, Weber J, Eschli B, McCoy KD, et al. Nonneutralizing antibodies binding to the surface glycoprotein of lymphocytic choriomeningitis virus reduce early virus spread. J Exp Med [Internet]. 2006 Aug 7;203(8):2033–42. Available from: https://rupress.org/jem/article/203/8/2033/46523/Nonneutralizing-antibodies-binding-to-the-surface

72. Seiler P, Senn BM, Bründler MA, Zinkernagel RM, Hengartner H, Kalinke U. In vivo selection of neutralization-resistant virus variants but no evidence of B cell tolerance in lymphocytic choriomeningitis virus carrier mice expressing a transgenic virus-neutralizing antibody. J Immunol [Internet]. 1999 Apr 15;162(8):4536–41. Available from: https://www.jimmunol.org/content/162/8/4536%0D

73. Kunz S, Sevilla N, Rojek JM, Oldstone MBA. Use of alternative receptors different than α-dystroglycan by selected isolates of lymphocytic choriomeningitis virus. Virology. 2004;325(2):432–45.

74. Smelt SC, Borrow P, Kunz S, Cao W, Tishon A, Lewicki H, et al. Differences in Affinity of Binding of Lymphocytic Choriomeningitis Virus Strains to the Cellular Receptor -Dystroglycan Correlate with Viral Tropism and Disease Kinetics. J Virol. 2001;75(1):448–57.

75. Smelt SC, Borrow P, Kunz S, Cao WEI, Tishon A, Lewicki H, et al. Differences in Affinity of Binding of Lymphocytic Choriomeningitis Virus Strains to the Cellular Receptor ⌣ -Dystroglycan Correlate with Viral Tropism and Disease Kinetics †. 2001;75(1):448–57.

76. Fedeli C, Torriani G, Galan-Navarro C, Moraz M-L, Moreno H, Gerold G, et al. Axl Can Serve as Entry Factor for Lassa Virus Depending on the Functional Glycosylation of Dystroglycan. J Virol. 2017;92(5):1–22.

77. Salvato M, Borrow P, Shimomaye E, Oldstone MB. Molecular basis of viral persistence: a single amino acid change in the glycoprotein of lymphocytic choriomeningitis virus is associated with suppression of the antiviral cytotoxic T-lymphocyte response and establishment of persistence. J Virol. 1991;65(4):1863–9.

78. Mueller SN, Matloubian M, Clemens DM, Sharpe AH, Freeman GJ, Gangappa S, et al. Viral targeting of fibroblastic reticular cells contributes to immunosuppression and persistence during chronic infection. Proc Natl Acad Sci U S A. 2007;104(39):15430–5.

79. Sevilla N, McGavern DB, Teng C, Kunz S, Oldstone MBA. Viral targeting of hematopoietic progenitors and inhibition of DC maturation as a dual strategy for immune subversion. J Clin Invest [Internet]. 2004 Mar 1;113(5):737–45. Available from: http://www.jci.org/articles/view/20243

80. Parajuli P, Mosley RL, Pisarev V, Chavez J, Ulrich A, Varney M, et al. Flt3 ligand and granulocyte-macrophage colony-stimulating factor preferentially expand and stimulate different dendritic and T-cell subsets. Exp Hematol [Internet]. 2001 Oct;29(10):1185–93. Available from: http://www.ncbi.nlm.nih.gov/pubmed/9286334

81. Brooks DG, Trifilo MJ, Edelmann KH, Teyton L, McGavern DB, Oldstone MBA. Interleukin-10 determines viral clearance or persistence in vivo. Nat Med. 2006;12(11):1301–9.

82. Brooks DG, Ha SJ, Elsaesser H, Sharpe AH, Freeman GJ, Oldstone MBA. IL-10 and PD-L1 operate through distinct pathways to suppress T-cell activity during persistent viral infection. Proc Natl Acad Sci U S A. 2008;105(51):20428–33.

83. Brown JA, Dorfman DM, Ma F-R, Sullivan EL, Munoz O, Wood CR, et al. Blockade of Programmed Death-1 Ligands on Dendritic Cells Enhances T Cell Activation and Cytokine Production. J Immunol. 2003;170(3):1257–66.

84. Richter K, Agnellini P, Oxenius A. On the role of the inhibitory receptor LAG-3 in acute and chronic LCMV infection. Int Immunol. 2009;22(1):13–23.

85. Balkhi MY, Wittmann G, Xiong F, Junghans RP. YY1 Upregulates Checkpoint Receptors and Downregulates Type I Cytokines in Exhausted, Chronically Stimulated Human T Cells. iScience [Internet]. 2018;2:105–22. Available from: https://doi.org/10.1016/j.isci.2018.03.009

86. Wherry EJ. T cell exhaustion. Nat Immunol [Internet]. 2011 Jun 18;12(6):492–9. Available from: http://dx.doi.org/10.1038/ni.2035

87. Brooks DG, Lee AM, Elsaesser H, McGavern DB, Oldstone MBA. IL-10 blockade facilitates DNA vaccine-induced T cell responses and enhances clearance of persistent virus infection. J Exp Med. 2008;205(3):533–41.

88. Ejrnaes M, Filippi CM, Martinic MM, Ling EM, Togher LM, Crotty S, et al. Resolution of a chronic viral infection after interleukin-10 receptor blockade. J Exp Med [Internet]. 2006 Oct 30;203(11):2461–72. Available from: https://rupress.org/jem/article/203/11/2461/46352/Resolution-of-a-chronic-viral-infection-after

89. Barber DL, Wherry EJ, Masopust D, Zhu B, Allison JP, Sharpe AH, et al. Restoring function in exhausted CD8 T cells during chronic viral infection. Nature. 2006;439(7077):682–7.

90. Blackburn SD, Shin H, Haining WN, Zou T, Workman CJ, Polley A, et al. Coregulation of CD8+ T cell exhaustion by multiple inhibitory receptors during chronic viral infection. Nat Immunol [Internet]. 2009 Jan 30;10(1):29–37. Available from: http://www.nature.com/articles/ni.1679

91. Elsaesser H, Sauer K, Brooks DG. IL-21 is required to control chronic viral infection. Science (80-). 2009;324(5934):1569–72.

92. Fallet B, Hao Y, Florova M, Cornille K, de los Aires AV, Girelli Zubani G, et al. Chronic Viral Infection Promotes Efficient Germinal Center B Cell Responses. Cell Rep. 2020;30(4):1013-1026.e7.

93. Ciurea A, Hunziker L, Klenerman P, Hengartner H, Zinkernagel RM. Impairment of CD4+ T cell responses during chronic virus infection prevents neutralizing antibody responses against virus escape mutants. J Exp Med. 2001;193(3):297–305.

94. Moskophidis D, Pircher H, Ciernik I, Odermatt B, Hengartner H, Zinkernagel RM. Suppression of virus-specific antibody production by CD8+ class I-restricted antiviral cytotoxic T cells in vivo. J Virol. 1992;66(6):3661–8.

95. Wei X, Decker JM, Wang S, Hui H. Antibody neutralization and escape by HIV-1. 2003;837(1988):835–7.

96. Choi YS, Kageyama R, Eto D, Escobar TC, Johnston RJ, Monticelli L, et al. ICOS Receptor Instructs T Follicular Helper Cell versus Effector Cell Differentiation via Induction of the Transcriptional Repressor Bcl6. Immunity [Internet]. 2011 Jun;34(6):932–46. Available from: http://dx.doi.org/10.1016/j.immuni.2011.03.023

97. Baumjohann D, Okada T, Ansel KM. Cutting Edge: Distinct Waves of BCL6 Expression during T Follicular Helper Cell Development. J Immunol [Internet]. 2011 Sep 1;187(5):2089–92. Available from: http://www.jimmunol.org/lookup/doi/10.4049/jimmunol.1101393

98. Kerfoot SM, Yaari G, Patel JR, Johnson KL, Gonzalez DG, Kleinstein SH, et al. Germinal Center B Cell and T Follicular Helper Cell Development Initiates in the Interfollicular Zone. Immunity [Internet]. 2011;34(6):947–60. Available from: http://dx.doi.org/10.1016/j.immuni.2011.03.024

99. Nurieva RI, Chung Y, Martinez GJ, Yang XO, Tanaka S, Matskevitch TD, et al. Bcl6 Mediates the Development of T Follicular Helper Cells. Science (80-) [Internet]. 2009 Aug 21;325(5943):1001–5. Available from: https://www.sciencemag.org/lookup/doi/10.1126/science.1176676

100. Johnston RJ, Poholek AC, DiToro D, Yusuf I, Eto D, Barnett B, et al. Bcl6 and Blimp-1 are reciprocal and antagonistic regulators of T follicular helper cell differentiation. Science (80-). 2009;325(5943):1006–10.

101. Yang Shih T-A, Meffre E, Roederer M, Nussenzweig MC. Role of BCR affinity in T cell–dependent antibody responses in vivo. Nat Immunol [Internet]. 2002 Jun 20;3(6):570–5. Available from: http://www.nature.com/articles/ni803

102. Schwickert TA, Victora GD, Fooksman DR, Kamphorst AO, Mugnier MR, Gitlin AD, et al. A dynamic T cell-limited checkpoint regulates affinity-dependent B cell

entry into the germinal center. J Exp Med. 2011;208(6):1243–52.

103. Victora GD, Schwickert TA, Fooksman DR, Kamphorst AO, Meyer-Hermann M, Dustin ML, et al. Germinal center dynamics revealed by multiphoton microscopy with a photoactivatable fluorescent reporter. Cell [Internet]. 2010;143(4):592–605. Available from: http://dx.doi.org/10.1016/j.cell.2010.10.032

104. Allen CDC, Ansel KM, Low C, Lesley R, Tamamura H, Fujii N, et al. Germinal center dark and light zone organization is mediated by CXCR4 and CXCR5. Nat Immunol. 2004;5(9):943–52.

105. Kitano M, Moriyama S, Ando Y, Hikida M, Mori Y, Kurosaki T, et al. Bcl6 Protein Expression Shapes Pre-Germinal Center B Cell Dynamics and Follicular Helper T Cell Heterogeneity. Immunity [Internet]. 2011;34(6):961–72. Available from: http://dx.doi.org/10.1016/j.immuni.2011.03.025

106. Bannard O, Horton RM, Allen CDC, An J, Nagasawa T, Cyster JG. Germinal center centroblasts transition to a centrocyte phenotype according to a timed program and depend on the dark zone for effective selection. Immunity [Internet]. 2013;39(5):912–24. Available from: http://dx.doi.org/10.1016/j.immuni.2013.08.038

107. Caron G, Le Gallou S, Lamy T, Tarte K, Fest T. CXCR4 Expression Functionally Discriminates Centroblasts versus Centrocytes within Human Germinal Center B Cells. J Immunol. 2009;182(12):7595–602.

108. Green JA, Suzuki K, Cho B, Willison LD, Palmer D, Allen CDC, et al. The sphingosine 1-phosphate receptor S1P2 maintains the homeostasis of germinal center B cells and promotes niche confinement. Nat Immunol [Internet]. 2011 Jul 5;12(7):672–80. Available from: http://dx.doi.org/10.1038/ni.2047

109. Voigt I, Camacho SA, de Boer BA, Lipp M, Förster R, Berek C. CXCR5-deficient mice develop functional germinal centers in the splenic T cell zone. Eur J Immunol [Internet]. 2000 Feb;30(2):560–7. Available from: https://www.ncbi.nlm.nih.gov/pubmed/10671212

110. Nie Y, Waite J, Brewer F, Sunshine M, Littman DR, Zou Y. The Role of CXCR4 in Maintaining Peripheral B Cell Compartments and Humoral Immunity. J Exp

Med [Internet]. 2004 Nov 1;200(9):1145–56. Available from: https://rupress.org/jem/article/200/9/1145/52441/The-Role-of-CXCR4-in-Maintaining-Peripheral-B-Cell

111. Huang C, Gonzalez DG, Cote CM, Jiang Y, Hatzi K, Teater M, et al. The BCL6 RD2 Domain Governs Commitment of Activated B Cells to Form Germinal Centers. Cell Rep [Internet]. 2014;8(5):1497–508. Available from: http://dx.doi.org/10.1016/j.celrep.2014.07.059

112. Ye BH, Cattoretti G, Shen Q, Zhang J, Hawe N, Waard R de, et al. The BCL-6 proto-oncogene controls germinal-centre formation and Th2-type inflammation. Nat Genet [Internet]. 1997 Jun;16(2):161–70. Available from: http://www.nature.com/articles/ng0697-161

113. Liu YJ, Malisan F, de Bouteiller O, Guret C, Lebecque S, Banchereau J, et al. Within Germinal Centers, Isotype Switching of Immunoglobulin Genes Occurs after the Onset of Somatic Mutation. Immunity [Internet]. 1996 Mar;4(3):241–50. Available from: https://linkinghub.elsevier.com/retrieve/pii/S107476130080432X

114. Muramatsu M, Kinoshita K, Fagarasan S, Yamada S, Shinkai Y, Honjo T. Class Switch Recombination and Hypermutation Require Activation-Induced Cytidine Deaminase (AID), a Potential RNA Editing Enzyme. Cell [Internet]. 2000 Sep;102(5):553–63. Available from: https://linkinghub.elsevier.com/retrieve/pii/S0092867400000787

115. Högerkorp C-M, Borrebaeck CAK. The Human CD77 − B Cell Population Represents a Heterogeneous Subset of Cells Comprising Centroblasts, Centrocytes, and Plasmablasts, Prompting Phenotypical Revision. J Immunol [Internet]. 2006 Oct 1;177(7):4341–9. Available from: http://www.jimmunol.org/lookup/doi/10.4049/jimmunol.177.7.4341

116. Roco JA, Mesin L, Binder SC, Nefzger C, Gonzalez-Figueroa P, Canete PF, et al. Class-Switch Recombination Occurs Infrequently in Germinal Centers. Immunity [Internet]. 2019 Aug;51(2):337-350.e7. Available from: https://doi.org/10.1016/j.immuni.2019.07.001

117. Masani S, Han L, Yu K. Apurinic/Apyrimidinic Endonuclease 1 Is the Essential

Nuclease during Immunoglobulin Class Switch Recombination. Mol Cell Biol [Internet]. 2013 Apr 1;33(7):1468–73. Available from: http://mcb.asm.org/cgi/doi/10.1128/MCB.00026-13

118. Stavnezer J, Linehan EK, Thompson MR, Habboub G, Ucher AJ, Kadungure T, et al. Differential expression of APE1 and APE2 in germinal centers promotes error-prone repair and A:T mutations during somatic hypermutation. Proc Natl Acad Sci [Internet]. 2014 Jun 24;111(25):9217–22. Available from: http://www.pnas.org/cgi/doi/10.1073/pnas.1405590111

119. Hanayama R, Tanaka M, Miyasaka K, Aozasa K, Koike M, Uchiyama Y. Autoimmune Disease and Impaired Uptake of Apoptotic Cells in MFG-E8 – Deficient Mice. Science (80-). 2004;VOl 304:1147–50.

120. Meyer-Hermann M, Mohr E, Pelletier N, Zhang Y, Victora GD, Toellner K-M. A Theory of Germinal Center B Cell Selection, Division, and Exit. Cell Rep [Internet]. 2012 Jul;2(1):162–74. Available from: https://linkinghub.elsevier.com/retrieve/pii/S2211124712001350

121. De Silva NS, Klein U. Dynamics of B cells in germinal centres. Nat Rev Immunol [Internet]. 2015;15(3):137–48. Available from: http://dx.doi.org/10.1038/nri3804

122. Kranich J, Krautler NJ. How follicular dendritic cells shape the B-cell antigenome. Front Immunol. 2016;7(JUN).

123. Ferguson AR, Youd ME, Corley RB. Marginal zone B cells transport and deposit IgM-containing immune complexes onto follicular dendritic cells. Int Immunol. 2004;16(10):1411–22.

124. Aguzzi A, Kranich J, Krautler NJ. Follicular dendritic cells: Origin, phenotype, and function in health and disease. Trends Immunol [Internet]. 2014;35(3):105–13. Available from: http://dx.doi.org/10.1016/j.it.2013.11.001

125. Junt T, Moseman EA, Iannacone M, Massberg S, Lang PA, Boes M, et al. Subcapsular sinus macrophages in lymph nodes clear lymph-borne viruses and present them to antiviral B cells. Nature. 2007;450(7166):110–4.

126. Park C, Kehrl JH. An integrin/MFG-E8 shuttle loads HIV-1 viral-like particles onto follicular dendritic cells in mouse lymph node. Elife. 2019;8:1–26.

127. Phan TG, Grigorova I, Okada T, Cyster JG. Subcapsular encounter and complement-dependent transport of immune complexes by lymph node B cells. Nat Immunol. 2007;8(9):992–1000.

128. Phan TG, Green JA, Xu Y, Cyster JG. Immune complex relay by subcapsular sinus macrophages and noncognate B cells drives antibody affinity maturation. Nat Immunol [Internet]. 2009;10(7):786–96. Available from: http://dx.doi.org/10.1038/ni.1745

129. Roozendaal R, Carroll MC. Complement receptors CD21 and CD35 in humoral immunity. Immunol Rev. 2007;219(1):157–66.

130. Sewald X, Ladinsky MS, Uchil PD, Beloor J, Pi R, Herrmann C, et al. Retroviruses use CD169-mediated trans-infection of permissive lymphocytes to establish infection. Science (80-). 2015;350(6260):563–7.

131. Bhalla DK, Braun J, Karnovsky MJ. Lymphocyte surface and cytoplasmic changes associated with translational motility and spontaneous capping of Ig. J Cell Sci. 1979;VOL 39:137–47.

132. Chen C-W, Saubi N, Joseph-Munné J. Design Concepts of Virus-Like Particle-Based HIV-1 Vaccines. Front Immunol [Internet]. 2020 Sep 30;11(September):1–8. Available from: https://www.frontiersin.org/article/10.3389/fimmu.2020.573157/full

133. Kranich J, Krautler NJ, Heinen E, Polymenidou M, Bridel C, Schildknecht A, et al. Follicular dendritic cells control engulfment of apoptotic bodies by secreting Mfge8. J Exp Med [Internet]. 2008;205(6):1293–302. Available from: http://www.jem.org/lookup/doi/10.1084/jem.20071019

134. Burgess BL, Abrams TA, Nagata S, Hall MO. MFG-E8 in the retina and retinal pigment epithelium of rat and mouse. 2006;(October):1437–47.

135. Miyasaka K, Hanayama R, Tanaka M, Nagata S. Expression of milk fat globule epidermal growth factor?8 in immature dendritic cells for engulfment of apoptotic cells. Eur J Immunol [Internet]. 2004 May;34(5):1414–22. Available from: http://doi.wiley.com/10.1002/eji.200424930

136. Hanayama R, Nagata S. Impaired involution of mammary glands in the absence

of milk fat globule EGF factor 8. 2005;

137. Chabannon C, The C De, Machy P. Identification of a factor that links apoptotic cells to phagocytes. 2002;417(May):4–9.

138. Hanayama R, Tanaka M, Miwa K, Shinohara A, Iwamatsu A, Nagata S. Identification of a factor that links apoptotic cells to phagocytes. Nature. 2002;417(6885):182–7.

139. Hanayama R, Miyasaka K, Nakaya M. MFG-E8-Dependent Clearance of Apoptotic Cells , and Autoimmunity. 2006;9:162–72.

140. Aziz M, Jacob A, Matsuda A, Wang P. Review: milk fat globule-EGF factor 8 expression, function and plausible signal transduction in resolving inflammation. Apoptosis [Internet]. 2011 Nov 7;16(11):1077–86. Available from: http://link.springer.com/10.1007/s10495-011-0630-0

141. Borisenko GG, Iverson SL, Ahlberg S, Kagan VE, Fadeel B. Milk fat globule epidermal growth factor 8 (MFG-E8) binds to oxidized phosphatidylserine: implications for macrophage clearance of apoptotic cells. Cell Death Differ [Internet]. 2004 Aug 19;11(8):943–5. Available from: http://www.nature.com/articles/4401421

142. Yamaguchi H, Fujimoto T, Nakamura S, Ohmura K, Mimori T, Matsuda F, et al. Aberrant splicing of the milk fat globule-EGF factor 8 (MFG-E8) gene in human systemic lupus erythematosus. Eur J Immunol. 2010;40(6):1778–85.

143. Zaitseva E, Zaitsev E, Melikov K, Margolis LB, Melikyan GB, Chernomordik L V, et al. Fusion Stage of HIV-1 Entry Depends on Virus- Induced Cell Surface Exposure of Article Fusion Stage of HIV-1 Entry Depends on Virus-Induced Cell Surface Exposure of Phosphatidylserine. Cell Host Microbe [Internet]. 2017;22(1):99-110.e7. Available from: http://dx.doi.org/10.1016/j.chom.2017.06.012

144. Moller-Tank S, Maury W. Phosphatidylserine receptors: Enhancers of enveloped virus entry and infection. Virology [Internet]. 2014;468:565–80. Available from: http://dx.doi.org/10.1016/j.virol.2014.09.009

145. Morizono K, Chen ISY. Role of Phosphatidylserine Receptors in Enveloped

Virus Infection. J Virol. 2014;88(8):4275–90.

146. Oshima K, Aoki N, Negi M, Kishi M, Kitajima K, Matsuda T. Lactation-Dependent Expression of an mRNA Splice Variant with an Exon for a MultiplyO-Glycosylated Domain of Mouse Milk Fat Globule Glycoprotein MFG-E8. Biochem Biophys Res Commun [Internet]. 1999 Jan;254(3):522–8. Available from: https://linkinghub.elsevier.com/retrieve/pii/S0006291X98901073

147. Kodigepalli KM, Bowers K, Sharp A, Nanjundan M. Roles and regulation of phospholipid scramblases. FEBS Lett [Internet]. 2015;589(1):3–14. Available from: http://dx.doi.org/10.1016/j.febslet.2014.11.036

148. Nagata S, Sakuragi T, Segawa K. Flippase and scramblase for phosphatidylserine exposure. Curr Opin Immunol [Internet]. 2020 Feb;62:31–8. Available from: https://doi.org/10.1016/j.coi.2019.11.009

149. Yamaguchi H, Takagi J, Miyamae T, Yokota S, Fujimoto T, Nakamura S, et al. Milk fat globule EGF factor 8 in the serum of human patients of systemic lupus erythematosus. J Leukoc Biol [Internet]. 2008 May;83(5):1300–7. Available from: http://doi.wiley.com/10.1189/jlb.1107730

150. Segawa K, Nagata S. An Apoptotic "Eat Me" Signal: Phosphatidylserine Exposure. Trends Cell Biol [Internet]. 2015;25(11):639–50. Available from: http://dx.doi.org/10.1016/j.tcb.2015.08.003

151. Toda S, Hanayama R, Nagata S. Two-Step Engulfment of Apoptotic Cells. Mol Cell Biol [Internet]. 2012 Jan 1;32(1):118–25. Available from: http://mcb.asm.org/cgi/doi/10.1128/MCB.05993-11

152. Turner DL, Korneev D V, Purdy JG, de Marco A, Mathias RA. The host exosome pathway underpins biogenesis of the human cytomegalovirus virion. Elife [Internet]. 2020 Sep 10;9:1–29. Available from: https://elifesciences.org/articles/58288

153. Véron P, Segura E, Sugano G, Amigorena S, Théry C. Accumulation of MFG-E8/lactadherin on exosomes from immature dendritic cells. Blood Cells, Mol Dis [Internet]. 2005 Sep;35(2):81–8. Available from: https://linkinghub.elsevier.com/retrieve/pii/S1079979605000628

154. Segura E, Nicco C, Lombard B, Véron P, Raposo G, Batteux F, et al. ICAM-1 on exosomes from mature dendritic cells is critical for efficient naive T-cell priming. Blood [Internet]. 2005 Jul 1;106(1):216–23. Available from: https://ashpublications.org/blood/article/106/1/216/103155/ICAM1-on-exosomes-from-mature-dendritic-cells-is

155. Lindenbergh MFS, Stoorvogel W. Antigen Presentation by Extracellular Vesicles from Professional Antigen-Presenting Cells. Annu Rev Immunol. 2018;36(1).

156. Zitvogel L, Regnault A, Lozier A, Wolfers J, Flament C, Tenza D, Ricciardi-Castagnoli P, Raposo G AS, Zitvogel L, Regnault A, Lozier A, Wolfers J, Flament C, et al. Eradication of established murine tumors using a novel cell-free vaccine: dendritic cell-derived exosomes. Nat Med [Internet]. 1998;4(5):594–600. Available from: http://www.ncbi.nlm.nih.gov/pubmed/9585234%0Ahttp://www.nature.com/natur emedicine

157. Gould SJ. As we wait: coping with an imperfect nomenclature for extracellular vesicles. 2013;1:3–5.

158. Kowal J, Arras G, Colombo M, Jouve M, Morath JP, Primdal-Bengtson B, et al. Proteomic comparison defines novel markers to characterize heterogeneous populations of extracellular vesicle subtypes. Proc Natl Acad Sci [Internet]. 2016 Feb 23;113(8):E968–77. Available from: http://www.pnas.org/lookup/doi/10.1073/pnas.1521230113

159. Théry C, Amigorena S, Raposo G, Clayton A. Isolation and Characterization of Exosomes from Cell Culture Supernatants and Biological Fluids. Curr Protoc Cell Biol. 2006;30(1):3.22.1-3.22.29.

160. O'Dea KP, Tan YY, Shah S, V Patel B, C Tatham K, Wilson MR, et al. Monocytes mediate homing of circulating microvesicles to the pulmonary vasculature during low-grade systemic inflammation. J Extracell Vesicles [Internet]. 2020;9(1). Available from: https://doi.org/10.1080/20013078.2019.1706708

161. Baietti MF, Zhang Z, Mortier E, Melchior A, Degeest G, Geeraerts A, et al. Syndecan-syntenin-ALIX regulates the biogenesis of exosomes. Nat Cell Biol [Internet]. 2012;14(7):677–85. Available from:

http://dx.doi.org/10.1038/ncb2502

162. Valadi H, Ekström K, Bossios A, Sjöstrand M, Lee JJ, Lötvall JO. Exosome-mediated transfer of mRNAs and microRNAs is a novel mechanism of genetic exchange between cells. Nat Cell Biol [Internet]. 2007 Jun 7;9(6):654–9. Available from: http://www.nature.com/articles/ncb1596

163. Skog J, Würdinger T, van Rijn S, Meijer DH, Gainche L, Curry WT, et al. Glioblastoma microvesicles transport RNA and proteins that promote tumour growth and provide diagnostic biomarkers. Nat Cell Biol [Internet]. 2008 Dec 16;10(12):1470–6. Available from: http://www.nature.com/articles/ncb1800

164. Gu J, Wu J, Fang D, Qiu Y, Zou X, Jia X, et al. Exosomes cloak the virion to transmit Enterovirus 71 non-lytically. Virulence [Internet]. 2020 Jan 1;11(1):32–8. Available from: https://doi.org/10.1080/21505594.2019.1705022

165. Andreu Z, MaríaYáñez-Mó. Tetraspanins in Extracellular Vesicle Formation and Function. Front Immunol [Internet]. 2014 Sep 16;5(September):1–12. Available from: http://journal.frontiersin.org/article/10.3389/fimmu.2014.00442/abstract

166. Denzer K, van Eijk M, Kleijmeer MJ, Jakobson E, de Groot C, J. Geuze H. Follicular Dendritic Cells Carry MHC Class II-Expressing Microvesicles at Their Surface. J Immunol [Internet]. 2000 Aug 1;165(3):1259–65. Available from: http://www.jimmunol.org/lookup/doi/10.4049/jimmunol.165.3.1259

167. Montecalvo A, Shufesky WJ, Beer Stolz D, Sullivan MG, Wang Z, Divito SJ, et al. Exosomes As a Short-Range Mechanism to Spread Alloantigen between Dendritic Cells during T Cell Allorecognition. J Immunol. 2008;180(5):3081–90.

168. Morelli AE, Larregina AT, Shufesky WJ, Sullivan MLG, Stolz DB, Papworth GD, et al. Endocytosis, intracellular sorting, and processing of exosomes by dendritic cells. Blood [Internet]. 2004 Nov 15;104(10):3257–66. Available from: http://dx.doi.org/10.1182/blood-2004-03-0824

169. Kranich J, Chlis NK, Rausch L, Latha A, Schifferer M, Kurz T, et al. In vivo identification of apoptotic and extracellular vesicle-bound live cells using image-based deep learning. J Extracell Vesicles [Internet]. 2020;9(1). Available from: https://doi.org/10.1080/20013078.2020.1792683

170. Näslund TI, Gehrmann U, Qazi KR, Karlsson MCI, Gabrielsson S. Dendritic Cell–Derived Exosomes Need To Activate Both T and B Cells To Induce Antitumor Immunity. J Immunol [Internet]. 2013 Mar 15;190(6):2712–9. Available from: http://www.jimmunol.org/lookup/doi/10.4049/jimmunol.1203082

171. Winau F, Weber S, Sad S, De Diego J, Hoops SL, Breiden B, et al. Apoptotic vesicles crossprime CD8 T cells and protect against tuberculosis. Immunity. 2006;24(1):105–17.

172. Segura E, Amigorena S, Théry C. Mature dendritic cells secrete exosomes with strong ability to induce antigen-specific effector immune responses. Blood Cells, Mol Dis [Internet]. 2005 Sep;35(2):89–93. Available from: https://linkinghub.elsevier.com/retrieve/pii/S107997960500063X

173. Segura E, Guérin C, Hogg N, Amigorena S, Théry C. CD8 + Dendritic Cells Use LFA-1 to Capture MHC-Peptide Complexes from Exosomes In Vivo. J Immunol [Internet]. 2007 Aug 1;179(3):1489–96. Available from: http://www.jimmunol.org/lookup/doi/10.4049/jimmunol.179.3.1489

174. You Y, Zhao H, Wang Y, Carter RH. Cutting Edge: Primary and Secondary Effects of CD19 Deficiency on Cells of the Marginal Zone. J Immunol [Internet]. 2009 Jun 15;182(12):7343–7. Available from: http://www.jimmunol.org/lookup/doi/10.4049/jimmunol.0804295

175. Papp K, Végh P, Prechl J, Kerekes K, Kovács J, Csikós G, et al. B lymphocytes and macrophages release cell membrane deposited C3-fragments on exosomes with T cell response-enhancing capacity. Mol Immunol. 2008;45(8):2343–51.

176. Clayton A, Clayton A, Harris CL, Court J, Mason MD, Paul B. Antigen-presenting cell exosomes are protected from complement-mediated lysis by expression of CD55 and CD59. 2003;522–31.

177. Qazi KR, Gehrmann U, Domange Jordö E, Karlsson MCI, Gabrielsson S. Antigen-loaded exosomes alone induce Th1-type memory through a B-cell-dependent mechanism. Blood [Internet]. 2009 Mar 19;113(12):2673–83. Available from: http://www.ncbi.nlm.nih.gov/pubmed/19176319

178. Colino J, Snapper CM. Dendritic Cell-Derived Exosomes Express a Streptococcus pneumoniae Capsular Polysaccharide Type 14 Cross-Reactive Antigen That Induces Protective Immunoglobulin Responses against Pneumococcal Infection in Mice. Infect Immun [Internet]. 2007 Jan;75(1):220–30. Available from: https://iai.asm.org/content/75/1/220

179. del Cacho E, Gallego M, Lee SH, Lillehoj HS, Quilez J, Lillehoj EP, et al. Induction of protective immunity against Eimeria tenella infection using antigen-loaded dendritic cells (DC) and DC-derived exosomes. Vaccine [Internet]. 2011 May;29(21):3818–25. Available from: http://dx.doi.org/10.1016/j.vaccine.2011.03.022

180. Yang X, Meng S, Jiang H, Zhu C, Wu W. Exosomes Derived from Immature Bone Marrow Dendritic Cells Induce Tolerogenicity of Intestinal Transplantation in Rats. J Surg Res [Internet]. 2011 Dec;171(2):826–32. Available from: http://dx.doi.org/10.1016/j.jss.2010.05.021

181. Verma NK, Kelleher D. Not Just an Adhesion Molecule: LFA-1 Contact Tunes the T Lymphocyte Program. J Immunol [Internet]. 2017 Aug 15;199(4):1213–21. Available from: http://www.jimmunol.org/lookup/doi/10.4049/jimmunol.1700495

182. Verma NK, Dempsey E, Long A, Davies A, Barry SP, Fallon PG, et al. Leukocyte Function-associated Antigen-1/Intercellular Adhesion Molecule-1 Interaction Induces a Novel Genetic Signature Resulting in T-cells Refractory to Transforming Growth Factor-β Signaling. J Biol Chem [Internet]. 2012 Aug;287(32):27204–16. Available from: https://linkinghub.elsevier.com/retrieve/pii/S0021925820479189

183. Pang X-L, Wang Z-G, Liu L, Feng Y-H, Wang J-X, Xie H-C, et al. Immature dendritic cells derived exosomes promotes immune tolerance by regulating T cell differentiation in renal transplantation. Aging (Albany NY) [Internet]. 2019;11(20):8911–24. Available from: http://www.ncbi.nlm.nih.gov/pubmed/31655796

184. Ma B, Yang J-Y, Song W, Ding R, Zhang Z, Ji H, et al. Combining Exosomes Derived from Immature DCs with Donor Antigen-Specific Treg Cells Induces Tolerance in a Rat Liver Allograft Model. Sci Rep [Internet]. 2016 Dec

19;6(1):32971. Available from: http://dx.doi.org/10.1038/srep32971

185. Nolte-'t Hoen ENM, Buschow SI, Anderton SM, Stoorvogel W, Wauben MHM. Activated T cells recruit exosomes secreted by dendritic cells via LFA-1. Blood [Internet]. 2009 Feb 26;113(9):1977–81. Available from: https://ashpublications.org/blood/article/113/9/1977/107987/Activated-T-cells-recruit-exosomes-secreted-by

186. Llorente A, Skotland T, Sylvänne T, Kauhanen D, Róg T, Orłowski A, et al. Molecular lipidomics of exosomes released by PC-3 prostate cancer cells. Biochim Biophys Acta - Mol Cell Biol Lipids [Internet]. 2013 Jul;1831(7):1302–9. Available from: https://linkinghub.elsevier.com/retrieve/pii/S1388198113000966

187. Théry C, Zitvogel L, Amigorena S. Exosomes: composition, biogenesis and function. Nat Rev Immunol [Internet]. 2002 Aug;2(8):569–79. Available from: http://www.nature.com/articles/nri855

188. Martínez MC, Freyssinet JM. Deciphering the plasma membrane hallmarks of apoptotic cells: phosphatidylserine transverse redistribution and calcium entry. BMC Cell Biol [Internet]. 2001;2:20. Available from: http://www.ncbi.nlm.nih.gov/pubmed/11701087

189. Zwaal RFA, Comfurius P, Bevers EM. Surface exposure of phosphatidylserine in pathological cells. Cell Mol Life Sci. 2005;62(9):971–88.

190. Heijnen HF, Schiel AE, Fijnheer R, Geuze HJ, Sixma JJ. Activated platelets release two types of membrane vesicles: microvesicles by surface shedding and exosomes derived from exocytosis of multivesicular bodies and alpha-granules. Blood [Internet]. 1999 Dec 1;94(11):3791–9. Available from: http://www.ncbi.nlm.nih.gov/pubmed/10572093

191. Dillon SR, Constantinescu A, Schlissel MS. Annexin V Binds to Positively Selected B Cells. J Immunol [Internet]. 2001 Jan 1;166(1):58–71. Available from: http://www.jimmunol.org/lookup/doi/10.4049/jimmunol.166.1.58

192. Gibson DG. Enzymatic assembly of overlapping DNA fragments. Methods Enzymol. 2011;498:349–61.

193. Gibson DG, Young L, Chuang R-Y, Venter JC, Hutchison CA, Smith HO.

Enzymatic assembly of DNA molecules up to several hundred kilobases. Nat Methods [Internet]. 2009;6(5):343–5. Available from: http://www.ncbi.nlm.nih.gov/pubmed/19363495

194. Einhauer A, Jungbauer A. The FLAG™ peptide, a versatile fusion tag for the purification of recombinant proteins. J Biochem Biophys Methods [Internet]. 2001 Oct;49(1–3):455–65. Available from: https://linkinghub.elsevier.com/retrieve/pii/S0165022X01002135

195. Stepanenko AA, Dmitrenko VV. HEK293 in cell biology and cancer research: phenotype, karyotype, tumorigenicity, and stress-induced genome-phenotype evolution. Gene [Internet]. 2015 Sep;569(2):182–90. Available from: http://dx.doi.org/10.1016/j.gene.2015.05.065

196. Belmokhtar CA, Hillion J, Ségal-Bendirdjian E. Staurosporine induces apoptosis through both caspase-dependent and caspase-independent mechanisms. Oncogene [Internet]. 2001 Jun 22;20(26):3354–62. Available from: http://www.nature.com/articles/1204436

ACKNOWLEDGEMENTS

AFFIDAVIT

Affirmation in lieu of an oath

Hilgendorff Henning Thomas

surname, first name

I hereby declare in lieu of oath that I have written the present dissertation with the title:

MFG-E8 - an antigen carrier to follicular dendritic cells

I have written this dissertation, entitled, independently, have not made use of any auxiliary materials other than those indicated, and have identified all findings that have been taken over in whole or in part from the literature as such and have provided individual proof of their origin, citing the source.

I further declare that the dissertation presented here has not been submitted in the same or a similar form to any other body for the purpose of obtaining an academic degree.

Munich, 04.01.2024   Henning Thomas Hilgendorff

place, date,   doctoral candidate's signature